Title
Developmental dysregulation of sensory-evoked responses in the somatosensory cortex of Fmr1 KO mice

Author
Arroyo, Erica Darlene

Publication Date
2018

Peer reviewed|Thesis/dissertation

UNIVERSITY OF CALIFORNIA

Los Angeles

Developmental dysregulation of sensory-evoked responses in the somatosensory cortex of *Fmr1* KO mice

A dissertation submitted in partial satisfaction of the

requirements for the degree Doctor of Philosophy

in Neuroscience

by

Erica Darlene Arroyo

2018

ABSTRACT OF THE DISSERTATION

Developmental dysregulation of sensory-induced responses

in the somatosensory cortex of *Fmr1* KO mice

by

Erica Darlene Arroyo

Doctor of Philosophy in Neuroscience

University of California, Los Angeles, 2018

Professor Carlos Portera-Cailliau, Chair

Autism spectrum disorders (ASD) are associated with atypical sensory processing and sensory hypersensitivity, which lead to maladaptive behaviors, such as tactile defensiveness, and possibly contribute to symptoms of inattention, anxiety and learning disabilities. Disruptions in experience-dependent maturation of circuits during early brain development could give rise to altered sensory perception in ASD, but this has not been thoroughly investigated. Focusing on Fragile X Syndrome (FXS), the most common inherited form of autism, I tested the hypothesis that neural circuits in primary somatosensory (S1) cortex do not mature properly in response to sensory inputs. during critical and sensitive periods. Cortical dendritic spines in adult *Fmr1* knockout (KO) mice,

a model of FXS, are known to be unstable and insensitive to sensory input deprivation, but when this begins in development is not known. I used chronic *in vivo* two-photon microscopy to image layer 2/3 of S1 cortex of wild type (WT) and *Fmr1* KO mice. Exposing 2-week-old WT mice to a brief (overnight) period of dramatically enhanced sensory experience led to a significant increase in spine density, whereas the numbers of spines in *Fmr1* KO mice did not change. Next, I tested whether manipulations of inhibition could rescue cortical circuit defects in *Fmr1* KO mice. I imaged intrinsic signals and found that single whisker maps in S1 cortex were abnormally large in *Fmr1* KO mice starting at 2 weeks of age. Early intervention with the NKCC1 inhibitor, bumetanide for 2 weeks starting at birth corrected the size of whisker maps, even up to adulthood. I conclude that *Fmr1* KO mice are unable to modulate post-synaptic dynamics in response to increased sensory input, at a time when sensory information processing first comes online in the cortex, which could play a role in altered sensory processing in FXS. Strategies that enhance inhibition could potentially rescue such circuit defects in FXS.

The dissertation of Erica Darlene Arroyo is approved.

Alvaro Sagasti

Alcino Jose Silva

Stephen Lawrence Zipursky

Carlos Portera-Cailliau, Committee Chair

University of California, Los Angeles

2018

In dedication to:

Dinah and Marcimilliano Baca

Vincente “Rocky” Arroyo

Paul Baca

Steve Sanchez

Craig Arroyo

and

Laura Padilla, PhD

Unable are the loved to die, for love is immortality.

-Emily Dickinson

Table of Contents

List of Figures

List of Tables

Acknowledgments + Permissions

I'd like to first thank my adviser and fearless leader, Dr. Carlos Portera-Cailliau. I am deeply grateful for his mentorship and consistent support throughout my tenure in his lab. His scientific prowess, passion for mentee success, and ease with which he conducts the lab creates an atmosphere of genuine respect and community. I also want to highlight the fact that he selects a diverse group of mentees and fosters inclusion of women in science. On a personal note, I'm continually dazzled with his uncanny ability to effortlessly balance his responsibilities as a mentor, PI and physician, all-the-while taking pride in his dedication to his family. When I first joined the lab, I immediately felt inspired by the people and scientific inquiry. However, when Carlos recognized the logo on my Battle Royale t-shirt and expressed enthusiasm, I knew I had found my new home. Now that it's time to leave, I'm excited but know that there is much to miss (just not the all-nighter experiments).

I thank my committee – Drs. Alvaro Sagasti, Alcino Silva and Larry Zupirsky - for their time and feedback. Since rotating in Alvaro's lab, he has been a source of positivity and encouragement. I also thank him for suggesting I contact Dr. Carlos Portera-Cailliau for my final rotation, a recommendation that I value dearly. I thank Alcino Silva for his constructive feedback and for reminding me to take a step back to think about my work in a larger context. I also thank Larry for his support and his contributions to science, which piqued my interest while I was an undergraduate. As required reading for a genetics class, I presented his landmark paper on Dscam1, which set in motion my resolve to study developmental neurobiology.

I would also like to thank the former and current members of the Portera-Cailliau lab starting with Dr. Amaya Miquelajauregui. Amaya played an instrumental role in my early progress by taking the time to train me in all of the surgical techniques I implemented in my thesis work (with the exception of P1 injections). Her teaching ability (and patience) continues to elicit admiration and appreciation from me. I thank Daniel Cantu for being a great resource ever since we joined the lab together many moons ago and for being the only one who, without miss, catches my movie quotes no matter how obscure. I thank Dr. Cynthia He for being a fantastic collaborator and for being my rock for a number of years, always willing to provide support, for example after repated experimental failures. For this I also thank Dr. Aaron Lulla. I see you, Aaron. I'd like to thank Dr. Anu Goel for her help over the years and for her remarkable even-keeled nature. I thank the physician-in-training formerly known as our "wundergrad", Sahana Kribakaran, for her friendship and for her Ghana music playlist I still enjoy. And I thank the rest of the lab members with whom I've had the pleasure of working: Luis Garza, Grant Higard, Annasha Vyas, Claire Huang, Aditi Newadkar, Gunvant Chaudhari, Sheyda Mesgarzadeh, Satvir Saggi, Gengming Liu, Anouk Heuvelmans, Drs. Máté Marosi, Ricardo Mostany, Anand Suresh, Nazim Kourdougli, and Will Zeiger. I thank Qionger He for our success of a collaboration; the two weeks we spent in lab working 14 hours a day non-stop was made enjoyable by her tireless work ethic and unflinching positive attitude.

A couple other individuals at UCLA I would like to acknowledge are Dr. Will Silkworth and Jaime Lopez. I thank Will for our ongoing series of heated scientific (and otherwise) discussions aided by only the finest whisky (garnished with a splash of our own tears). He is a dear friend, a gentleman and a scholar. I thank Jaime Lopez for being a good friend, often at 3am when I would haunt the corridors of Reed in between experiments. I thank him, in part, for my weight gain due to the Domino's pizza he so often procured. Our comradery is a great reminder that friendship can be forged even when one is sleep-deprived and decidedly grumpy.

I thank my previous mentors Drs. Daniela Cimini and Nagaraj Vinay Janthakahalli for their guidance and support during my early years of training.

I thank Dr. Ed Smith for the competitive program he built for underrepresented minorities in science at Virginia Tech, the VT post baccalaureate research education program (VT-PREP). It is through the mentorship of Ed and the other advisors that I was able to transition into graduate school envigored and determined.

I'd like to thank my family for their unconditional love and support. Without my parents, Joyce and Bill pushing me to pursue my goals, I would not be where I am today. Growing up, my dad used to tell me I would be going to college, "kicking and screaming" if need be. Luckily when it was time, that wasn't necessary. My parents are two of the most selfless people I have ever known. I thank my sisters Katerina, EmaLee and Alma who, I am proud to say, are my best friends. I thank them for being the strong, driven, loving individuals that they are. Katerina and her wonderful partner, Clem hosted me for 6 months during my 4th year - their warmness and generosity during that time is something for which I will always be grateful. I thank EmaLee, my surrogate twin, for her contagious laughter and for being a bright ray of sunshine consistently counteracting my propensity for darkness. I am fortunate to be a part of the strongest support structure for which one can hope.

In keeping with the tradition Carlos established by thanking the Grateful Dead in his doctoral thesis, I would like to thank Nina Hagen, Riz Ortolani and Britney Spears for providing the soundtrack of my work.

My thesis work was supported by the Eugene V. Cota-Robles Fellowship, UCLA; the Neurobehavioral Genetics Training Grant, NIH T32 5T32MH073526-08 and the Dissertation Year Fellowship, UCLA.

Chapter 1 in this thesis includes a subset of material derived from the article entitled "Critical period inhibition of NKCC1 rectifies synapse plasticity in the somatosensory cortex and restores adult tactile response maps in fragile X mice" recently published in *Molecular Psychiatry,* 2018 for which I am a co-author (He et al., 2018) (doi:10.1038/s41380-018-0048-y). The complete author list is as follows: Qionger He, Erica D. Arroyo, Samuel N. Smukowski, Jian Xu, Claire Piochon, Jeffrey N. Savas, Carlos Portera-Cailliau & Anis Contractor (corresponding author). In **Figure 2**, I performed the daily injections of bumetanide (blind), all the cranial window implantations, data analysis and statistical tests. Qionger He performed the OIS. Jeffrey N. Savas, Carlos Portera-Cailliau and Anis Contractor wrote the manuscript. I thank the authors for permission to reproduce the contents of this article.

The contents of **Chapter 2** are derived from a manuscript in preparation titled, "Dendritic spines in early postnatal Fragile X mice are insensitive to novel sensory experience" for which I am lead author. The complete author list is: Erica D. Arroyo, Daniel Fiole, Shilpa Mantri, Claire Huang, and Carlos Portera-Cailliau (corresponding author). I performed all experiments and wrote the manuscript with Carlos Portera-Cailliau who also provided direction for the study. Daniel Fiole generated the Matlab code used for EPB volume measurements. Shilpa Mantri and Claire Huang helped with EPB analysis. I would like to also thank Annasha Vyas for helping with early troubleshooting of EPB analysis.

The contents of **Chapter 3** are reproduced from the manuscript, "A versatile method for viral transfection of calcium indicator in the neonatal mouse brain" recently submitted to *Frontiers in Neuroscience* for which I am co-first author along with Cynthia He. The full author list is as follows: Cynthia X. He‡, Erica D. Arroyo‡, Daniel A. Cantu, Anubhuti Goel, and Carlos Portera-Cailliau (corresponding author). Cynthia He developed the protocol and wrote the manuscript along with Carlos Portera-Cailliau. I contributed to the writing of the manuscript and performed all the imaging experiments and the analysis thereof. Daniel Cantu wrote the Matlab code used for GCaMP6s analysis. Anubhuti Goel performed the electrophysiology experiments and data analysis.

Vita

EDUCATION + RESEARCH EXPERIENCE

2011 – **Interdepartmental PhD Program for Neuroscience**
Chronic in vivo two-photon imaging of experience-dependent synaptic development in a mouse model of Fragile X Syndrome: dysregulated spine dynamics
Lab of Dr. Carlos Portera-Cailliau

2010 – 2011 **Post Baccalaureate Research Education Program at Virginia Tech**
Imaging the mitotic effects of the small molecule drug boric acid on DU-145 prostate cancer cells
Lab of Dr. Daniela Cimini

2005 - 2010 **Arizona State University**

- Bachelors in Science - Biological Chemistry with medicinal chemistry concentration
- Bachelors in Science - Biological Sciences with an emphasis on animal physiology & behavior

ACADEMIC HONORS + AWARDS

2006 - 2010	National Hispanic Recognition Program (NHRP) scholarship
2010 - 2011	Virginia Tech Post-baccalaureate Research Education Program
2011	Competitive Edge Summer Research Program, UCLA
2011/12-2014/15	Eugene V. Cota-Robles Fellowship, UCLA
2012 - 2014	Neurobehavioral Genetics Training Grant, NIH T32 5T32MH073526-08
2014	Carl Storm Fellowship Underrepresented Minority (CSURM) Fellowship, Gordon Research Conference: Fragile X and Autism-Related Disorders
2015	Advanced Techniques in Molecular Neuroscience Cold Spring Harbor course attendee
2015	Brain Research Institute / Semel Institute Neuroscience Graduate Travel Award, UCLA
2017 – 2018	Dissertation Year Fellowship, UCLA

PUBLICATIONS

Arroyo ED, Fiole D, Mantri S, Huang C and Portera-Cailliau, *Regulation of sensory experience-dependent layer 2/3 spine dynamics is impaired in neonatal Fragile X mice following environmental enrichment*. Manuscript in preparation, 2018.

He CX*, Arroyo ED*, Cantu DA, Goel A and Portera-Cailliau C*, A versatile method for viral transfection of calcium indicator in the neonatal mouse brain*. Manuscript submitted to Frontiers in Neuroscience, 2018.

Ricard C, Arroyo ED, He CX, Portera-Cailliau C, Lepousez G, Canepari M, Fiole D, *Two-photon probes for in vivo multicolor microscopy of the structure and signals of brain cells.* Brain Structure and Function, 2018. https://doi.org/10.1007/s00429-018-1678-1

He Q, Arroyo ED, Smukowski SN, Xu J, Piochon C, Savas JN, Portera-Cailliau C and Contractor A, *Critical period inhibition of NKCC1 rectifies synapse plasticity in the somatosensory cortex and restores adult tactile response maps in fragile X mice.* Molecular Psychiatry, 2018. https://doi.org/10.1038/s41380-018-0048-y

PRESENTATIONS

Arroyo ED. *Linking sensory experience to abnormal synaptic development in the Fragile X Syndrome mouse model, Fmr1 KO*. Neurobehavioral Genetics Annual Retreat, UCLA, Jan 9, 2014.

Selected poster presentations:

Arroyo ED, Huang C and Portera-Cailliau C, *Linking sensory experience to abnormal synaptic development in Fragile X mice*. Society for Neuroscience, 2015.

Arroyo ED, Mantri S, Huang C and Portera-Cailliau C, *Linking sensory experience to abnormal synaptic development in Fragile X mice*. Society for Neuroscience, 2017.

TEACHING EXPERIENCE

2015 **Invited lecture**: *Abnormal spine dynamics in a mouse model of Fragile X Syndrome during development*. Virginia Tech Post-baccalaureate Research Education Program. October 8, 2015.

2016 Teaching Assistant: Biology of Cells, Molecular, Cell, and Developmental Biology – UCLA, Winter 2016

Introduction

Sensitive and critical periods during development

Early brain development involves a well-orchestrated series of events by which circuits are assembled and refined through experience, ultimately giving rise to sophisticated computations necessary for a variety of basic autonomic functions as well as complex cognitive tasks. These complex cascades of events are controlled by transcriptional programs and epigenetic interactions that, together, serve as instructions for building the brain by generating a myriad of interconnected molecular pathways (Lambroso and Rubenstein, 1998; Jessell and Sanes, 2000; Tam et al., 2016; Cariaga-Martínez et al., 2018). The gross architecture of the brain is constructed in many developmental stages, including cell proliferation, signal-guided navigation of cells, neuronal process extension and pathfinding via guidance and avoidance cues, and activity-dependent refinement of short- and long-range circuit connectivity (Jessell and Sanes, 2000; Pencea et al., 2001; Rash and Grove, 2006; Ghashghaei et al., 2007; Bystron et al., 2008; Tau and Peterson, 2010). As individual neurons pair with their appropriate synaptic partners, the basic organization of circuitry emerges, followed by synaptic refinement and maturation (Molliver et al., 1973; Fiala et al., 1998; Tashiro et al., 2003). In the somatosensory cortex, the latter steps depend on sensory input (Landers and Sullivan, 1999; Erzurumlu and Gaspar, 2012; Begum and Sng, 2017). Critical periods are defined as distinct windows of time during which specific circuits become "hard-wired" in the brain, such that disruptions after the window has closed lead to irreversible consequences (Hensch, 2005; Meredith, 2015). The classic example of this phenomenon is detailed in the Hubel and Wiesel's elegant studies wherein the authors sutured one eye of a cat during development. This led to preferential ocular dominance columns associated with the open eye, and demonstrated that after critical window was closed, opening of the sutured

eyelid could not reverse ocular dominance (Hubel and Wiesel, 1970). Similarly, sensitive periods are characterized by important windows of time when developmental trajectories associated with massive changes occur, such as elevated synaptic plasticity, but whose repercussions are less well understood and may or may not be irreversible (Knudsen, 2004; Meredith et al., 2012; Meredith, 2015). How and when these sequential events unfold have significant consequences, as slight perturbations of genetic and epigenetic components, even if only transiently, can lead to lifelong dysregulation of brain function (Hensch, 2005; Cariaga-Martínez et al., 2018). Therefore, the brain is especially vulnerable to genetic and environmental deviations during certain epochs of development (Meredith et al., 2012).

Neurodevelopmental disorders and autism spectrum disorders

Symptoms of neurodevelopmental disorders, such as autism spectrum disorders (ASD) and intellectual disability (ID), emerge in early childhood and are characterized by a series of developmental delays including in motor learning, language development and cognitive functions (Filipek et al., 1999). Because the succession of developmental milestones in typically developing individuals is thought to reflect neural circuit maturation across brain regions (Tau and Peterson, 2010), ASDs are collectively thought of as disorders of circuit function arising from altered developmental trajectories (Belmonte et al., 2004; Fagiolini and Leblanc, 2011). Furthermore, ASD exhibit a wide-range of phenotypes (and severities thereof) including sensory hyper – and hypo – sensitivity, social communication impairments, restricted interests, repetitive behaviors and epilepsy. ASD also often shows comorbidity with other disorders such as depression, anxiety and attention-deficit hyperactivity disorder

(ADHD), which has the highest co-occurrence (30-50%) (Leitner, 2014). Although the hallmarks of ASD appear variegated, they share an underlying commonality of circuit dysfunction. One such manifestation of circuit dysfunction is sensory hypersensitivity, which is one of the most prominent features across different forms of ASD (Belmonte et al., 2004; Cascio, 2010). Sensory hypersensitivity is also one of the first indications of ASD beginning in childhood and coincides with a period of development when external sensory information instructs the refinement of sensory circuits required for proper integration (Miyazaki et al., n.d.; Leekam et al., 2007; Cascio, 2010; Tau and Peterson, 2010). Sustained sensory processing deficits therefor indicate problems with circuit assembly during early critical and sensitive periods.

In light of sensitive and critical periods, delays in circuit maturation likely have profound ramifications that extend beyond development into adulthood (Knudsen, 2004; LeBlanc and Fagiolini, 2011; Meredith, 2015). Determining the most efficacious treatment options for ASD and ID may therefore require early time-specific interventions (Filipek et al., 1999; Winarni et al., 2012; Gliga et al., 2014). But which brain circuits are affected in ASD and ID is poorly understood. Moreover, even less is known about how circuit assembly and refinement is affected in ASD.

Of particular interest is Fragile X Syndrome (FXS), which is a neurodevelopmental disorder characterized by ID, hyper-activity, hypersensitivity to sensory stimuli, and behavioral symptoms associated with idiopathic ASD such as social communication and interaction deficits, language delay and repetitive motor behaviors (Smith et al., 2012; Chang et al., 2013). FXS is one of the

most common inherited forms of ASD and shows comorbidity prevalence in 7-25% of individuals with FXS (Gabis et al., 2011), although more recent estimates are as high as 15-52% (Bailey et al., 2008; Hernandez et al., 2009).

Fragile X Syndrome is a disorder of synapses

FXS is caused by the silencing of the *Fmr1* gene, which encodes a translational repressor, the fragile X mental retardation protein (FMRP). Silencing is caused by an expansion of CGG repeats in the 5' UTR of the *Fmr1* gene (Fu et al., 1991; Verkerk et al., 1991). When the repeat expansion exceeds 200 repeats, hypermethylation of the gene leads to near complete silencing across brain regions (Malter et al., 1997). FMRP expression is developmentally regulated and is widely thought to be critical for proper synapse development both structurally and functionally. It also plays a role in synaptic plasticity: in response to the glutamatergic receptor (mGlur) 1/5 activation, FMRP forms complexes with ribonucleoproteins within which it negatively regulates the expression of key synaptic targets such as MAP1B, PSD-95, and CamKII (Lu et al., 2004; Zukin et al., 2009; Darnell et al., 2011). Notably, FMRP targets may comprise as much as 30% of the post synaptic density (PSD) proteome (Darnell et al., 2011; Darnell and Klann, 2013). Because FMRP is silenced in FXS, excess translation of synaptic protein occurs (Peñagarikano et al., 2007; Darnell and Klann, 2013), which likely leads to persistent alterations in synaptic plasticity. Likewise, other forms of ASD and ID are also considered synaptopathies (Won et al., 2013). More specifically, pathways regulated by FMRP have been implicated in other ASD (Nomura et al., 2008; Jiang et al., 2013; Abekhoukh and Bardoni, 2014) suggesting that FXS and ASD likely share a suite of common endophenotypes.

The main neuro-anatomical defect observed in human FXS brains is the presence of immature, filopodia-like, dendritic spines (Rudelli et al., 1985; Hinton et al., 1991; Irwin et al., 2000). Similarly, cortical neurons of the best-studied mouse model of ASD and FXS, *Fmr1* knockout (KO) mice, also show immature spines and reduced concentrations of mushroom-like spines, which tend to be more stable (Dutch-Belgian Fragile X Consortium, 1994; Comery et al., 1997; Yuste and Bonhoeffer, 2001; Irwin et al., 2002). Previous work from our lab and others have shown that dendritic spines of neocortical pyramidal neurons in FXS mutant mice are also abnormally unstable during both early postnatal development (Cruz-Martín et al., 2010) and in adulthood (Pan et al., 2010; Padmashri et al., 2013). The same phenotype appears to occur in other ASD mouse models (Isshiki et al., 2014). Because the dynamics of dendritic spines are regulated by sensory experience (Holtmaat and Svoboda, 2009), it is conceivable that one problem with *Fmr1* KO mice is that their spines are not modulated by changes in sensory inputs. Unfortunately, to date no study has investigated the role of sensory experience in shaping synapses in *Fmr1* KO mice during early postnatal development.

In one study where adult wild type (WT) mice were exposed to environmental enrichment (EE), an increased rate of new spine generation was observed in layer (L) 2/3 and L5 pyramidal neurons in S1 cortex (Yang et al., 2009; Jung and Herms, 2014). In contrast, L5 spines in adult *Fmr1* KO mice do not show a response to changes in sensory experience (Pan et al., 2010). This failure of spine modulation and maturation in response to sensory experience could potentially give rise to hyper-excitability and sensory hypersensitivity, which arguably contribute to the most problematic symptoms of FXS, including ID (Miller et al., 1999; Knoth et al., 2014). Furthermore, dysfunction in structural (and functional) spine dynamics could lead to alterations in how neurons respond to

sensory input (experience-dependent plasticity), meaning that elevated turnover of spines and altered plasticity may be intricately connected. However, little is known about how individual spines respond to sensory stimulation both structurally and functionally. Given the important role of spine dynamics in experience-dependent plasticity and learning (Knott and Holtmaat, 2008; Yu and Zuo, 2011), the increase in spine turnover in cortical pyramidal neurons of the somatosensory cortex could lead to alterations in sensory perception and cognition.

Another possibility is that presynaptic sites on axons, or 'en passant' boutons (EPB), contribute to sensory dysregulation, although little is known about EPB dynamics in the neocortex. In rodents during early development, when axonal processes extend and navigate to their proper destinations, FMRP is expressed at the growth cones and along the shaft in puncta near synapses (Antar 2005, Christie 2009, Akins 2012). At the growth cones, FMRP is thought to play a role in motility and actin dynamics since in its absence, hippocampal growth cones are less motile and have more filopodia extensions as compared to WT mice (Antar 2006). During early synapse development, FMRP is first expressed in dendritic spines and later appears in axonal EPBs suggesting potential roles in synaptic maturation (Till et al., 2012). After the first two post-natal weeks, FMRP is massively down-regulated, although it continues to be expressed at pre (and post) synaptic sites throughout adulthood suggesting additional roles in synaptic plasticity in EPBs. Indeed, studies in the hippocampus, cortex and amygdala suggest that EPB dysregulation may also contribute to errors in plasticity in FXS mice (Ruthazer and Stryker, 1996; Hanson and Madison, 2007; Akins et al., 2009; Suvrathan et al., 2010; Deng et al., 2013; Ferron et al., 2014; Wang et al., 2014). Given the localization and involvement in synaptic plasticity, FMRP function appears to be necessary for proper synapse maturation at both pre- and post-synaptic elements during

development (Till et al., 2012) and later in synaptic plasticity. Thus, spine immaturity/instability and presynaptic hyperexcitability in FXS likely have far-reaching effects, from cell-to-cell communication, to circuit establishment/maintenance, and to behavior, making the study of synaptic structures a critical facet in understanding FXS pathology, and one with potential broader implications for ASD in general.

The fact that synaptic maturation may be delayed in FXS could of course explain the myriad neurological and psychiatric symptoms of affected individuals. But it remains a mystery how subtle defects in such a profoundly important developmental milestone that takes place throughout the brain (i.e., synaptogenesis) could lead to specific symptoms, such as anxiety, attention deficit, or impaired learning. One possibility is that different symptoms are caused by specific synaptic defects in different brain regions (e.g., amygdala, neocortex, hippocampus). Hence, during my thesis, I focused on a specific symptom in FXS (hypersensitivity to sensory stimuli) and set out to identify how sensory experience shapes synapses in the somatosensory cortex.

Sensory over-reactivity in Fragile X Syndrome and autism

A common feature between ASD, FXS and other neurodevelopmental disorders is aberrant sensory processing (Tomchek and Dunn, 2007) that often manifests (but is not limited to) as tactile defensiveness. In fact, a majority of young children with autism respond inappropriately to sensory stimulation (Leekam et al., 2007; Ben-Sasson et al., 2009); and in FXS, virtually all patients have tactile defensive behaviors (Rogers et al., 2003; Baranek et al., 2008). For example,

FXS patients may show over-reactivity to tactile sensory stimuli, such as human touch or contact with certain textures (Cascio, 2010). Tactile defensiveness may have other implications since touch is the first sense to develop (Pihko and Lauronen, 2004) and because the tactile modality is important for motor control development associated with posture / walking (Metcalfe et al., 2005) and for fine motor movements, such as grasping and tool manipulation (Soechting and Flanders, 2008). It is possible that problems with sensory processing and sensory hypersensitivity (auditory and somatosensory) contribute to delays in language development. Prior to verbal communication, social communication transpires primarily through touch, suggesting tactile defensiveness may also infringe upon early social bonding with caregivers (Cascio, 2010), in which case, tactile defensiveness could manifests as an early form of a social deficit. Furthermore, recent studies evaluating the intersection between sensory processing abnormalities and social/behavioral irregularities, suggest that rather than occurring independently, sensory and behavioral phenotypes are the product of cooperative interplay (Gliga et al., 2014; Ronconi et al., 2016; Thye et al., 2018). The fact that sensory processing abnormalities exacerbate social and behavioral problems suggests that targeting and correcting sensory abnormalities may have non-linear ameliorative outcomes.

The *Fmr1* knockout mouse model of FXS:

Because symptoms of FXS (including sensory overreactivity) begin in childhood, it is reasonable to look for cortical abnormalities in brain development when meaningful activity patterns are being established in response to sensory inputs. However, studying the precise circuits that encode sensory information is not possible in humans given the limitations of brain imaging resolution. Aforementioned, a prominent phenotype in FXS is the overabundance of immature cortical

dendritic spines, which can only be studied in humans' post mortem. Notably, imaging studies reveal similar spine phenotypes in *Fmr1* KO mice (Dutch-Belgian Fragile X Consortium, 1994; Comery et al., 1997; Yuste and Bonhoeffer, 2001; Irwin et al., 2002), which serves as a more effective way to study circuit development due to: relative ease of genetic manipulation, ability to study behavior, and because the brain can be interrogated using combinations of genetic tools and *in vivo* imaging techniques. In addition to phenocopying spine abnormalities in FXS, *Fmr1* KO mice exhibit many behaviors that correlate to FXS behaviors in humans including learning and memory deficits, task inflexibility, social interaction abnormalities, and heightened sensory responsiveness, making it an ideal model to study sensory processing abnormalities in ASD.

Our lab recently showed that tactile defensive behaviors are present in early post-natal *Fmr1* KO mice (He et al., 2017), around the time when mice begin exploratory behavior. This is a sensitive period when cortical cell populations transition from highly correlated firing patterns to desynchronized patterns, and when sensory stimuli-dependent processing first comes online (Golshani et al., 2009; Rochefort et al., 2009; Frye and MacLean, 2016). This study also showed maladaptive responses of layer 2/3 excitatory barrel cortex neurons during whisker stimuli: repeated stimuli lead to a gradual reduction in neuronal firing (adaptation) in WT mice but not in *Fmr1* KO mice. This suggests that aberrant cortical sensory processing is already present at the onset of initial sensory integration, specifically around the second post-natal week.

Fmr1 KO mouse model studies have provided invaluable insights into some of the major molecular mechanisms that are, at least in part, responsible for circuit defects. One of the

central dogmatic theories in FXS is that activation of the metabotropic glutamate receptor, mGluR, leads to secondary messenger-dependent initiation of translation of synaptic proteins (Bear et al., 2004; Matta et al., 2011). This activation of translation is counterbalanced with FMRP translation repression. In FXS, however, excessive translation occurs in the absence of FMRP, which leads to errors in synaptic plasticity (Bear et al., 2004; Muddashetty et al., 2007; Nakamoto et al., 2007; Bassell and Warren, 2008). These studies championed the notion that targeting mGluR pharmacologically would yield potential therapeutic options for the treatment of FXS. Despite early success in mouse models and somewhat promising pre-clinical trials, these strategies have not yielded viable treatments due to trials ending either due to lack of phenotypic improvement and, in some cases, due to detrimental side effects (Jacquemont et al., 2011; Bailey et al., 2016; Quiroz et al., 2016; Youssef et al., 2018). Another parallel hypothesis is that hyperexcitability in FXS is caused by underperformance of GABAergic interneurons, the main inhibitory neuronal population of cells (Rubenstein and Merzenich, 2003; Belmonte and Bourgeron, 2006; Moy and Nadler, 2008; Lozano et al., 2014). Although FMRP is thought of as a translational repressor, it also has non-canonical functions and can lead to activation of translation (Willemsen and Kooy, 2017). In the absence of FMRP, GABA receptor subunit (A) expression is reduced (D'Hulst et al., 2006; Gantois et al., 2006) while catabolism of GABA is increased (Maravall et al., 2000; Adusei et al., 2010) leading to an overall decrease in GABAergic inputs throughout the brain, which is thought to underpin hyperexcitability. Indeed, evidence in the amygdala and subicular neurons demonstrates that postsynaptic inhibitory GABA currents are reduced in *Fmr1* KO mice (Curia et al., 2009; Olmos-Serrano et al., 2010). Importantly, as has been the case with mGluR antagonists, clinical trials targeting GABA have been unsuccessful (Berry-Kravis et

al., 2012; Erickson et al., 2017; Ligsay et al., 2017). The reasons preclinical trials and animal studies have yet to translate into treatment options have been heavily debated, with reasons ranging from unreliable outcome measures due to parental reporting, to issues with dosage. Another possibility is that these targets are too far upstream and whose antagonism interferes with molecular cascades important for circuit function. It is also possible that targeted early intervention in combination with the pharmacological tools can reverse synaptic phenotypes. What is clear is that the impact of these studies has ushered in a new chapter in FXS research, wherein new targets must be identified and new paradigms for animal studies must be generated. I propose that studies focused on development will be the key to future treatment of FXS both for predictions of treatment efficacy and to provide insights into timing-dependent circuit dysfunction.

The second post-natal week is important for development of sensory modalities in the rodent cortex

The second post-natal week is an important time for proper maturation in the somatosensory cortex. By P14, eyes are (newly) opened and integration of sensory information necessary for sensorimotor coordination begins - as mice start actively exploring their environments. Exploration is primarily mediated by movement of vibrissae on their snout, a.k.a., whisking, which is perhaps not surprising given rodents are nocturnal animals and have poor vision. Whisking is a tactile behavior used to detect objects, interpret surroundings and interact socially (Wolfe et al., 2011; Bobrov et al., 2014). Although non-patterned whisking occurs prior to eye opening, P14 coincides with the onset of oriented high-frequency active whisking (Arakawa and Erzurumlu,

2015), which is necessary for scanning surfaces and texture delineation (Zucker and Welker, 1969; Arakawa and Erzurumlu, 2015). Active whisking is also required for object recognition and perisomatic spatial interpretation, key aspects of navigation. Thus, sensory feedback at P14 is important for mature whisking behaviors, which is vital for navigation.

Another study that points to the second post-natal week as being a sensitive period suggests that a developmental switch occurs, during which spike timing-dependent plasticity (STDP) properties undergo significant changes wherein timing-dependent LTP (t-LTP) becomes less dominant. STDP is thought to be a strong contributor to sensory evoked activity responses, indicating that this window is important for the proper developmental circuit organization (Itami and Kimura, 2012).

Significance of thesis work

The breadth of this work was conducted to address outstanding questions and to develop strategies so that future work can be done in early post-natal mice. The 3 major achievements presented here can be described as follows: 1.) evidence that early intervention is a viable strategy for treatment of FXS, 2.) establishment of a novel structural synaptic phenotype related to sensory experience in early neonates, and finally 3.) a detailed protocol for imaging activity in neonatal mice, which was previously hampered by technical limitations of mouse lines and traditional plasmid transduction techniques.

A strength of my work is that it focuses on early cortical development precisely because FXS is a neurodevelopmental disease. The bulk of prior rodent studies were conducted using adult mice, and while those experiments were important for developing treatments of symptoms of FXS in adolescents and adults, understanding how FXS originates and progresses is important for precise timing-specific target options for early intervention, a strategy that has already shown merit in individuals with FXS (Winarni et al., 2012).

In **chapter 1** I show that an early intervention strategy that targets NKCC1 (whose down-regulation during a sensitive period in WT mice serves as a switch for GABA polarity but remains abnormally high in *Fmr1* KO mice) is sufficient to rescue the abnormally large size of whisker-evoked barrel field maps in the second post-natal week and in adult mice. This empirical evidence suggests that targeted early intervention can potentially lead to long-lasting reversal of a FXS phenotype thought to contribute to sensory hypersensitivity.

In **chapter 2** I show that two-week old *Fmr1* KO mice are insensitive to a brief period of novel sensory experience (enriched environment). Establishing early sensory-related synaptic phenotypes is crucial for FXS and ASD research because they elucidate specific types of sensory dysfunction, timing of dysfunction for future targeting, and may provide unbiased measures that can be used in the future as readouts of treatment efficacy (since a battery of behavioral tests is not possible in neonates).

In **chapter 3** I present a research protocol that facilitates early post-natal *in vivo* calcium imaging of neuronal and synaptic activity. Given the many technical challenges inherent to neonatal

experiments, the importance of protocol-sharing and improvement is vital for building a foundation on which neurodevelopmental disorder research can be built. That only a few labs are capable of performing neonatal *in-vivo* imaging experiments reflects the need for resource-sharing. By generating this protocol, the hope is that others will implement our strategies, develop additional strategies and help move the field forward in a unified effort.

Chapter 1

Rescue of expansive whisker-responsive maps in early post-natal FXS mice: empirical support for early intervention efficacy

As discussed in the introduction, FXS is characterized be a series of developmental delays in the neocortex. One of particular importance is the delay in the maturation of the $GABA_A$ receptor equilibrium potential (E_{GABA}) (He et al., 2014). E_{GABA} sets the efficacy of GABA transmission and the immature depolarized reversal potential has been proposed to have trophic effects on the developing central nervous system (CNS) (Wang and Kriegstein, 2009). E_{GABA} becomes increasingly hyperpolarized in many neuronal types with age, which affects the driving force through $GABA_A$ receptors (Ben-Ari et al., 2007). This developmental change is mediated by alterations in intracellular chloride $[Cl^-]_{INT}$ which is maintained by the expression of two Cl^- co-transporters; Na^+-K^+-Cl^- co-transporter (NKCC1) is expressed early in development and elevates $[Cl^-]_{INT}$, and K^+-Cl^- co-transporter (KCC2) expresses at increasing levels later in development and which extrudes Cl^- from the cell (Kaila et al., 2014). *Fmr1* KO mice have an abnormally high expression of NKCC1 in the cortex at P10 (He et al., 2014). This high expression of NKCC1 could primarily drive the prolonged depolarized E_{GABA} in layer IV neurons. Because GABA-mediated depolarization can directly induce synaptogenesis and the maturation of glutamatergic synapses (Chancey et al., 2013; Oh et al., 2016), mistimed maturation of E_{GABA} may cause the aberrant development of glutamatergic synapses in *Fmr1* KO mice. But as yet, it has not been demonstrated whether the prolongation of a depolarized E_{GABA} is causally related to the altered development of excitatory synapses in the somatosensory cortex in *Fmr1* KO mice. This work demonstrates that daily administration of the NKCC1 inhibitor, bumetanide, to *Fmr1* KO mice early in development corrected the enlarged whisker response maps in barrel cortex in early post-natal mice and persisted through adulthood.

Whisker evoked responses in the cortex are normalized by repeated bumetanide treatment during early post-natal development

Prior work has demonstrated that there is a heightened neural response in the adult barrel cortex of *Fmr1* KO mice to tactile whisker stimuli (Arnett et al., 2014; Zhang et al., 2014; He et al., 2017). We used optical imaging of intrinsic signals (OIS) to measure the cortical response to single whisker stimulation in order to determine whether sensory responses were affected by recurring bumetanide treatment during the neonatal development (**Fig. 1**).

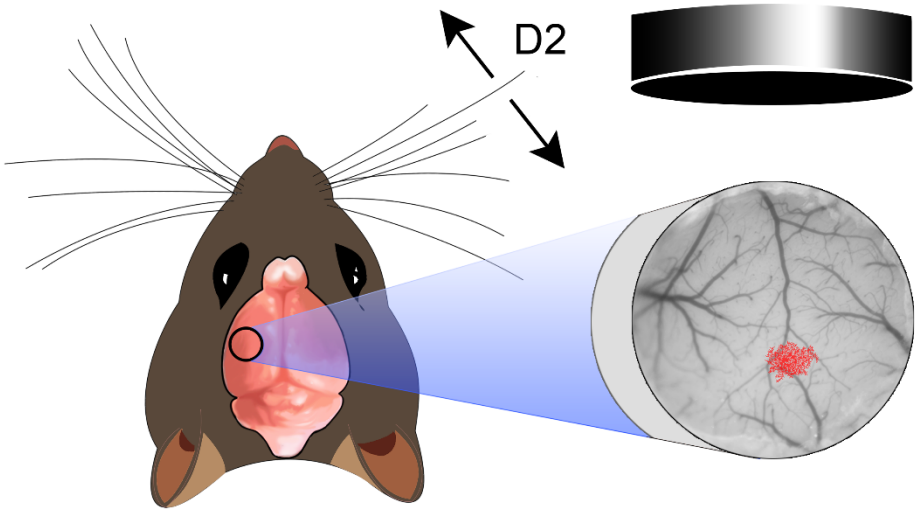

Figure 1: Scheme of OIS mapping of D2 whisker.
Barrel cortex maps of primary whisker D2 generated by OIS. The D2 whisker is stimulated with a piezo electric actuator. Tactile responsive maps are generated by contrast imaging of the barrel cortex though a cranial window.

Fmr1 KO and littermate *Fmr1* WT mice were administered bumetanide (0.2 mg/kg) or vehicle during the first two postnatal weeks when E_{GABA} is more depolarized in *Fmr1* KO mice than

WT littermates (He et al., 2014) (daily from P 0-14; **Fig. 2a**). At P14, mice underwent surgeries to implant cranial windows over the somatosensory cortex and imaging was first performed at P 16/17 and then again at 2 months of age (in the same animals). The sensory representation map evoked by high frequency (100 Hz, 1.5 s) stimulation of the D2 whisker was measured in all the groups. At P16/17, the vehicle-treated *Fmr1* KO group had a significantly larger cortical response (thresholded area) compared to vehicle-treated *Fmr1* WT controls (2396 ± 336 vs. 1124 ± 311 μm^2, respectively, $p = 0.003$, two-way ANOVA with Bonferroni adjustment; **Fig. 2B–D**), demonstrating that the previously reported increase in map size in 3-month-old *Fmr1* KO mice (Arnett et al., 2014) is already apparent by 2 weeks of age. In the bumetanide-treated *Fmr1* KO group the cortical whisker response was significantly reduced and indistinguishable from that of either the vehicle- or drug-treated WT animals (892 ± 68 μm^2 $p = 0.992$ vs WT two-way ANOVA with Bonferroni adjustment; **Fig. 2B-D**). Therefore, the enhanced sensory response in early post-natal *Fmr1* KO mice can be normalized by bumetanide treatment. To determine whether drug administration during the first two post-natal has long-lasting effects on cortical responses, I also measured the whisker-evoked intrinsic signals in the same animals at 2 months of age. Vehicle-treated adult *Fmr1* KO mice also had abnormally large cortical representations of whisker responses in comparison to the vehicle-treated *Fmr1* WT mice ($p = 1 \times 10^{-6}$, two-way ANOVA with Bonferroni adjustment; **Fig. 2E–G**). However, in the group treated with bumetanide, the OIS neural activity map was no different from the WT groups (map area WT bumetanide vs KO bumetanide, $p = 0.21$, two-way ANOVA with Bonferroni pairwise comparisons). Therefore, bumetanide treatment during the early cortical development corrects the circuit response to sensory whisker stimulation, an effect that persists through adulthood despite cessation of drug administration.

Figure 2: Long lasting correction of cortical whisker evoked responses after critical period treatment with bumetanide

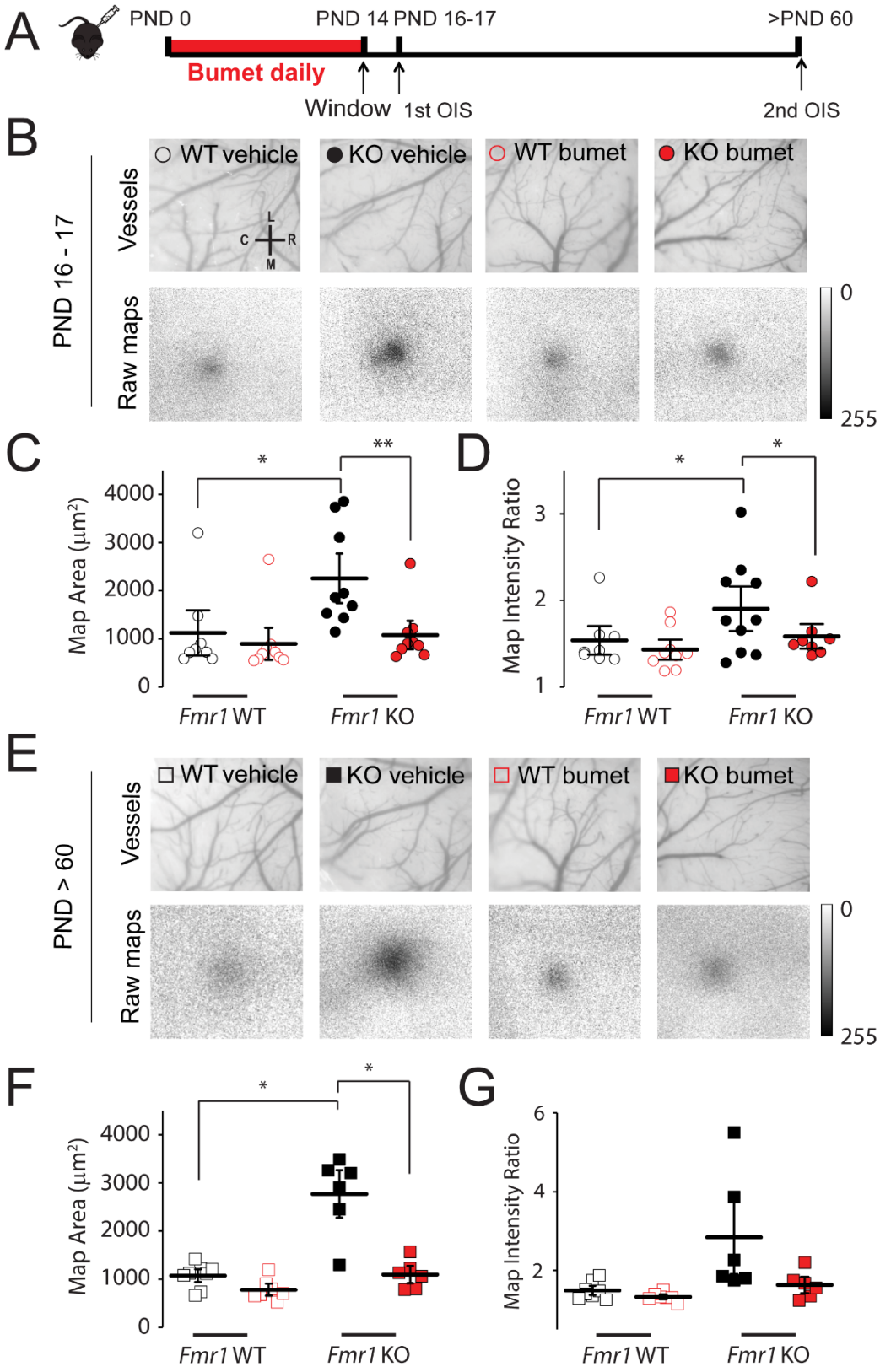

Figure 2: Long lasting correction of cortical whisker evoked responses after critical period treatment with bumetanide

(A) Schematic representation of time-course of OIS experiments.

(B) Top: vasculature of S1 somatosensory cortex of P16-17 *Fmr1* WT and *Fmr1* KO mice; Bottom: corresponding cortical excitation maps collected during D2 whisker stimulation. Calibration: 0.5 mm

(C) Map area measured in P16-17 *Fmr1* WT and *Fmr1* KO mice in vehicle (black) and bumetanide (red).

(D) Map intensity ratio measured in P16-17 mice.

(E) Vasculature and cortical excitation maps for mice older than P60; same representative mice as shown in (B). Calibration: 0.5 mm

(F) Map area measured in adult mice

(G) Map intensity ratio measured in adult mice. Significance was determined using two-way ANOVA with Bonferroni correction *$p < 0.05$ ** $p < 0.01$.

METHODS FOR CHAPTER 1

Reagents

All reagents were from Sigma-Aldrich unless otherwise noted.

Drug Administration

Animals were housed in trio breeding with a male *Fmr1*$^{-/y}$ and two *Fmr1*$^{-/+}$ females. Births of new litters were monitored daily to ensure treatment started on the day of birth (P 0). Intraperitoneal (i.p.) injections were made of bumetanide (0.20mg/kg), furosemide (20mg/kg), mannitol (750mg/kg). The vehicle used in for bumetanide was 0.9% saline and 0.1% ethanol, and for furosemide and mannitol experiments the vehicle was 0.9% saline. Minimal handling of pups and use of nestlets in cages was used to avoid disruption to new litters. For electrophysiology experiments, pups were injected daily from P0 until the day of experimentation. For OIS and mass spectrometry experiments, pups were injected from P0 to P14.

Cranial Windows

Chronic glass-covered cranial windows were implanted as previously described [53, 54]. Briefly, P 14 mice were anesthetized with isoflurane (5% induction, 2% maintenance via nose cone) and placed in a stereotaxic frame over a warm water re-circulating blanket. Dexamethasone (0.2 mg/kg; Baxter Healthcare Corp.) and carprofen (5 mg/kg; Pfizer) were administered subcutaneously to reduce brain edema and local tissue inflammation. A 2-3 mm craniotomy was performed with a pneumatic dental drill. The center of the craniotomy was placed over the left hemisphere barrel

cortex. A sterile round 5 mm glass cover slip (#1; Electron Microscopy Sciences) was gently laid over the dura matter and glued to the skull with cyanoacrylate-based glue. Dental acrylic was then applied to the skull surface and up to the wound edges. A titanium bar (0.125 x 0.375 x 0.05 inch) was embedded in the dental acrylic to secure the mouse on to the stage for imaging. Following recovery for ~1 h, mouse pups were returned to their cages with their dam and littermates.

Optical intrinsic signal imaging

Rodents rely on whiskers sensory feedback for navigation of their surroundings by utilizing a sensory information from of active whisking and from passive whisker deflection. This provides information about distance and texture of the objects over which the whiskers deflect as they move through space. This sensory information is relayed through the VPM to the thalamus and ultimately to the neocortex in a somatotopic organization called the barrel field. Whisker-evoked tactile response maps can be visualized through cranial windows by stimulating whiskers and using contrast imaging in a procedure called optical imaging of intrinsic signals (OIS). (**Fig 1**).

Optical intrinsic signal (OIS) imaging of the D2 whisker (D2W) sensory receptive field was done at two different time points in the same mice: P16-17 and at 2 months (not all mice were imaged at both times due to window clarity issues). Whiskers surrounding the D2W were gently trimmed with Vannas scissors (down to a length of ~ 2 mm) just prior to imaging to facilitate single whisker stimulation. OIS imaging was performed through the cranial window on mice under light anesthesia with 0.5-0.75% isoflurane and a single dose of chlorprothixene (3 mg/kg, i.p., Sigma-Aldrich). The cortical surface was illuminated by green (535 nm) and red (630 nm) light-emitting diodes (LEDs) mounted around a 'front-to-front' tandem arrangement of objective lenses (135 mm and 50 mm focal lengths, Nikon). The green LEDs were used to visualize the superficial

vasculature and the red LEDs were used for IOS imaging. The microscope was focused to ~350 μm below the cortical surface for 2-month mice and about ~300 μm for P16-17 mice. Imaging was performed at 10 Hz using a fast camera (Pantera 1M60, Dalsa), frame grabber (64 Xcelera-CL PX4, Dalsa) and custom routines written in MATLAB. Each session consisted of 30 trials (at 10 s intervals) of mechanical stimulation for 1.5 s (100 Hz) using a glass micropipette coupled to a piezo bender actuator (Physik Instrumente). Frames 0.9 s before the onset of stimulation (baseline) and 1.5 s after stimulation (response) were collected. Frames were binned 3 times temporally and 2 x 2 spatially. Stimulated cortical areas were identified by dividing the response signal by the averaged baseline signal (DR/R) for every trial and then summing all trials. Response maps were then thresholded at 50% of maximum response to get the responsive cortical areas for D2W. For a subset of mice and time points, maps at different depths were averaged to account for slight variations in signal.

Analysis for OIS

Cortical sensory representation map sizes were defined by ImageJ software (National Institutes of Health, Bethesda, MD). To compute statistical differences between genotype and treatment interactions, two-way ANOVAs were performed followed by 2-tailed pairwise comparisons with Bonferroni corrections. For comparisons between WT bumetanide - *Fmr1* KO vehicle and WT vehicle – *Fmr1* KO bumetanide groups, T-Tests for independent samples with Bonferroni correction (alpha = 0.05 / 2; confidence level = 97.5%) were used to compute statistical differences. All statistical tests were conducted in SPSS 23 software (IBM Corporation, USA). All data are presented as the mean ± standard error of the mean. Significance was set at $p < 0.05$*, $p < 0.001$**, $p < 0.0001$***.

Chapter 2

Dendritic spines in early postnatal FXS mice are insensitive to novel sensory experience: an early post-natal phenotype

One way to understand how sensory experience modulates synapses, is to image dendritic spines *in vivo* before and after a period of sensory deprivation (Trachtenberg et al., 2002; Holtmaat et al., 2006; Hofer et al., 2009; Pan et al., 2010; Miquelajauregui et al., 2015). Spines in adult *Fmr1* KO mice are also less responsive to sensory deprivation and motor learning (Pan et al., 2010; Padmashri et al., 2013), which might reflect an inability to make and maintain stable synapses. But whether spines in FXS are insensitive to new sensory experiences has never been tested *in vivo* during development. To address this, I used a brief period of dramatic novel sensory experience environmental enrichment (EE) in P14 mice.

For chronic two-photon imaging of synaptic structures, *in utero* electroporation (IUE) was performed at embryonic day (E) 16 to express green fluorescent protein (GFP) in L2/3 pyramidal neurons of S1 cortex (**Fig. 3A**). To ensure sparse labeling of GFP-expressing and minimal overlap of their apical dendrites and axons in L1 (**Fig. 3B**), a low concentration of pCAG-GFP (500 ng/μL) was injected into the lateral ventricle during the IUE procedure. At P10-12, cranial windows were implanted over the barrel field of S1 cortex. Only mice with windows that were optically transparent with no signs of bleeding or dural damage were used for subsequent imaging (**Fig. 3C**). Starting at P14, mice were anesthetized and head-fixed to the stage of a two-photon microscope for longitudinal *in vivo* imaging of dendrites and axons of L2/3 neurons (**Fig. 3D, E**).

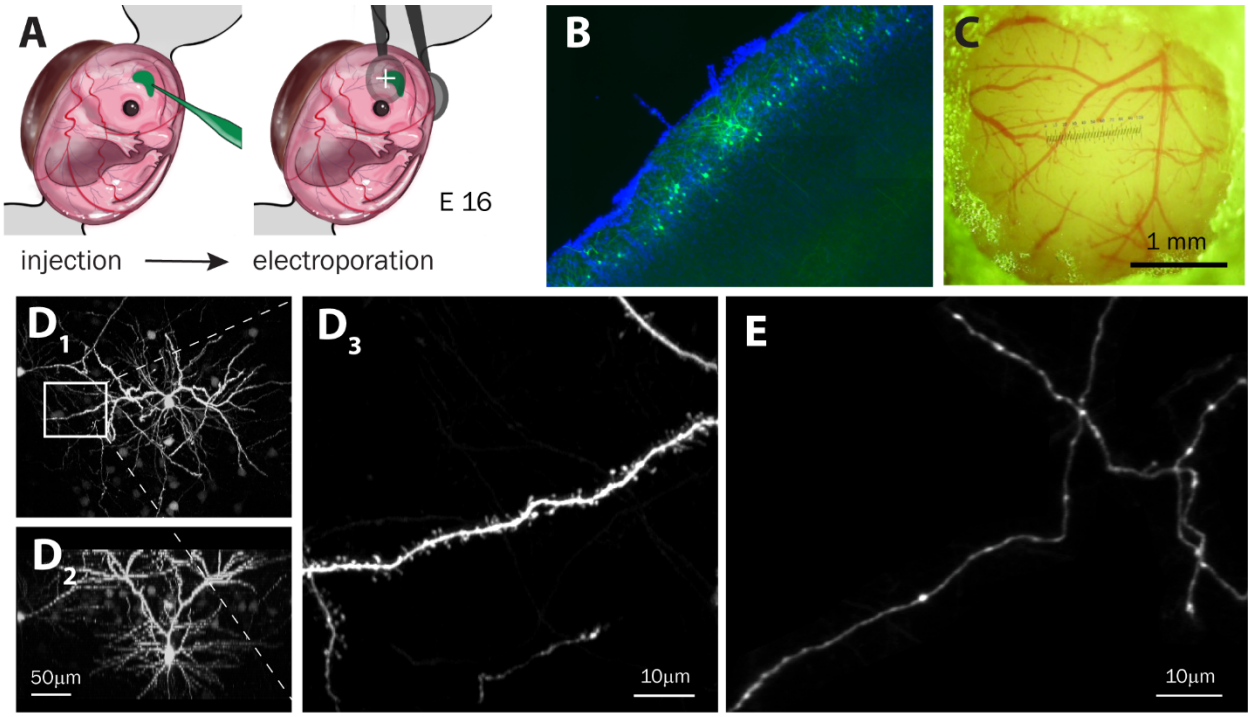

Figure 3: Embryonic day 16 *in utero* electroporation and *in vivo* imaging of somatosensory L2/3 neurons at P14

Cartoon of E16 IUE scheme. The lateral ventricle is injected with pCAG-GFP (left panel) and electroporated with the positive electrode over the filled ventricle (right panel).

A. GFP expression localized at S1 in L2/3 pyramidal cells. Coronal slice of 2mo. old WT brain that underwent E16 IUE with pCAG-GFP (green) and counterstained with DAPI (blue).

B. Cranial window implanted over the somatosensory cortex at postnatal day (P) 12 and imaged at P14 (photo taken just prior to imaging). Notes: photo was taken through the microscope eyepiece while the window was illuminated with a green light; the line transecting the window is a ruler bar on the eye piece.

D1. Low magnification of a L2/3 neuron imaged *in vivo* at an x-y (top-down) view. Image z-stack was collected at 5µm steps and 3D projection in FIJI.

D2. Low magnification of a L2/3 neuron (same as D1) imaged *in vivo* at an z-y (orthogonal) view. Image z-stack was collected at 5µm steps and 3D projection in FIJI.

D3. Max projection of representative L2/3 apical dendritic segment. Zoomed in view of inset in D1.

E. Best projection of representative L2/3 axon

High resolution *in vivo* imaging of L2/3 dendrites was performed at P14 (**Fig. 4A**) in n= 81 cells of 18 WT mice and n= 73 cells of 15 *Fmr1* KO mice. I found that spine density was the same in WT and *Fmr1* KO mice (0.68 ± 0.014 spines/mm vs. 0.65 ± 0.015 spines/μm respectively; **Fig. 4B**), which is in agreement with several prior *in vivo* imaging studies during development and adult (Cruz-Martin 2010, Pan 2010; Padmashri 2013). Because immature dendritic protrusions are often longer and thinner (filopodia-like) than their mature counterparts (Portera-Cailliau The Neuroscientist 2012), I also compared the length of spines in both genotypes. I find that spines in *Fmr1* KO mice at P14 were significantly longer than those of WT mice, though the difference was rather small (1.5 ± 0.03 μm vs. 1.38 ± 0.028 μm; p = 0.005; **Fig 4C**).

FMRP is expressed in axons at the growth cones where it plays a role in growth cone navigation in the hippocampus (Antar 2005, Christie 2009, Akins 2012). Also, as discussed in the **Introduction**, *Fmr1* KO mice exhibit defects in synaptic plasticity in many brain regions (Ruthazer and Stryker, 1996; Hanson and Madison, 2007; Akins et al., 2009; Suvrathan et al., 2010; Deng et al., 2013; Ferron et al., 2014). Therefore, I also imaged axons of L2/3 neurons coursing through L1 at P14 in n=33 cells from 8 WT mice and n=27 cells from 6 *Fmr1* KO mice and did not find any significant differences in EPB density between WT and *Fmr1* KO mice (**Fig. 4D;** 0.12 ± 0.008 EPBs/ μm vs. 0.11 ± 0.009 EPBs/ μm, respectively).

A previous study of wild-type (WT) mice, where EPBs were imaged *in vivo* with two-photon microscopy, suggests that there's a positive correlation between EPB volume and network activity (Grillo et al., 2013). There is also indirect evidence of links between EPB volume and activity: release probability of neurotransmitter is intimately tied to the size of the active zone of the EPB,

which in turn shows a weak positive correlation with EPB volume (Holderith et al., 2012). Because there is evidence of altered presynaptic plasticity in FXS (see the **Introduction** section), I investigated the possibility that plasticity errors are accompanied by volumetric differences in FXS EPBs. At baseline, Hippocampal CA3-CA1 EBPs have normal release properties in FXS mice but following repeated stimuli, the release probability becomes abnormally high (Patel et al., 2013). I therefor expected to detect no differences in EPB volumes in FXS mice at baseline. I imaged n/N = 43/13 in WT animals and n/N = 38/10 *Fmr1* KOs, averaged EPB EPBs for each cell and found no differences between genotypes (data normally distributed, one-way ANOVA).

Figure 4: Spine density of L2/3 neurons is equal in WT and *Fmr1* KO mice at P14 but *Fmr1* KO spines are longer.

A. Representative *in vivo* two-photon images of dendrites in WT and *Fmr1* KO mice were acquired at P14. Scale bar is 10 µm.

B. Density of spines in L2/3 neurons in WT is not different than *Fmr1* KO L2/3 dendrites. I analyzed n=81 cells in 18 WT mice and n=73 dendrites in 15 *Fmr1* KO mice (one-way ANOVA; normally distributed data).

C. *Fmr1* KO spines are 11% longer than WT spines in L2/3 dendrites. I analyzed 77 neurons from 19 WT mice and 74 neurons from 16 mice. One-way ANOVA was used for statistical significance; normally distributed data.

D. *Fmr1* KO EPB density appears normal in L2/3 neurons. I imaged n=33 cells from 8 WT mice and n=27 cells from 6 *Fmr1* KO mice. Data were

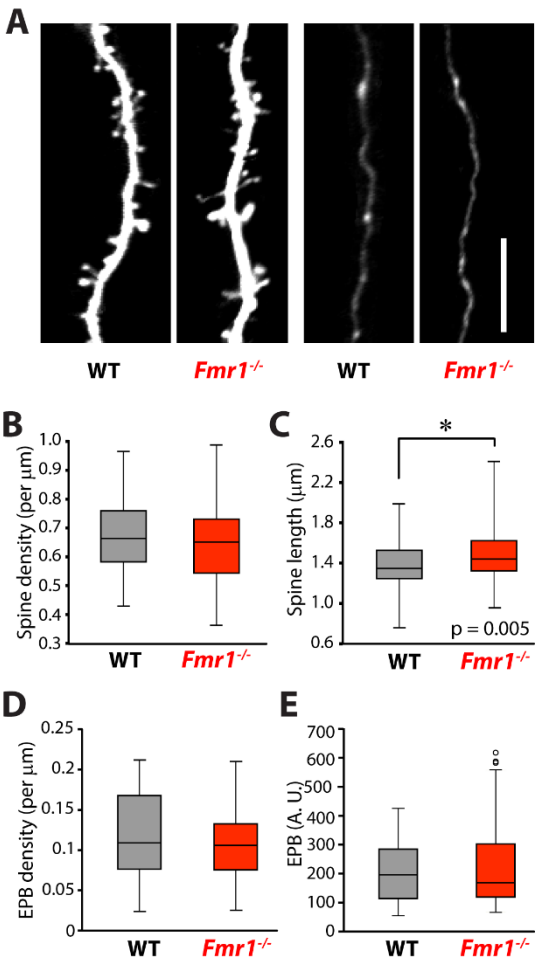

not normally distributed. For statistical significance testing, the Mann-Whitney U test was used.

E. Volumes of EPBs in FXS are not statistically significant from WT. I imaged n=43 cells from 13 WT mice and n=38 cells from 10 *Fmr1* KO mice. One-way ANOVA was used for statistical significance testing; normally distributed data.

Rather than finding alterations in the density of dendritic spines in juvenile or adult *Fmr1* KO mice, previous *in vivo* imaging studies have revealed a significant increase in spine turnover (Cruz-Martin 2010, Pan 2010; Padmashri 2013). I interpreted this synaptic instability to mean that neurons in *Fmr1* KO mice are unable to respond to new sensory inputs related to novel sensory experiences or learning (He CX & Portera-Cailliau, Neuroscience, 2013). To test the hypothesis that heightened sensory input affects synaptic dynamics, mice were placed in either an enriched environment (EE) overnight at P14-15 or kept in their standard environment (SE) cage (**Fig. 5**). The EE cages provided a dramatic novel sensory experience across visual, auditory and, especially, tactile modalities (**Fig. 5**). Dendrites were imaged at P14 twice, 4 h apart, and then placed overnight in either EE or SE cages, and then imaged again at P15 twice, 4 h apart (**Fig. 5**).

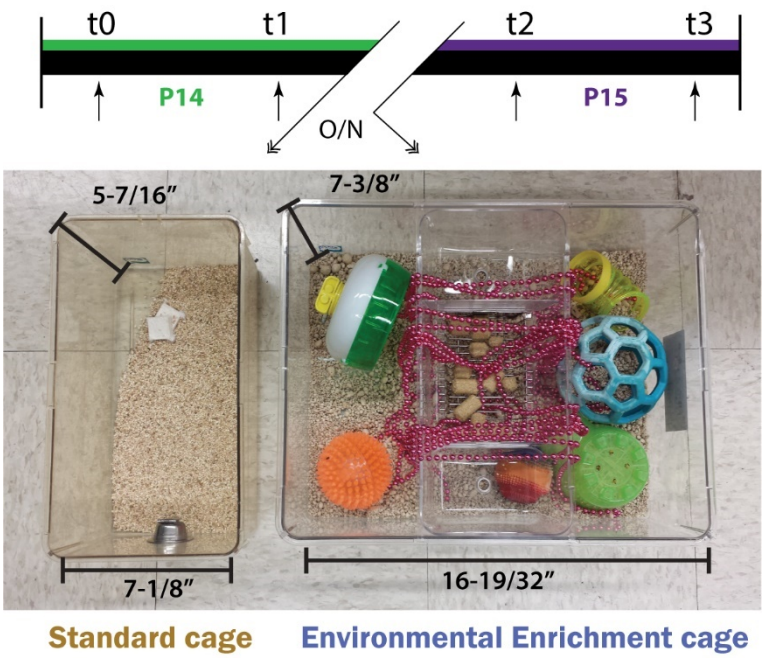

Figure 5: Experimental time line for environmental enrichment experiments

At P14, mice are imaged twice with four hours inter-imaging intervals, then placed overnight (O/N) in either a standard cage (left), which is smaller and only contains bedding and nesting pads or in and enriched environment (right). Enriched environments contain many elements chosen to engage in different sensory modalities including bright colors (vision), variegated shapes, sizes and textures (whisking) and a running wheel (sensorimotor). At P15, mice were returned to their home cages and the same field of views were imaged again twice with 4 hours between each imaging session.

As far as axons, I imaged axons before and after EE or SE (**Fig. 6A**). I find that neither the turnover rate (ToR) nor EPB density were significantly different in 32 axons from 10 WT mice or 32 axons from 8 *Fmr1* KO mice housed in EE vs. 33 axons in 8 WT mice and 27 axons in 6 *Fmr1* KO mice housed in SE (**Fig. 6B,** data were not normal, statistical tests used: Wilcoxon signed ranks tests for density*;* Kruskal-Wallis H test for ToR).

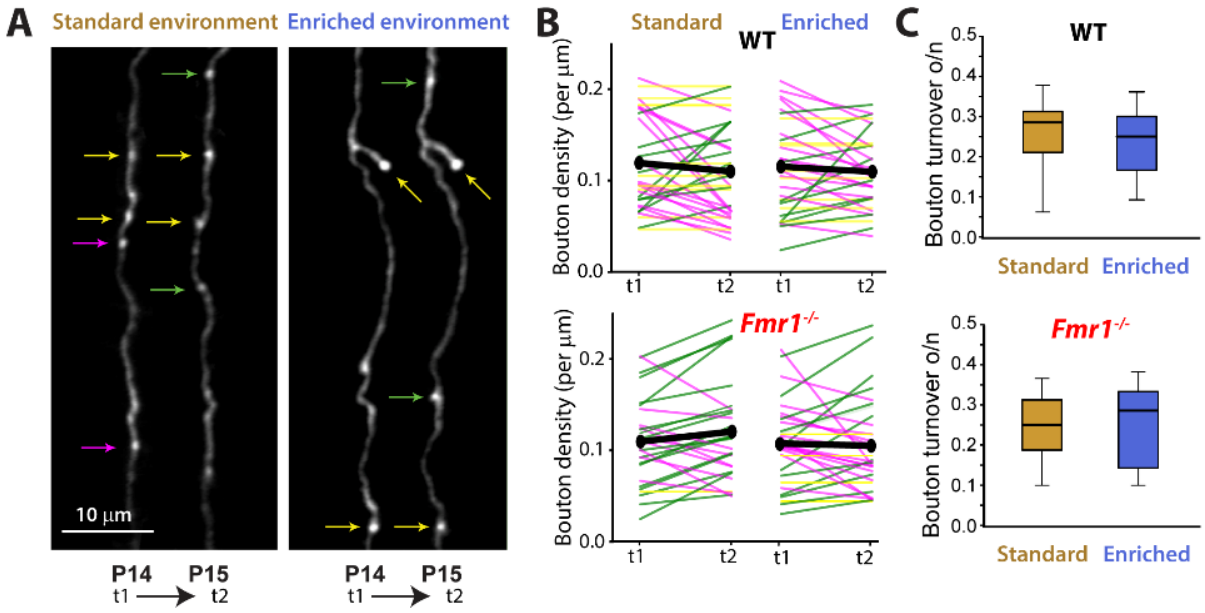

Figure 6: EPB volume and spine density of L2/3 neurons is equal in WT and *Fmr1* KO mice at P14 but *Fmr1* KO spines are abnormally long

A. *In vivo* two-photon images of axonal EPBs in WT mice were acquired at P14, (t1). Animals were then housed overnight (for 8-10 h) either in standard environment (SE) or in an enriched environment (EE) and imaged again at P15, (t2). Subsets of representative EPBs are tracked with arrows: yellow indicates persistent EPBs, magenta indicates lost EPBs and green indicates newly formed EPBs (with respect to overnight period).

B. Density of EPBs does not change from P14 to P15 regardless of genotype and or housing condition. Top: density of EPBs in L2/3 neurons of WT mice housed overnight in SE or EE (repeated measures mixed-design ANOVA; normally distributed data). Each line represents the spine density for an individual neuron. Green, magenta and yellow lines indicate an increase, a reduction or no change in EPB density, respectively. Black lines represent the average for all the cells. I analyzed n=33 cells from 8 WT mice in SE and 32 cells from 10 WT mice in EE. Bottom: Density of EPBs in L2/3 neurons of *Fmr1* KO mice housed overnight in SE or EE at P14. There was no significant change in spine density after EE or SE. For *Fmr1* KO mice, I analyzed n=27 cells from 6 mice in SE, and 32 cells from 8 mice in EE.

C. Turnover of axonal EPBs of L2/3 neurons in WT mice (top) and *Fmr1* KO mice (bottom) in SE and EE mice. No statistical difference was found among all four groups, although there seems to be a trend for WT EE EPB turnover to be lower than WT SE EPB turnover but not in *Fmr1* KO animals. I analyzed n=34 cells from 8 WT mice in SE and 33 cells from 10 WT mice in EE and n= 27 cells from 6 *Fmr1* KO mice in SE, and 32 cells from 8 *Fmr1* KO mice in EE (two-way ANOVA).

When I examined spine density in 40 cells from 9 WT mice in SE and 40 cells from 9 WT mice in EE, I found a significant increase in spine density in WT mice following the novel sensory experience in EE (from 0.66 ± 0.02 spines/μm to 0.70 ± 0.02 spines/μm; mixed-model repeated measures ANOVA was used to compare across all groups, p-values reported were corrected via Bonferroni, p= 0.023 for WT EE; **Fig. 7B**, top) but not in WT after standard housing. The spine density in WT following enrichment was also significantly higher than both *Fmr1* KO groups (p = 0.02 compared to *Fmr1* KO SE, p = 0.044 compared to *Fmr1* KO EE, data not shown). In contrast, the density of spines in 32 cells from 7 *Fmr1* KO mice in SE and 41 cells from 8 *Fmr1* KO mice in EE did not significantly increase at P15 (0.636 ± 0.21 spines /μm to 0.609 ± 0.022 spines /μm, for *Fmr1* KO SE; and 0.643 ± 0.018 spines /μm to 0.621 ± 0.019 spines /μm, for *Fmr1* KO EE; **Fig. 7B**, bottom). Although the increase in spine density with EE in WT mice was subtle (~6 %), the vast majority (67.5%, 27/40 cells) of the neurons analyzed added spines with this relatively brief period of novel sensory experience, whereas the majority of neurons in WT mice that remained in impoverished sensory experience (SE), showed a decrease in spine density (62.5%, 25/40 cells) (**Fig. 7B**, top).

Changes in spine density are due to changes in the rates at which spines are added or eliminated, and/or to changes in their lifetime. Thus, the higher spine density in WT mice after a novel sensory experience (EE) could arise from a gain in new spines or from a loss of preexisting spines. I calculated the rates of spine formation and spine elimination before and after EE and in WT mice and discovered that spine generation was 16% higher following EE (from 0.14 ± 0.01 spines/µm before vs. 0.16 ± 0.01 spines/µm after EE; signed-rank test, p = 0.035; **Fig. 7C**). In contrast, the rate of spine gains remained constant in WT mice that remained in SE (0.14 ± 0.01 spines/µm at P14 and 0.15 ± 0.01 spines/µm, signed rank test, n.s.). *Fmr1* KO mice housed overnight in EE showed no change in the rates of spine formation or elimination; (formation: 0.155 ± 0.01 spines/µm before vs. 0.143 ± 0.01 spines/µm, signed rank test; n.s.); **Fig. 7C, bottom;** elimination: **Fig. 8**). Together, these data indicate that neurons in *Fmr1* KO mice are insensitive to novel sensory stimuli at P14.

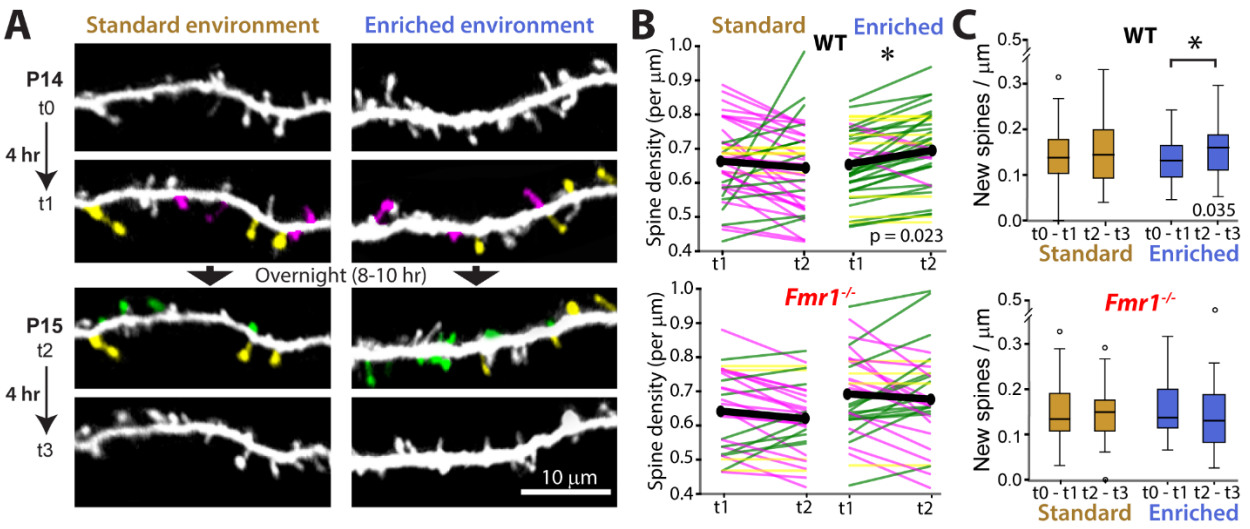

Figure 7: Spine density of L 2/3 neurons in WT mice increases after environmental enrichment at P14 but not in *Fmr1* KO mice.

A. *In vivo* two-photon images of dendritic spines in WT mice were acquired at P14, 4 h apart (t0 and t1). Animals were then housed overnight (for 8-10 h) either in a standard environment

(SE) or in an enriched environment (EE) and imaged again twice at P15, 4 h apart (t2 and t3). Subsets of representative spines are pseudo-colored: yellow indicates persistent spines, magenta indicates lost spines and green indicates newly formed spines (with respect to overnight period).

B. Density of spines in L2/3 neurons of WT (top) and *Fmr1* KO (bottom) mice housed overnight in SE or EE. Note the significant increase in spine density after EE in WT mice (*p = 0.023; repeated measure mixed-design ANOVA with Bonferroni correction; normally distributed data). Each line represents the average of all ROIs for an individual neuron. Green, magenta and grey lines indicate an increase, a reduction or no change in spine density, respectively, for individual cells. Black lines represent the average for all the cells. I analyzed n=40 cells (1,738 spines) from 9 WT mice in SE and 40 cells (2,225 spines) from 9 WT mice in EE. For *Fmr1* KO mice I analyzed n= 33 cells (1671 spines) from 7 mice in SE, and 41 cells (1760 spines) from 8 mice in EE.

C. Rates of formation and elimination of dendritic spines of L2/3 neurons in WT mice (left) and *Fmr1* KO mice (right). Note that the rate of spine formation was significantly higher in WT mice immediately after environmental enrichment (*p = 0.035 signed rank test; normal data), but not in *Fmr1* KO mice or WT mice housed in standard cages. I analyzed n=41 cells from 9 WT mice in SE and 45 cells from 9 WT mice in EE. For *Fmr1* KO mice I analyzed n= 34 cells from 7 mice in SE, and 41 cells from 8 mice in EE.

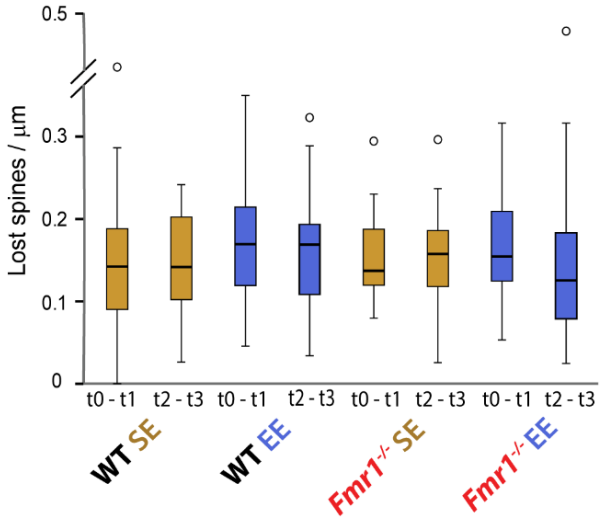

Figure 8: Spine elimination rate is not different in *Fmr1* KO mice and is not affected by EE

Elimination of spines before and after SE or EE is the same in WT and *Fmr1* KO mice. A mixed-design repeated measures ANOVA was used to determine statistical differences with significance set at $p < 0.05$ (n=44 cells from 10 WT mice in SE, n=45 cells from 9 WT mice in EE, n=34 cells from 7 *Fmr1* KO mice in SE, and n=44 cells from 8 *Fmr1* KO mice in EE).

METHODS FOR CHAPTER 2

Reagents:

The plasmid vector pCAG-GFP was obtained through Addgene (Plasmid #11150). All other reagents were from Sigma-Aldrich unless otherwise noted.

Experimental animals:

All experiments followed the U.S. National Institutes of Health guidelines for animal research, under an animal use protocol (ARC #2006-016) approved by the Chancellor's Animal Research Committee and Office for Animal Research Oversight at the University of California, Los Angeles. I used male and female C57/BL6J mice (HSD C57Bl/6NHsd) housed in a vivarium with a 12-h light-dark cycle and food/water ad libitum. Imaging was performed during the light cycle and enrichment experiments were performed during the dark cycle. Animals were housed with their dam until P21-22.

In utero electroporation for GFP expression in L2/3 pyramidal cells:

In utero electroporation was performed as previously reported (Cruz-Martín et al., 2010; Cruz-Martin et al., 2012). Briefly, pregnant female mice at gestation day E16 were anesthetized with isoflurane (5% induction, 1.5-2% maintenance vol/vol). Under sterile conditions, a medial incision was made along the abdomen to expose the uterine horns were. Using ringed forceps to gently hold embryos, I pressure injected a plasmid encoding pCAG-GFP (500ng/μl) into the left

lateral ventricle with a Picospritzer (Parker; 40 PSI, 10 ms pulses). A set of 3 square pulses (50 ms duration, 35 V, with 500 ms between each pulse) was administered to each embryo via a custom-built electroporator with the positive electrode paddle placed over the left somatosensory cortex. Throughout the procedure, the embryos were frequently irrigated with warm saline (37ºC). The embryos were placed back inside the mother and the dam's abdominal wall was sutured with absorbable sutures (muscle: Surgical specialties LOOK, nylon 0.7 metric, 1279B) and nylon sutures (skin: Surgical specialties LOOK, polysyn 0.7 metric, 492B). The dam was observed for 2 hours following the surgery to monitor full recovery.

Cranial window surgery for chronic *in vivo* two-photon microscopy:

I followed a previously described protocol (Cruz-Martin et al., 2010; Cruz-Martin and Portera-Cailliau, 2010; Mostany and Portera-Cailliau, 2008). In short, pups (P10-12) were anesthetized with isoflurane and placed in a stereotaxic frame. A 2.5 mm diameter circular craniotomy was performed over the electroporated somatosensory cortex in the left hemisphere and covered with a 3 mm glass coverslip (Electron Microscopy Sciences). The coverslip was secured to the skull with Krazy Glue and dental cement. At P14 a small titanium headbar was attached to the skull with dental cement in order to secure the animal to the microscope stage for imaging.

Histology:

2-month old mice were perfused intracardially with ice-cold 4% paraformaldehyde in 0.1 M phosphate buffer. The brains were harvested and post-fixed overnight at 4ºC and then sliced (100 µm-thick sections) on a vibratome. Sections were then stained with DAPI (Life Technologies) and mounted onto coverslips with Gold-Mount media. Sections were imaged with a structure

illumination Zeiss Apotome microscope and 10x objective. Images were acquired and stitched via ZEN.

***In vivo* two-photon imaging:**

Structural synaptic imaging was performed on a custom-built two-photon microscope with a Chameleon Ultra II Ti:Sapphire laser (Coherent), a 40X objective (0.8 NA, Olympus), and ScanImage software (Pologruto et al., 2003). Mice were anesthetized for imaging sessions with isoflurane (1-2% maintenance vol/vol) and kept warm with an electric heating blanket (Harvard Apparatus). Throughout imaging, mice were monitored for taxed breathing and proper coloration of paws/ears. Z-stacks with 1 μm steps were collected at 512 x 512 pixels and a digital zoom of 1x for low magnification images (0.71 μm/pixel x 0.73 μm/pixel) (**Fig. 3**) and 5x for dendrite and axon imaging (0.153 μm/pixel x 0.154 μm/pixel) (**Fig. 5,6,7**). Imaging sessions were performed in the evening at P14 and in the morning at P15 after being housed with their dam and littermates in either standard cages or enriched cages (see **Environmental enrichment**).

Environmental enrichment:

Animals were housed in their home cages for standard enrichment or in enriched cages overnight (8-10 hours) between P14-15 during the dark cycle when rodents are most active and awake. Standard cage dimensions were 13-1/4" x 7-1/8" x 5-7/16" with two pads for nest-building and a layer of bedding. Enriched environment cage dimensions were 13-1/4" x 16-19/32" x 7-3/8″ (1800 Moue Cage, Lab Products) and contained brightly-colored balls and plastic tunnels, a running wheel, beaded necklaces strewn from the top of the cage, and a variety of toys, multiple nest pads and a layer of bedding (**Fig 4**).

Measurement of axonal bouton volume:

Z-stacks with 1 μm steps were collected at 512 x 512 pixels and a digital zoom 5x for imaging (0.153 μm/pixel x 0.154 μm/pixel) (**Fig. 5**). Raw images were sum-projected and were manually binarized prior to skeletonization. Then, the signal baseline along the skeleton was estimated on the projected images using the asymmetric least squares smoothing algorithm by Eilers and Boelens (unpublished manuscript). Peaks along the skeleton of the axon were detected utilizing the Fast 2D Peak Finder algorithm. The volume of boutons was defined as the sum of the pixel intensities of the sub-regions segmented by the Fast 2D Peak Finder algorithm, divided by the baseline local value for normalization. Statistical analysis was performed using MATLAB (Mathworks®, Natick, MA, USA) for each peak along the axonal shaft.

Experimental design and statistical analysis:

Spine imaging data were analyzed using the semi-automated ScanImage (r3.8RC4) spine analysis software in MATLAB. With the exception of brightness and contrast toggling, raw images were used for the analysis. If a time point was missing or one or more imaging sessions was poor quality, the field-of-view was eliminated from analysis for time-series calculations. Spines longer that 5 μm were categorized as filipodia and excluded from analysis. Dendritic and axonal segments were analyzed in: 1) regions at a distance of at least 10 μm from branch points and process tips, 2) if the segment was at least 15 μm in length, and 3) if the segment was isolated (minimal overlap with other processes). The average length of dendritic segments analyzed per cell was 37.74 +/- 2.25 μm, 43.97 +/- 2.59 μm, 42.5 +/- 2.82 μm and 43.22 +/- 1.97 μm for WT SE, WT EE, *Fmr1* KO SE, *Fmr1* KO respectively. For axonal EPB experiments, custom-written MATLAB code was used to determine EPB volume.

All statistical tests and pertinent values are listed in **table 1**. In all experiments, n represents the number of neurons analyzed and N represents the number of animals used. All statistical analysis where ANOVAs were used, data were distributed normally as determined by the Shapiro-Wilk test for normality (with the p-value set at < 0.05) and met the criteria for Levene's test of homogeneity of variances in each group. Outliers were defined as data that were more or less than two standard deviations from the mean. For baseline length, density and turnover of WT and *Fmr1* KO spines, One-way ANOVAs were used. Turnover was calculated as follows: $\frac{(\boldsymbol{lost\ spines + gained\ spines})}{(\boldsymbol{2\ x\ total\ number\ of\ spines})}$. All pairwise comparisons were corrected for multiple comparisons with the Bonferroni method. For baseline density of WT and *Fmr1* KO EPB, data were non-normal, so comparisons were made using the Mann-Whitney U test.

For environmental enrichment spine imaging experiments, mixed-design or split plot repeated measure ANOVAs (SPANOVAs) were used with Bonferroni-corrected pairwise comparisons across all groups with the exception of spine formation rate at P14 vs. P15 (**Fig. 7D)**. Because the *Fmr1* KO SE group was not distributed normally, comparisons for all groups were determined using the non-parametric signed ranks test (with significance set at $p < 0.05$, two-tailed). For EE EPB analysis, data were non-normal; Kruskal-Wallis H tests were used for ToR comparisons between groups. For within group comparisons of EPB density, Wilcoxon signed-rank tests were used (with significance set at $p < 0.05$, two-tailed). All statistics were performed with SPSS 24 (IBM). Graphs were generated using Microsoft Excel 2017 and SigmaPlot 13 (Systat). In box and whisker plots, error bars indicate SEM and horizontal bars indicate medians. Figures were generated with SPSS 24 (IBM), Microsoft Excel 2017, FIJI (ImageJ), Adobe Photoshop 2018 and Adobe Illustrator 2018.

Figure	*Comparison*	*Statistical test* *Normality* [¥]	*Group*	*n value /* *N value*	*Test statistic*	*p-value*
4B	Spine density	one-way ANOVA normal	WT *Fmr1* KO	81 / 18 73 / 15	*F (1, 152) = 1.61*	0.21
4C	Spine length	one-way ANOVA normal	WT *Fmr1* KO	89 / 18 78 / 15	*F (1,165) = 8.069*	*0.005 [a] *0.005 [b]
4D	EPB density	Mann-Whitney U non-normal	WT *Fmr1* KO	33 / 8 27 / 6	*U = 408*	0.58
6B	EPB density (within group)	Wilcoxon signed ranks non-normal	WT SE WT EE *Fmr1* KO SE *Fmr1* KO EE	33 / 8 32 / 10 27 / 6 32 / 8	*Z = -1.55* [c] *Z = -1.06* [c] *Z = -1.66* [c] *Z = -0.096* [c]	0.12 [d] 0.29 [d] 0.096 [d] 0.92 [d]
6C	EPB ToR (between group)	Kruskal-Wallis H non-normal	WT SE WT EE *Fmr1* KO SE *Fmr1* KO EE	33 / 8 32 / 10 27 / 6 32 / 8	χ^2 (3) = 1.97[e]	0.58 [d]
7B[l]	Spine density	Split-plot ANOVA (SPANOVA) normal	Group * time WT SE WT EE *Fmr1* KO SE *Fmr1* KO EE *t0* *t1* *t2* *t3* WT: EE vs. SE [j] WT EE vs. KO SE [j] WT EE vs. KO EE [j]	 40 / 9 40 / 9 32 / 7 41 / 8	*F (3, 147) = 1.94* [f,g] <u>Within groups</u> *F (3, 147) = 2.46* [f,g] *F (3, 147) = 2.96* [f,g] *F (3, 147) = 2.78* [f,g] *F (3, 147) = 2.46* [f,g] between groups *F (3, 149) = 0.54* [a] *F (3, 149) = 0.39* [a] *F (3, 149) = 3.71* [a] *F (3, 149) = 2.58* [a]	*0.045 [k] 0.065 *0.034 *0.023 [b,h] *0.043 [i] 0.066 0.66 0.76 *0.013 0.056 0.33 [b] *0.020 [b] *0.044 [b]
7C	Spine formation (within group)	Signed ranks non-normal	WT SE WT EE *Fmr1* KO SE *Fmr1* KO EE	44 / 9 45 / 9 34 / 7 44 / 8	*Z = -0.16* *Z = -2.11* *Z = -0.19* *Z = -1.11*	0.87 [d] *0.035 [d] 0.85 [d] 0.27 [d]
8	Spine elimination	Split-plot ANOVA (SPANOVA) normal	Group * time WT SE WT EE *Fmr1* KO SE *Fmr1* KO EE	 44 / 9 45 / 9 34 / 7 44 / 8	*F (3, 163) = 0.74* [f,g]	0.53

Table 1: Detailed statistical reports for Chapter 2

¥ Data were considered normal if they passed the Shapiro Wilk's test (significance was set at $p < 0.05$)

* The difference is significant at the .05 level.

a. Univariate test

b. Post-hoc pairwise comparisons with Bonferroni adjustment

c. Based on positive ranks

d. Asymptotic significance (2-sided test)

e. The test statistic is adjusted for ties.

f. Multivariate test

g. Exact statistic

h. Comparisons between t1 – t2

i. Post-hoc pairwise comparisons with Bonferroni adjustment not significant ($p = 1, 0.053, 0.080, 0.447, 0.730$)

j. Comparisons at t2

k. Pillai's Trace

Chapter 3

Post-natal day 1 GCaMP6s viral injections: a method to image cortical activity in early post-natal mice

The first three postnatal weeks in the mouse brain are of great interest to neuroscientists because they coincide with critical periods of experience-dependent plasticity (Hensch, 2005) and a phase of massive synaptogenesis (Micheva and Beaulieu, 1996; Holtmaat et al., 2009; Cruz-Martin et al., 2012). In particular, the time period around postnatal day (P) 12 is one of drastic sensory transitions as mice open their eyes, start whisking, and begin to actively explore their environment (Arakawa and Erzurumlu, 2015; van der Bourg et al., 2016). These developmental processes are critically important for understanding the causes of circuit dysfunction in a variety of developmental brain disorders, such as autism, schizophrenia, epilepsy and intellectual disability.

In the last two decades, we have witnessed a large number of technological innovations for investigating neural circuits, from optogenetics and chemogenetics to rabies virus tracing and tissue clearing methods for fluorescence microscopy. Two of the most notable advancements have been the development of novel fluorescent calcium and voltage sensors, which allow researchers to record neuronal activity with synaptic resolution (Grewe and Helmchen, 2009), and the enhanced microscopy capabilities for imaging the anatomy and function of circuits across time in behaving animals (Wilt et al., 2009). These developments, combined with the ability to use a growing array of genetically encoded fluorescent molecules (e.g., fluorescent proteins, channels, pumps, etc.) via mouse genetics or viral transduction, now make it possible to trace the inputs and outputs of individual neurons and to record activity of specific neuronal cell populations in awake behaving mice.

The development of the ultrasensitive fluorescent genetically encoded calcium indicators (GECIs), especially GCaMP6 (Chen et al., 2013), has dramatically improved the action potential detection capability of two-photon calcium imaging. When combined with Cre-Lox genetics, this approach is particularly well suited for chronic recordings of neural activity in awake, behaving animals at the single cell level, and in identified neuronal populations. The conventional approach for *in vivo* two-photon calcium imaging with GECIs typically consists of injecting a recombinant adeno-associated virus (rAAV) encoding the sensor at the time of implanting a cranial window over the desired cortical region. Imaging is typically performed 2-4 weeks after surgery to allow for sufficient expression of the virus (Tian et al., 2009; Chen et al., 2012, 2013; Zariwala et al., 2012). Unfortunately, this delay between injection and optimal GCaMP expression precludes calcium imaging experiments during the early postnatal period in rodents.

Overcoming this technological limitation would allow investigations to investigate how experience shapes circuits during the first postnatal weeks and other important developmental milestones in the mouse brain. For example, previous calcium imaging studies demonstrated that sensory cortices undergo a rapid desynchronization of network activity at postnatal day (P) 12 (Golshani et al., 2009; Rochefort et al., 2009; Siegel et al., 2012). However, those studies employed synthetic calcium indicators that could only be imaged acutely for a few hours. Thus, the approach we outline here, which makes it possible to express GECIs (or other proteins) during early postnatal development and allows longitudinal imaging over several days to weeks in the same animals (for example, before *and* after P12), is a significant advance.

An alternative to the rAAV injection-based approach presented here is to use transgenic mice that express GCaMP. Unfortunately, in popular genetic mouse lines that drive expression of GCaMP, the promoters come online after this developmental period. For example, *Thy1*-GCaMP6 mice show stable expression of GCaMP6 in multiple cortical regions across months without apparent toxicity, but only after the third postnatal week (Dana et al., 2014). Similarly, the Ai38 mouse line expresses GCaMP3 when treated with tamoxifen at P7, but showed very low expression at 4 weeks of age (Zariwala et al., 2012). A different problem may occur when you drive neuronal GCaMP6s expression too early, during embryonic development, namely toxicity. For example, when we tried using *in utero* electroporation at embryonic day 16 with plasmids encoding GCaMP6s, we were able to visualize a few synchronously active neurons at around P7-P9, but just a few days later all expression was lost, presumably due to neuronal cell death (unpublished observations). We surmise that the expression of GCaMP6s at early stages of neuronal differentiation or migration is irreversibly toxic to neurons, and therefore, a transgenic mouse line taking advantage of a promoter that would drive GECI expression during embryonic development is likely to be toxic to neurons.

Here we describe a novel protocol for neonatal injection of rAAV encoding GCaMP6s at P1, which enables *in vivo* two-photon imaging of cortical neurons as early as P10. At P1, a modified burr hole surgery was used to inject the rAAV encoding GCaMP into the desired cortical area, and then at P7 or later, a cranial window was implanted over the previously injected area. Starting at day P11, repeated *in vivo* two-photon calcium imaging of layer (L) 2/3 neurons was possible with adequate GCaMP expression that persisted for weeks. We demonstrate the major advantage of this approach to chronically image the same population of neurons from P11 through young

adulthood, allowing us to characterize the developmental desynchronization of cortical network activity and the evolution of sensory-evoked network during this critical period. We believe this approach will be valuable to the neuroscience community because the same neonatal viral injection approach could be used to express other genetically encoded calcium and voltage indicators, chemogenetic or optogenetic actuators, rabies virus tracers, or a variety of other fluorescent proteins, in different brain regions.

We performed intracranial rAAV-hSyn-GCaMP6s injections in anesthetized mouse pups at P1 through a small burr hole over primary somatosensory cortex (**Fig. 9 and Fig. 10**).

Figure 9: P1 injection setup and procedure (drawings by Kim Battista)

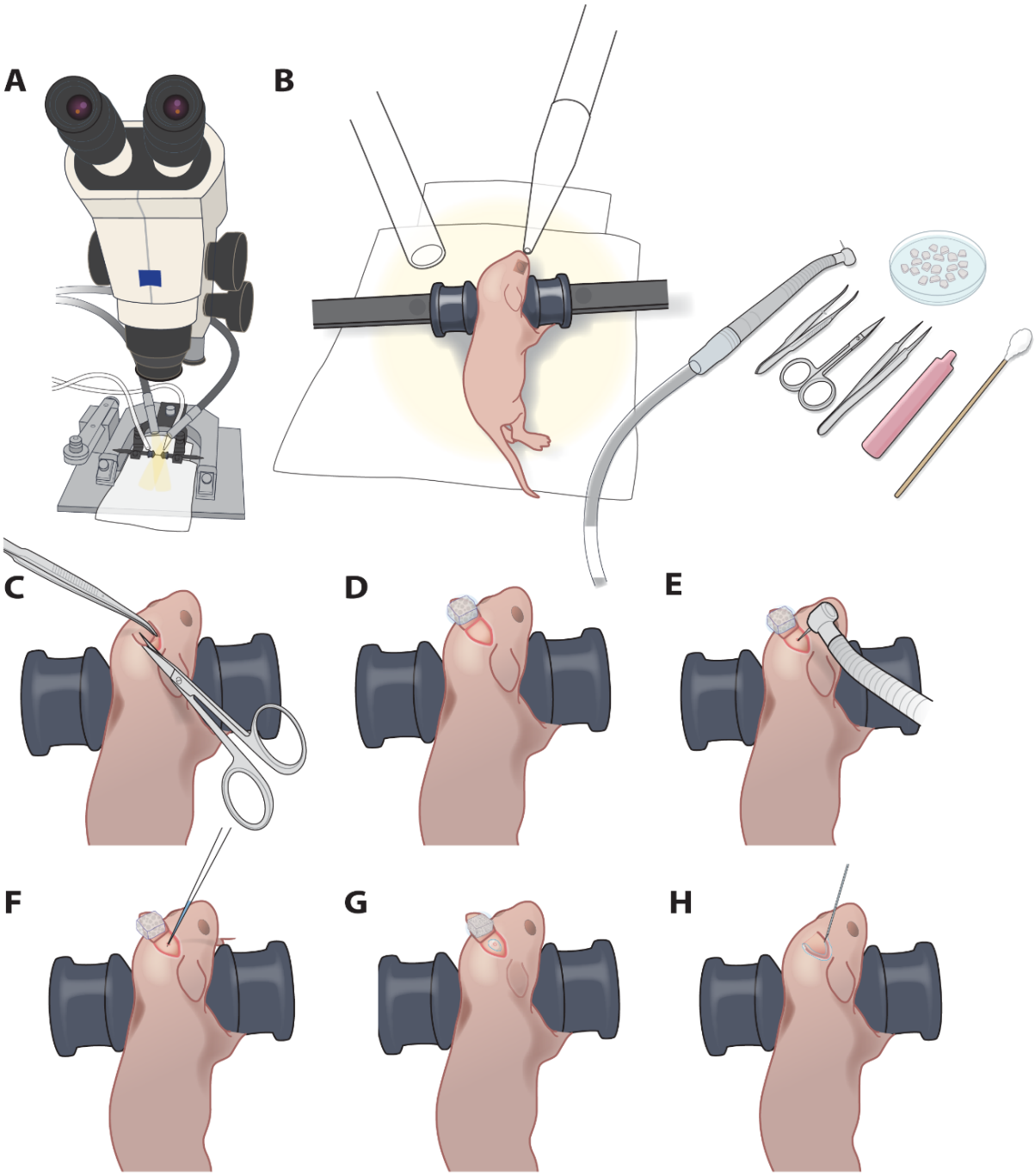

Figure 9: P1 injection setup and procedure

C. Dissecting microscope with goose-neck illumination.
D. Positioning of P1 pup with blunt ear bars, isoflurane delivery and exhaust tubes, pneumatic dental drill, forceps, iridectomy scissors, fine forceps, sterile saline vial, sterile cotton swab, and petri dish with Gelfoam sponges soaking in sterile saline.
E. Creating a 3-4 mm triangular skin flap over the desired injection area.
F. Folding back the skin flap and covering with wet Gelfoam to prevent the skin flap from drying out.
G. Light drilling of exposed skull to crack the bone slightly.
H. Injection of rAAV-GCaMP with glass micropipette.
I. Sealing of injection site with VetBond.
J. Sealing of skin flap with VetBond.

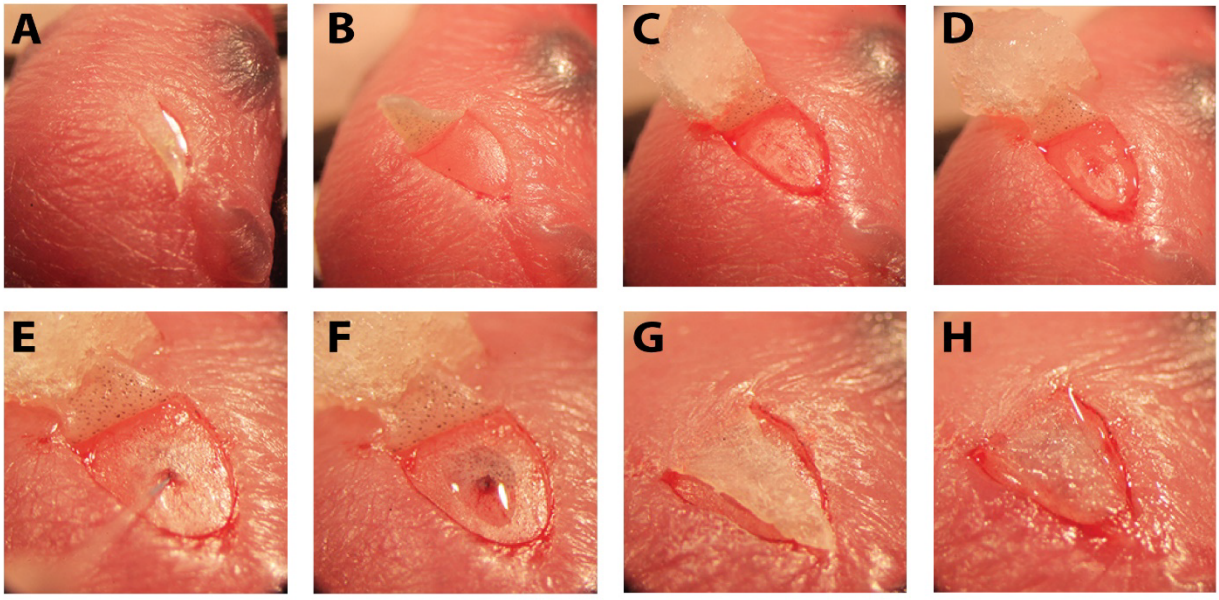

Figure 10: Surgical photographs of P1 injection procedure.

A. Creating a 3-4 mm triangular skin flap over the desired injection area.

B. Folding back the skin flap and covering with wet Gelfoam to prevent the skin flap from drying and shrinking.
C. Covering the skin flap with wet Gelfoam to prevent drying and shrinking; exposed skull is dry after light scraping with dental drill.
D. Small crack in skull after drilling.
E. Injection of rAAV-GCaMP with glass micropipette.
F. Sealing of injection site with VetBond.
G. Replacement of skin flap.
H. Sealing of skin flap with VetBond.

To confirm that neonatal GCaMP6 expression does not have cytotoxic effects on neurons, we used patch-clamp recordings in acute brain slices from two P16-17 pups that had been injected at P1, and two uninjected littermates at the same age, as previously described (Goel and Buonomano, 2016). We did not find statistically significant differences in either the input resistance (R_m) or the resting membrane potential (V_m) between GCaMP-expressing cells and cells from uninjected controls ($p= 0.51$ and $p=0.12$, respectively; unpaired rank-based comparisons with bootstrapping; n= 6 cells per group) **(Fig. 11**), suggesting that neonatal GCaMP expression does not have adverse effects on the neurons.

To assess the suitability of neonatal viral injections for investigating cortical circuits in early postnatal mice, I used *in vivo* two-photon calcium imaging to record neuronal activity. I specifically chose to perform an experiment that could not have been possible without neonatal viral injections. We and others have previously demonstrated that cortical network activity undergoes a major network transformation at around the 2nd postnatal week, such that neuronal activity becomes desynchronized (Golshani et al., 2009; Rochefort et al., 2009; Siegel et al., 2012;

Goncalves et al., 2013). However, those studies had recorded from different mice at different ages, so to this date, it had not been possible to record form an identified ensemble of neurons across time in a single animal. In order to achieve this, I injected three mice at P1 with rAAV-hSyn-GCaMP6s. Next, I permanently implanted glass-covered cranial windows at P10, following

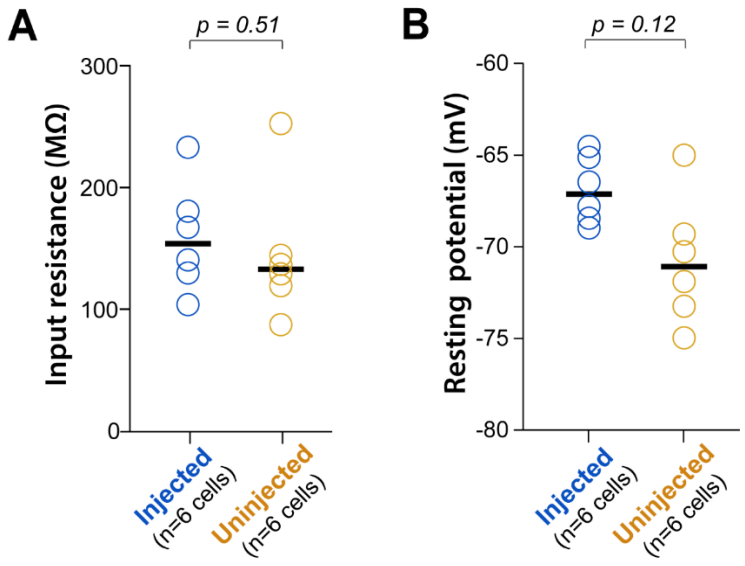

Figure 11: L2/3 neurons expressing GCaMP6s since P1 show normal electrophysiology.

A. Input resistance (R_m) during whole-cell recordings of L2/3 neurons from P16-17 mice injected with AAV-GCaMP6s at P1, or from uninjected littermates (n=2 mice each). Each circle represents data for one cell, bars represent group medians, and p-values are from unpaired rank-based two-group comparison with 10,000 resamples.

B. Resting membrane potential (V_m) for the same comparison.

protocols we have previously established (Portera-Cailliau et al., 2005; Cruz-Martín et al., 2010; Cruz-Martin et al., 2012). There are, however, important considerations when performing cranial

window implants in mice previously injected with rAAV at P1. For example, the P1 injection can cause scarring in the injected area, which can make the subsequent cranial window surgery more difficult and reduce experimental efficiency. Scarring can be minimized by the following considerations during the virus injection: 1) a rapid surgical procedure with carefully calibrated anesthesia levels; 2) gentle burr hole drilling (with the drill at a 45° angle to the skull) that produces only a small crack in the skull through which the glass pipette can be smoothly inserted, without any visible signs of bleeding; 3) careful cleaning of the periosteum prior to and after the injection to prevent granulation tissue from forming at the site of injection, which would otherwise soften the bone and make the cranial window surgery more difficult; 4) careful application of the minimal amount of VetBond to seal the drilled area and, separately, the skin edges so that the skull and skin are not glued to each other. Injections done at P2 or later will drastically increase the chances of scarring. If there is scarring, then the subsequent cranial window surgery may be much less successful, reducing the experimental success rate. In the **Table 2** in the **Methods** section, we also provide recommendations for ensuring that windows remain clear for repeated imaging in previously injected neonatal mice (**Fig. 12**).

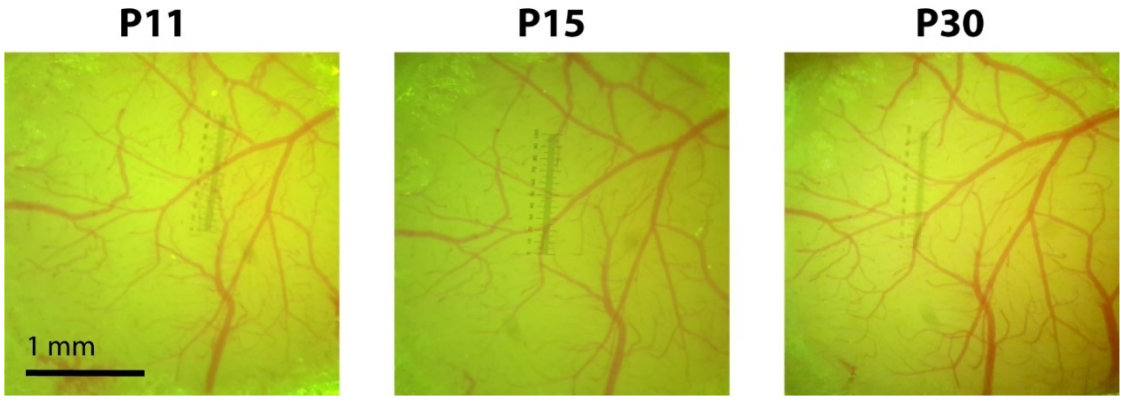

Figure 12: Cranial windows implanted at P10 remain optically transparent for weeks. Photographs of the cranial window at P11, P15, and P30 for a representative mouse injected with rAAV-GCaMP6s at P1.

In order to more easily identify the same ensemble of neurons over time (**Fig. 14A**), I used *in utero* electroporation to express Td-Tom in L2/3 neurons in S1 cortex (**Fig. 13**).

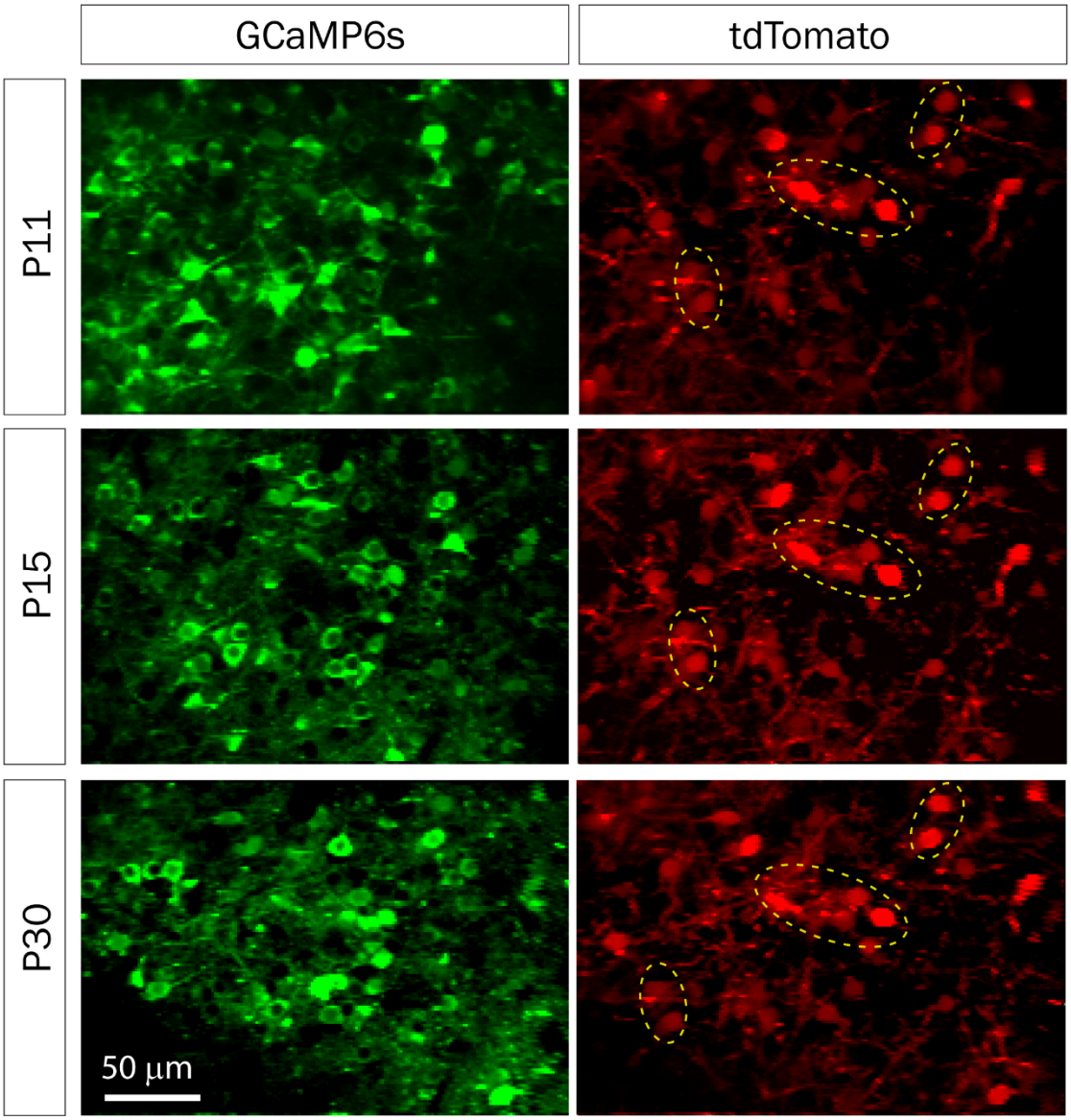

Figure 13: Td-Tomato expression to help identify same GCaMP6s field of view for calcium imaging.

Representative fields of view of GCaMP6s and Td-Tom expressing neurons in barrel cortex of a mouse at three different postnatal ages. This animal was electroporated *in utero* at E16 with a plasmid encoding the red fluorescent protein, Td-Tomato and then was injected with rAAV-

GCaMP6s at P1. Expression of Td-Tom allowed us to identify the same field of view throughout postnatal development because of stable expression of clusters of neurons in the red channel (yellow doted ellipses).

I performed *in vivo* calcium imaging of spontaneous network activity in slightly sedated, head-retrained mice from P11 to P30. At P11, L2/3 neurons in barrel cortex exhibit large but infrequent spontaneous calcium transients that are synchronous across the bulk of the neurons (**Fig. 14B**). These giant network depolarizations are the same early network oscillations that were originally described in acute cortical slices (Garaschuk et al., 2000) and *in vivo* (Golshani et al., 2009; Rochefort et al., 2009; Siegel et al., 2012; Goncalves et al., 2013). In contrast, by P15, activity has become largely desynchronized and this sparse firing of neurons prevailed at P30. To quantify the magnitude of this change in network behavior, I computed pairwise Pearson's correlation coefficients for all possible pairs of neurons that had been imaged at all 3 ages from their deconvolved calcium traces (**Fig. 14C, D**). The mean correlation coefficient of all cell pairs decreased significantly from 0.24 ± 0.01 at P11 to 0.06 ± 0.01 at P15 and 0.02 ± 0.01 at P30 (**Fig. 14D**).

I also recorded whisker-evoked activity at these same postnatal ages and observed clear whisker evoked activity as early as P15 (**Fig. 14E**). At P11, bursts of activity during ENOs were so broad (sometimes lasting several seconds) that it was not possible to determine whether neurons were indeed responding to tactile stimulation. I calculated the proportion of L2/3 neurons that responded to whisker stimulation in a time-locked fashion, as previously described (He et al., 2017) and found that the fraction of L2/3 neurons with activity that is time locked to the epochs of whisker stimulation appears to decrease from P15 to P30 (**Fig. 14H**).

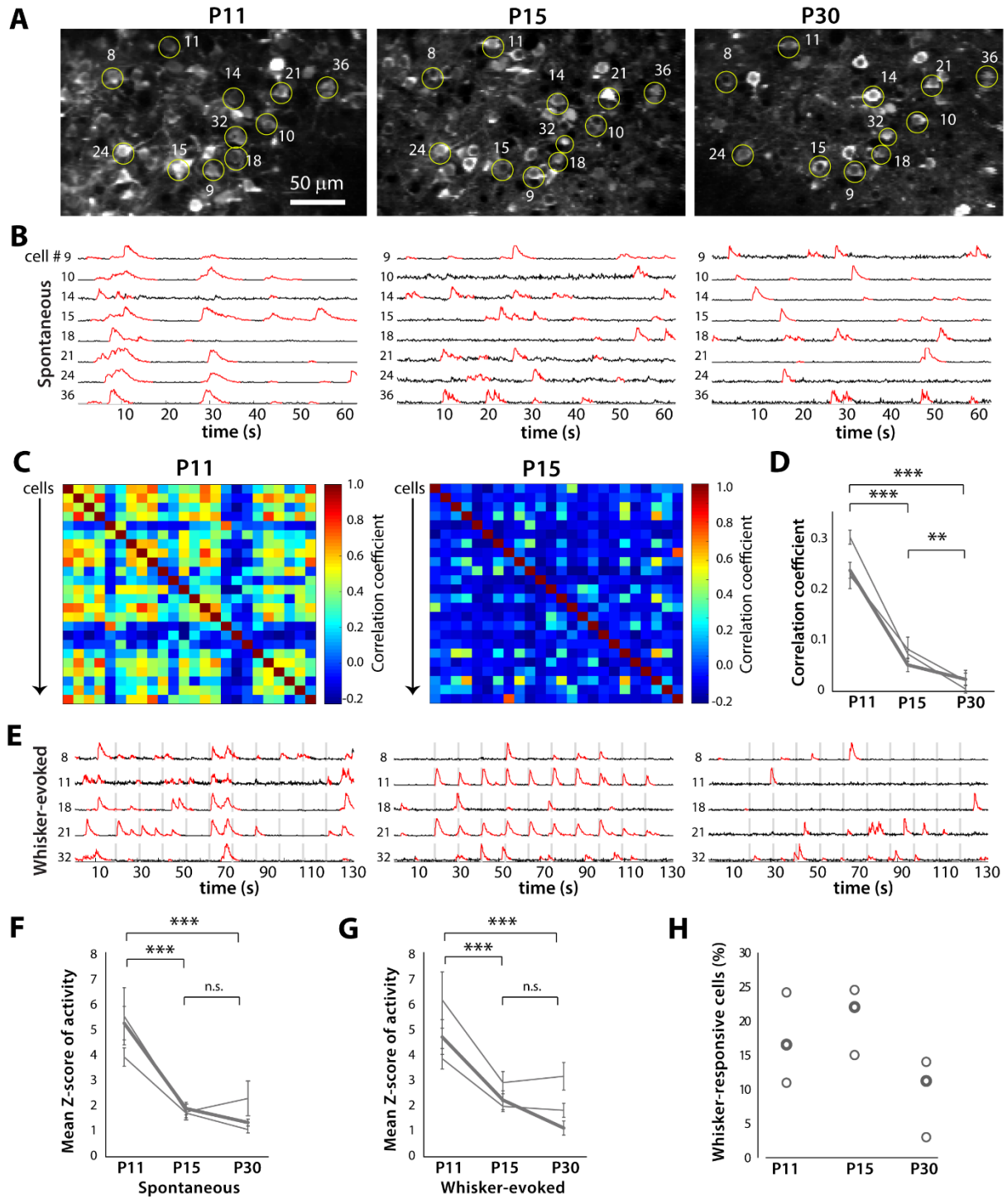

Figure 14: Developmental desynchronization of network activity in barrel cortex

A. Example field of view for a two-photon imaging recording of GCaMP6s-expressing layer (L) 2/3 neurons in barrel cortex from a representative *in vivo* experiment at P11, P15, and

P30 (*xyt* standard deviation projection of 1,040 consecutive frames at 7.8 Hz). Example cells that could be identified at all three ages are labeled by yellow circles and numbers. For some of these cells, the corresponding fluorescence calcium traces are shown in panels *B* and *E*.

B. Spontaneous activity ΔF/F calcium traces of 8 individual L2/3 neurons from the same field of view as in *A*, at P11, P15, and P30.
C. Correlation matrices displaying the correlation coefficients between the deconvolved calcium traces of all possible pairs of cells (n= 24) shown imaged in *A*.
D. Pair-wise correlation coefficients across developmental ages for 3 different mice. The bold line indicates data from the example recording shown in panels *A*-*C* and *E*). ** $p < 10^{-3}$, *** $p < 10^{-5}$.
E. Whisker-evoked activity ΔF/F calcium traces of 8 individual L2/3 neurons from the same field of view as in panel *A*, at P11, P15, and P30. Vertical gray bars represent epochs of whisker deflection (10 Hz, 1 s duration, 5 s i.s.i.)
F. Magnitude of spontaneous activity (as determined by average Z scores of calcium traces). In panels F & G, the bold line indicates data from the example recording shown in panels *A*-*C* and *E*. *** $p < 10^{-5}$.
G. Magnitude of whisker-evoked activity (average Z scores). *** $p < 10^{-5}$.
H. Percentage of all L2/3 neurons imaged whose activity was time-locked to epochs of whisker stimulation (see **Methods**) for all 3 mice (n= 296, 401 and 248 neurons respectively).

The neonatal viral injection approach also allowed us to record GCaMP6 signals in individual dendrites and dendritic spines of L2/3 neurons in early postnatal mice. I find that even by P15, individual dendritic spines display whisker-evoked activity (**Fig. 15**). Interestingly, amongst neighboring spines within the same dendritic shaft some exhibited whisker signals, while others did not. Hence, this approach will be useful to unravel the role of individual dendritic spines in local circuit computations during early postnatal development.

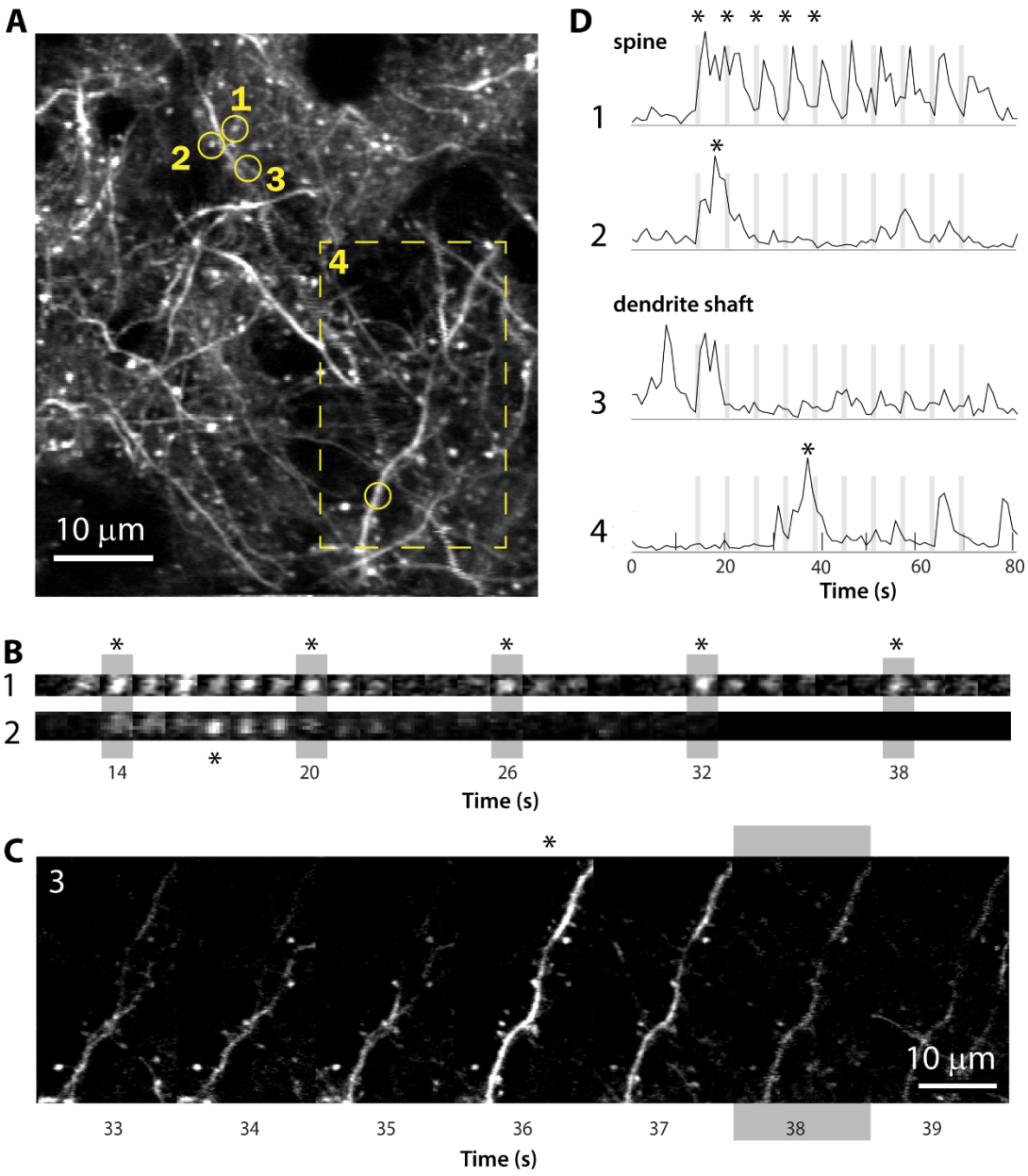

Figure 15: Imaging of GCaMP6s signals in dendritic spines of L2/3 neurons in barrel cortex at P15

A. Field of view of apical dendrites from a representative experiment in a P15 mouse injected at P1 with rAAV-GCaMP6s (*xyt* st-dev projection of 80 slices over ~80 sec). Time-lapse images of calcium recording of spines 1 and 2 (circles) and dendrite 4 (boxed region) are shown in *B* and *C*.

B. Time lapse imaging sequence of dendritic spines 1 and 2 shown in *A* over 5 consecutive whisker stimulations (vertical gray bars). Each image is one frame (0.98 Hz image acquisition). Asterisks for each spine in *B* correspond to those in panel *D*.

C. Time lapse imaging sequenced of the dendrite shown in *A* (box 4) over several seconds and a whisker stimulation (gray bar). Each image is one frame (0.98 Hz image acquisition). The asterisk above the time frame at 36 s corresponds to the asterisk in panel *D*.

D. ΔF/F traces for the calcium fluorescence signals for the dendritic spine and dendrite shaft regions of interest 1-4 shown in *A*, over 10 sequential whisker stimulations.

METHODS FOR CHAPTER 3

Detailed protocol for P1 injections:

Set-up

- Pipette preparation for injection: Pull a custom micropipette from a 1.5 mm outer diameter, 0.86 mm inner diameter glass capillary tube so that the length of the tapered tip is approximately 8 mm. Break pipette tip slightly by gently touching the tip to the side of sterilized forceps. The o.d. of the tip should be 12.5-25 μm. If the tip is too wide, the viral vector may reflux around the needle during the injection.
- Gelfoam preparation: Use sterilized scissors to cut small pieces of Gelfoam, approx. 1 x 1 mm. Soak them in a small petri dish filled with sterile saline.
- Surgical instruments: Sterilize instruments in a glass bead sterilizer and spray with ethanol before use.
- Heating blanket: Turn on the water recirculating heating blanket 15 min before start of each surgical procedure.

Step-by-Step Procedures:

rAAV injection at P1 (timing 15-20 min)

1) *Preoperative care:* Administer Carprofen (5 mg/kg BW, s.c.) to the mouse. Note: we do not use dexamethasone for the virus injection in newborn pups.

2) Anesthetize the mouse with 5% isoflurane for induction, followed by 1.5-2% isoflurane for maintenance (vol/vol, via nosecone).
3) Use blunt ear bars to position the mouse on the stereotax so that the desired injection area is as flat as possible (**Fig. 9B**). Ensure that the mouse pup remains warm (on the heating pad) throughout the procedure, and monitor breathing carefully, including tail and toe pinches. The ear bars should prevent movement of the pup during subsequent manipulations, without applying excessive pressure to its soft skull. Ensure that the heating blanket is functioning correctly. Note: Newborn pups can stop breathing suddenly, making close monitoring under anesthesia crucial.
4) Sterilize operating field using three alternating wipes of betadine and 70% alcohol.
5) Using the scissors, make one snip to create a 3-4 mm triangular skin flap over the desired injection area (**Fig. 9C, Fig. 10A**). Fold back the skin flap and cover it with a piece of saline-soaked Gelfoam to prevent the skin from drying (**Fig. 9D, Fig. 10B-C**).
6) Immediately apply a small drop of lidocaine/epinephrine onto the exposed skull. After 30 s, dry the surface of the skull with sterile cotton swab or dry Gelfoam.
7) Using the pneumatic dental drill, gently stroke the drill bit tip onto the skull surface to clear the periosteum. Use Gelfoam soaked in saline to clean the area of bone dust, then let the area dry. Note: do not push hard on the skull or the drill bit might pierce the bone and damage the dura/brain.
8) Once the exposed skull is clear of periosteum and dry, apply repeated light touches of the drill bit tip at the desired injection site until the bone has cracked enough to permit insertion of the glass micropipette (**Figs. 9E, Fig. 10D**). Clean up any bleeding with moist Gelfoam. Ideally, there should be no bleeding. Note: If a large hole in the skull is created during the drilling it

will likely delay healing and result in a larger scar, which will make the later cranial window surgery less successful. The animal will likely not be suitable for imaging.

9) Load glass micropipette with approximately 200 nL of rAAV-GCaMP (working titer 2E13) with FastGreen and position for injection at a 45^{o} angle to the skull surface.

10) Lower pipette until its tip has pierced through the cracked bone and into superficial cortex (**Figs. 9F, Fig. 10E**). Inject rAAV using the Picospritzer using approximately 30 puffs of 3-5 ms durations at 40 PSI. Leave the pipette in place for 15 s and then withdraw pipette. Note: If fluid comes out of the skull surface around the pipette after withdrawal, it is an indication that its tip was not sufficiently small. The animal will likely not be suitable for imaging.

11) Using a needle tip (e.g., 18-gauge), apply a very small drop of VetBond to the injection site (just enough to seal the cracked area but not enough to reach the skin edges) and let dry completely (**Figs. 9G, Fig. 10F**).

12) Replace the skin flap and seal the skin edges with a small amount of VetBond (**Figs. 9G, Fig. 10G-H**).

13) Allow VetBond to dry before placing mouse in warm recovery cage. After the mouse completely recovers from anesthesia, return it to the litter. Carefully monitor the dam to ensure reintegration of the post-operative pup(s). Minimize rearrangements of the litter in the cage to minimize stress on the dam and reduce the possibility of cannibalism. Placing a small cardboard shed in the cage can also reduce stress for the dam.

Cranial window procedure at P8-P10 (timing 45 min – 1 hr) (modified slightly from Cruz-Martín et al., 2010; Holtmaat et al., 2012)

1) Anesthetize the mouse with 5% isoflurane for induction, followed by 1.5-2% isoflurane for maintenance. Monitor anesthesia level throughout surgery by watching breathing, as well as using tail and toe pinches, and ensure that heating blanket is functioning correctly.
2) Use rodent trimmer to shave from the neck to the eyes, being careful not to trim any whiskers.
3) Use blunt ear bars to position mouse on stereotaxic frame, with anesthesia nose cone. The ear bars must be secured with just enough pressure such that the mouse's head does not shift during surgery. The skull is still soft at P10 and care must be taken not to excessively squeeze the skull between the bars, as this will affect respiratory rate.
4) Administer Carprofen (5 mg/kg BW, s.c.) and dexamethasone (0.2 mg/kg BW, s.c.).
5) The original injection site should be apparent as a well-healed triangular scar on the skin, not raised or inflamed. If a large plug of granulation tissue is present at the original injection site and the skin is attached to the skull underneath, there is likely an excessive amount of scarring that will preclude a successful window surgery. The animal will likely not be suitable for imaging.
6) Sterilize the skin with three alternating wipes of betadine and 70% alcohol.
7) Using the scissors, remove the skin on top of the skull, as well as the periosteum. Apply lidocaine/epinephrine to skin edges. After 30 s, dry the skull surface using cotton swabs.
8) Apply a small amount of cyanoacrylate glue to the skin edges, but do not apply glue over the bony sutures.
9) Use a pneumatic dental drill to very lightly carve a circular craniotomy, 3 mm in diameter. Apply lidocaine/epinephrine, let sit for 30 s, then dry skull. The skull at P10 is still very soft

and the bone near the original burr hole may be particularly brittle. Drilling should proceed with minimal pressure to reduce the chance of sudden penetration and excessive bleeding.

10) Continue to gently drill along a circular groove until bone has been cracked all around the perimeter of the craniotomy. Clean up any bleeding on the bone with Gelfoam. The drilling can stop when the skull at the center of the craniotomy gives way as one pushes gently on it with the dental drill tip.

11) Soak the entire drilled area with saline using Gelfoam for at least 1 min. Then use fine-tipped forceps to gently lift the skull flap. Use Gelfoam to wipe away any residual scar tissue from the original burr hole and injection. Note: Apply Gelfoam to stop any minor bleeding on the surface of the dura. Minimal bleeding at the edge of the window, if readily stopped with Gelfoam, will not impede imaging that same day. However, significant bleeding, bruising, or damage of the dura in the center of the window will preclude same-day imaging and, if severe, may also preclude subsequent imaging.

12) After the skull is removed use copious saline to irrigate the surface of the dura to remove bone dust. Note: If some bone dust remains, this will increase the chances of subsequent bone re-growth under the glass window.

13) While the dura is moist with saline, gently position a 3 mm glass coverslip over the craniotomy.

14) Hold the coverslip by applying gentle pressure on the center of the glass with the wooden end of a cotton swab (or with forceps) so that the glass is firmly resting against the bone edges. With the other hand, apply small drops of cyanoacrylate around the edges of the coverslip at two or three points, then drag it around the perimeter of the window. Cyanoacrylate should not seep under the glass and onto the dura. Let cyanoacrylate dry completely. Note: if some glue seeps under the glass, the animal will likely not be suitable for imaging.

15) Mix dental acrylic and apply over the entire skull surface around the window, sealing the edges of the coverslip. Use the same acrylic to secure a custom titanium headbar to an area of the head cap that will not interfere with the positioning of the microscope objective during *in vivo* imaging. The plane of the headbar should be parallel to that of the coverslip. Also use dental acrylic to make a small well around the window to hold water for the 20X immersion objective.
16) Allow the dental acrylic to cure for 5-10 minutes, and then move the mouse to a warm recovery cage. When the mouse has recovered from anesthesia completely, return to the litter. Monitor the dam closely to ensure the pups are safely reintegrated. Placing a cardboard shed in the cage can improve the dam's caretaking of pups.
17) The mouse can be imaged later the same day, as long as the dental acrylic on the head cap and head bar is fully cured.

Detailed materials list

- O_2 tank
- Artificial Tears eye lubricant ophthalmic ointment (Henry Schein, cat no. 048272)
- Sterile NaCl (Addipak, Teleflex cat no. 200-59)
- AAV vector encoding GCaMP (U. Penn virus core), diluted to 2E13 concentration with 1% Fast Green
- 70% ethanol (Sigma-Aldrich, cat no. R3154-1GA)
- Betadine (Purdue Products, NDC 67618-155-16)
- Sterile Gelfoam (absorbable gelatin sponge) (Ethicon, Devine Medical cat no. MED-ETH1975)
- Cyanoacrylate glue (Krazy Glue, Office Depot, cat no. 366490)

- Ortho-Jet dental acrylic powder and liquid (Lang Dental, cat nos. B1330 and 1306)

Drugs

- Lidocaine HCl 2% + epinephrine 1:200,000 (Fresenius-Kabl, cat no. 480927)
- Dexamethasone 2 mg/mL (Henry Schein, cat no. 002459)
- Carprofen (Rimadyl, 50 mg/ml, Pfiezer)
- Isoflurane (Henry Schein, cat no. 029405). Note: Procedures using isoflurane should be conducted in well-ventilated areas and should follow relevant animal care guidelines.

Equipment

- Glass capillary puller (Narashige, model PC-10)
- Glass capillaries, O.D. 1.5 mm, I.D. 0.86 mm (Sutter Instruments, cat no. BF150-86-10)
- Picospritzer injection device (Parker Hannifin, model Picospritzer III)
- Glass bead sterilizer (Fine Science Tools, cat no. 18000-45)
- Water recirculating heating blanket (Stryker, cat no. 8002-062-012) and pump (Gaymar, cat no. 07999-000)
- Rodent trimmer (Wahl, cat no. 9962-717)
- Dissecting microscope (Zeiss, model Stemi 2000)
- Gooseneck light source (Dolan-Jenner MI-150, Edmund Optics cat no. 59-236)
- Stereotaxic frame and mouse adaptor (Kopf, cat nos. 900 and 926)
- Anesthetic vaporizer (Surgivet Classic T3) with airflow meter (Porter, cat no. GL-616)
- Induction chamber (VetEquip, cat no. 941443)

- Pneumatic dental drill (Midwest Tradition, Henry Schein, cat no. 7726063) with FG ¼ carbide burr drill bits (Henry Schein, cat no. 100-7205)
- Dumont tweezers #4 and #5, straight dissecting scissors, 10 cm (World Precision Instruments cat nos. 500231, 14098, 14393)
- Small petri dish (35-mm diameter, Fisher, cat no. FB0875711YZ)
- Sterile cotton swabs (Henry Schein, cat no. 100-9175)
- Glass coverslips, 5 mm (Electron Microscopy Sciences, cat no. 72195-05)
- Needle tips, 18-gauge (BD, cat no. 305195)
- Titanium head bars (custom design: (0.125 x 0.375 x 0.05 inches)
- 2-photon microscope (custom built) (Cruz-Martín et al., 2010)
- Tunable Ti:Sapphire laser (Chameleon Ultra II, Coherent)
- Objectives, 4x (0.8 NA) and 20x (0.95 NA) water immersion (Olympus, UPLFLN 4x, XLUMPLFLN 20x)
- ScanImage (Pologruto et al., 2003)

Animals:

All experiments followed the U.S. National Institutes of Health guidelines for animal research, under an animal use protocol (ARC #2007-035) approved by the Chancellor's Animal Research Committee and Office for Animal Research Oversight at the University of California, Los Angeles. We used male and female FVB.129P2 WT mice (JAX line 004828) and C57/BL6J mice (HSD C57Bl/6NHsd) housed in a vivarium with a 12-h light-dark cycle. Experiments were performed

during the light cycle. Animals were weaned at P21-22 and afterward housed with up to five mice per cage. Before P21, pups were housed with their dam.

Reagents:

All reagents were obtained from Sigma unless otherwise specified. All viral vectors were obtained from the University of Pennsylvania Vector Core.

Virus injection at P1:

In **figures 9** and **10**, we provide detailed instructions for virus injections in newborn mice that have been optimized for targeting of GCaMP6s to L2/3 neurons of barrel cortex for *in vivo* two-photon calcium imaging of spontaneous and whisker-evoked activity starting in the 2nd postnatal week. Adjustments may be necessary for targeting deeper layers, different brain regions, or for injecting different viral serotypes. Minimizing tissue damage and the resulting inflammation is key for successful cranial window implantation and optimal window clarity within 10 days of viral injection.

The pCAG-tdTomato plasmid was introduced to layer (L) 2/3 precursor cortical neurons via *in utero* electroporation at E16. As we previously reported (He et al., 2017), for P1 injections we used rAAV (AAV1.Syn.GCaMP6s.WPRE.SV40) (Chen et al., 2013) diluted to a working titer of 2E13 together with 1% filtered Fast Green FCF dye (to visualize the spread of the injection). Pups were anesthetized with isoflurane (5% induction, 1.5-2% maintenance via a nose cone, vol/vol) and

positioned in a stereotaxic frame (Kopf model 900 with adaptor model 926) (**Fig. 10A-B**). After a subcutaneous injection of Carprofen (Rimadyl, Pfizer; 5 mg/kg) and scalp sterilization with betadine and 70% alcohol, a small (2-3 mm) skin flap was made over the somatosensory cortex (**Fig. 10C**). A dental drill was used to gently clear the periosteum under the skin flap. At the intended injection site, the bone was lightly drilled to the point of a slight crack without exposing the dura and without penetration by the drill (**Fig. 10E)**. A pulled glass micropipette (Sutter Instrument, 1.5 mm outer diameter, 0.86 mm inner diameter) was used to inject ~0.2 μL of rAAV at a depth of 0.2 mm below the dura, using a Picospritzer (General Valve) (**Fig. 10F**). After pipette removal, the injection site was cleaned gently with Gelfoam and sealed with VetBond (3M), and the skin flap was replaced and also sealed with VetBond (**Fig. 10H**). After full recovery on a warm water circulation blanket, the pup was returned to the dam.

Electrophysiology:

The brains were quickly removed and transferred to ice-cold artificial CSF (ACSF) containing (in mM): 119 NaCl, 2.5 KCl, 1.3 MgSO4, 1 NaH2PO4, 2.5 CaCl2, 26.2 NaHCO3, and 10 dextrose, bubbled with oxygenated 95% O2 / 5% CO2 to a final pH of 7.4. Acute coronal brain slices (300μm) through the barrel cortex were cut on a vibratome (Leica VT1000S). The acute slices were incubated at 37°C in oxygenated ACSF for 1 hour and then placed on a chamber maintained at 35–37°C on the stage of an upright Olympus BX51 microscope. Slices were submerged in ACSF, perfused at a rate of 2-4 ml/min, and bubbled with 95% O2 / 5% CO2. L2/3 pyramidal neurons were identified using differential interference contrast optics with a 60X 0.8 NA water immersion objective (Olympus). Cells were patched for 15-30 min and recordings were performed

using whole-cell patch-clamp technique in current clamp configuration (Axon Instruments, Multiclamp 700B). Series resistances were manually compensated for standard patch pipettes (6–9 MΩ tip resistance) pulled on a Brown/Flaming microelectrode puller (Sutter Instruments, model P-97). Pipettes were filled with an intracellular solution containing (in mM): 130 K-gluconate, 5 KCL, 2 MgCl2, 10 HEPES, 4 Mg-ATP, 0.3 Na-GTP, 10 phosphocreatine, and 2 Alexa-488, adjusted to a final pH of 7.3. The ACSF solution in which slices were maintained was consistent between recordings with the exception of the [KCl], which ranged from 1.25 mM to 5 mM. The input resistance (R_m) or membrane potential (V_m) did not change more than 10% during the course of recording for each cell. All electrophysiological recordings were sampled at 10 kHz, digitized with custom written MATLAB software controlling an A-D board (National Instruments, PCI-6723), and saved for off-line analysis. All analyses were performed using custom-written software in MATLAB.

Cranial window surgery:

We followed a protocol that we have described extensively in previous publications (Cruz-Martin et al., 2010; Cruz-Martin and Portera-Cailliau, 2010; Mostany and Portera-Cailliau, 2008). Briefly, pups (P10-12) were anesthetized with isoflurane (5% induction, 1.5-2% maintenance vol/vol) and placed in a stereotaxic frame. A 2.5 mm diameter craniotomy was performed over the injected barrel cortex in one hemisphere and covered with a 3 mm glass coverslip (Electron Microscopy Sciences). The coverslip was secured to the skull with Krazy Glue and dental cement. A headbar was attached to the skull with dental cement in order to secure the animal to the microscope stage for imaging.

***In utero* electroporation:**

In utero electroporation was performed as previously reported (Cruz-Martín et al., 2010; Cruz-Martin et al., 2012). In short, pregnant female mice at gestation day E16 were anesthetized with isoflurane (5% induction, 1.5-2% maintenance vol/vol). A medial incision along the abdomen was made exposing the abdominal cavity. The uterine horns were gently exposed and each embryo was pressure injected with a plasmid encoding pCAG-tdTomato (500ng/μl) in the left lateral ventricle with a Picospritzer. A set of 3 square pulses (50 ms duration, 35 V with 500 ms between each pulse) was administered to each embryo via a custom-built electroporator with the positive electrode paddle placed over the left somatosensory cortex. Throughout the procedure, the embryos were frequently irrigated with warm saline (37ºC). The embryos were placed back inside the mother and the dam's abdominal wall was sutured with absorbable sutures (muscle) and nylon sutures (skin).

Optical Intrinsic Signal (OIS) imaging:

After the cranial window placement, OIS imaging was used at P16 to obtain whisker-responsive maps and confirm appropriate targeting of rAAV injection to the barrel cortex. Following a protocol previously described (Johnston et al., 2012), the contralateral whisker bundle was attached using bone wax to a glass needle coupled to a piezo-actuator (Physik Instrumente). Each whisker stimulation trial consisted of a 100 Hz sawtooth stimulation lasting 1.5 s. In order to delineate the cortical representation of whisker stimulation, the response signal was divided by the averaged baseline signal, summed for all trials, then thresholded at 50% of maximum response.

OIS signal intensities were used solely for localization during calcium imaging and were not compared between animals.

***In vivo* two-photon calcium imaging in head-restrained mice :**

Calcium imaging was performed on a custom-built two-photon microscope, with a Chameleon Ultra II Ti:Sapphire laser (Coherent), a 20X objective (0.95 NA, Olympus), and ScanImage software (Pologruto et al., 2003). Mice were lightly sedated with chlorprothixene (2 mg/kg, i.p.) and isoflurane (0-0.5%), and kept warm with an electric heating blanket (Harvard Apparatus). Isoflurane was manually adjusted to maintain a breathing rate ranging from 100-150 breaths/min for P11-16 mice. Both spontaneous activity and whisker-evoked barrel cortex activity were recorded in the same mice at three postnatal ages, P11, P15 and P30. Whisker stimulation was delivered by bundling the contralateral whiskers (typically all macrovibrissae of at least ~1 cm in length) to a glass needle coupled to a piezo-actuator with soft bone wax. Whiskers were stimulated for 1 s at 10 Hz with 5 s interstimulus intervals (i.s.i.), for a total of 10 stimuli (**Fig. 14**) or with an i.s.i. of 5 s (**Fig. 15**). Whole-field images were acquired at 7.8 Hz (1024 x 128 pixels down-sampled to 256 x 128 pixels) for **Fig. 14** and 0.98 Hz for **Fig. 15** (512 x 512 pixels). Spontaneous activity recordings lasted 60 s.

Data analysis for calcium imaging:

Calcium-imaging data were analyzed using custom-written MATLAB routines, as described (He et al., 2017). All relevant data and MATLAB code are available upon request to the authors. X-Y drift in the movies was corrected using a cross-correlation-based, non-rigid alignment algorithm

(Mineault et al., 2016). The choice of registration algorithm did not affect the data analysis, since the fluorescence data for each neuron was always normalized to its own baseline. A semi-automated algorithm (Chen et al., 2013) was used to select regions of interest, each representing a single cell body, and extract the fluorescence signal ($\Delta F/F$) for each neuron. A "modified Z-score" Z_F time series for each neuron was calculated as

$$Z\_F(t) = \frac{F(t) - mean(quietest\ period)}{std(quietest\ period)}$$

where the quietest period is the 10 s period with the lowest variation (standard deviation) in $\Delta F/F$. All subsequent analyses were performed using the Z_F(t) time series.

For analysis of aggregate activity within a particular time range, as in **Fig. 14**, the mean of Z_F (t) within that time range was calculated for each ROI, and for each animal imaged, these means were compared across P11, P15, and P30. Only cells that had at least one calcium transient during the recording at all three postnatal ages were analyzed. To define whether an individual cell was "whisker-responsive," i.e., showed time-locked responses to whisker stimulations (**Fig. 14 C, F)** we used a probabilistic bootstrapping method, wherein we compared correlations between the stimulus time-course vs. the Z_F time series with correlations between the stimulus time-course and 1,000 scrambles of all calcium activity epochs in Z_F(t) (epoch = consecutive frames wherein Z_F(t) $\geq$ 3), as was previously described (He et al., 2017).

Statistical analyses:

Graphs in **Fig. 14** show data from neurons that were active across all time points P11, P15 and P30. For each ROI the Z_F(t) averages were calculated. To calculate statistical significance,

Friedman's two-way analysis of variance (ANOVA) by ranks for related samples was used with post-hoc pairwise comparisons corrected with Bonferroni adjustments. Pearson's correlations were determined using custom MATLAB code and Friedman's two-way ANOVAs by ranks were determined using SPSS 24 software (IBM). Graphs in **Fig. 14** show all data points, as well as group medians. Based on the group sizes of n=6, we used unpaired rank-based comparisons with bootstrapping (10,000 resamples), implemented using custom-written R code. Two-sided p-values were calculated, and the threshold for significance was set at $p<0.05$.

Table 2: Troubleshooting for P1 injection and P10-13 cranial window

Problem	**Possible reason**	**Solution**
Mouse is moving	Insufficient anesthesia	1. Check that isoflurane delivery system: Check all tubing, valves, vaporizer settings. 2. Ensure nose cone immediately adjacent to or covering the nose. 3. Check that ear bars are not too tight and uncomfortable for the animal. 4. Increase maintenance anesthesia to 2.5% 5. If mouse is still moving, remove the mouse from the stereotax and re-induce at 5%, then reposition on stereotax.
Mouse gasping or dies during surgery	Excessive anesthesia, hypothermia, or excessive cranial pressure.	1. Adjust isoflurane level to ensure that mouse is still breathing regularly, though slowly, during surgery, and without response to toe or tail pinches. 2. Keep duration of surgery (anesthesia time) under 20 min. 3. Ensure that heating blanket temperature is appropriate. 4. Check that ear bars are not too tight. Skull should be immobile but only barely bulging between the ear bars.
Bleeding during drilling	Damaged blood vessels, or the drill bit punctured the dura.	1. Apply wet Gelfoam to the drilled area and let sit for 30-60 s. If bleeding stops, then proceed with surgery. If bleeding does not stop, irrigate with sterile saline and then apply wet Gelfoam. 2. If the drill bit has clearly punctured through the skull and into the dura, terminate the experiment.

Vector does not exit the pipette tip	The pipette is clogged	1. Increase the Picospritzer pulse duration and apply a single larger pulse of pressure to try and unclog the pipette; then proceed with the injection at lower duration. 2. If the pipette tip remains clogged, retract the pipette and switch to a new pipette.
rAAV solution refluxes around pipette tip emerges from burr hole	The pipette tip is too wide	1. Avoid using pipettes with a large tip diameter; Use minimal pressure to break the pipette tip or by gently touching to moistened Kimwipe. 2. Reduce the Picospritzer pulse duration and increase the pause time between pulses (i.e., reduce the volume injected per pulse), to allow time for the injected solution to be absorb around the pipette tip. 3. After injection is complete and the pipette is retracted, use wet Gelfoam to thoroughly clean the skull surface before applying VetBond.
Skin at injection site has adhered to the skull (excessive scarring)	Removal of too much bone, excessive VetBond application, or skin flap replacement before VetBond on skull was dry	1. If the skin at the injection site is adhered to the skull, a good cranial window surgery can still be performed (i.e., the dura and skull may not be adhered). 2. If the skull flap cannot be lifted due to adhesion, terminate the surgery.
Bleeding occurs upon bone flap removal	Blood vessel damage or dura damage	1. Apply Gelfoam soaked in saline to the drilled area and let it sit for 30 s. If bleeding stops, proceed with surgery. If bleeding does not stop, irrigate with sterile saline and then apply wet Gelfoam. 2. If the drill bit has clearly punctured through the dura, or if the bone flap has ripped the dura, terminate the surgery.

Chapter 4

Discussion

Early intervention with bumetanide shows potential for a long-term rescue of network-level sensory dysfunction in FXS mice

Many of the synaptic perturbations, either functional or morphological, that have been described in the sensory cortex of *Fmr1* KO mice are present only during the first two post-natal weeks and seem to normalize as mice mature (Nimchinsky et al., 2001; Cruz-Martín et al., 2010; Harlow et al., 2010). However, circuit level defects and abnormal sensory-related behaviors persist in adult mutant mice (Arnett et al., 2014; Zhang et al., 2014; He et al., 2017). It has been speculated that the correct timing of the development of synapses during a critical period is required for the refinement of the circuit early in development (Meredith, 2015). However, this has not been formally tested. Therefore, I tested whether correction of the developmental profile of synapses by manipulation of inhibition during the first two post-natal weeks was sufficient to restore the circuit alteration in mature cortex of *Fmr1* KO mice. Specifically, I tested the drug bumetanide, a NKCC1 inhibitor that can reverse the delayed switch in GABA polarity that is seen in *Fmr1* KO mice. I chose bumetanide because it is an FDA approved drug (diuretic) that crosses the blood brain barrier and because it shows promise for treating symptoms in children with ASD (Hadjikhani et al., 2018). I found that administration of bumetanide to young adult *Fmr1* KO mice limited to this time frame was sufficient to correct the enlarged whisker-evoked maps in the barrel cortex, which could have therapeutic implications for the symptom of sensory hypersensitivity and tactile defensiveness. It is important to note that the intrinsic optical signal is the integration of many different responses of cortical neurons and interneurons. Therefore, the normalization of the map size and intensity suggests that the overall cortical response is corrected by bumetanide administered during a critical period. This provides strong evidence that correcting synaptic maturation during development can have long lasting effects on the function of the circuit and

supports the idea that the correct temporal refinement of synapses during early vulnerable periods is important to the correct function of the adult circuit. Prior work that has targeted metalloproteinases with minocycline to rescue dendritic spine development have also found that treatment during early development produces a long lasting improvement in some behaviors in *Fmr1* KO mice, further demonstrating the importance of early intervention (Dansie et al., 2013).

Excitatory neurons in the somatosensory cortex of FXS are insensitive to sensory stimuli

I set out to investigate whether L2/3 dendritic spines of *Fmr1* KO mice are affected by novel sensory experience at a time during early post-natal brain development when sensory information must begin to guide the behavior in terms of navigation, object recognition, social interaction and sensorimotor function. This was an important question because, previously, *in vivo* imaging studies of synaptic plasticity had focused only on sensory deprivation, which is not something that happens during typical brain development. I used a very brief period (8-10 hours) of EE at P14. Our main findings are that: 1. Spine density is normal in *Fmr1* KO mice; 2. The density and size of axonal EPBs are not different between genotypes and are unaltered by EE and; 3. EE leads to a significant increase in spine density in WT mice, due to an increase in the rate of spine formation; and 4. Dendritic spines of *Fmr1* KO mice are insensitive to EE.

The fact that spine density was normal in the somatosensory cortex of *Fmr1* KO mice is in line with several other *in vivo* imaging studies (Cruz-Martin 2010, Pan 2010, Padmashri 2013), and helps support once again the notion that prior reports of higher spine density in mutant mice from fixed tissue studies may have been due to sampling bias or selective effects of the Golgi method (He & Portera-Cailliau, Neuroscience 2013).

Even though some FMRP is also expressed presynaptically, I found that axon EPB density and volume in L2/3 neurons of *Fmr1* KO and WT mice were comparable. This could mean that, because of the relative abundance of FMRP in dendrites (compared to axons), dendritic spines are selectively affected by its absence in *Fmr1* KO mice. However, because of much lower density of EPBs compared to spines, it is conceivable that with a greater sample size (i.e., more mice), I might have detected differences in EPBs in *Fmr1* KO mice. Indeed, during normal aging, *in vivo* imaging studies have revealed significant changes in spine density but not in EPB density (Mostany 2013), which again could be due to the smaller sample size.

Our previous work shows that between P10-12, L2/3 spine lengths in the barrel cortex in *Fmr1* KO animals are comparable to that of WT mice, but that overall, spine length decreases from P7-8 to P21-24 (Cruz-Martin 2010). Spine density was determined to be around 0.35 spine /μm at P10-12 but increases to ~1.0 /μm by P21-24. Here, I show that by P14, spine density nearly doubles from that of P10-12, reaching 0.68 spines /μm in WT and 0.65 /μm in *Fmr1* KO mice. Because *Fmr1* KO spines are slightly longer than in WT at P14, but not P10-12 or P21-24, this rapid increase in spine density in *Fmr1* KO neurons is due to generation of protrusions that appear more morphologically immature.

The most significant and novel findings of our study are that a novel sensory experience leads to new spines being added onto dendrites of L2/3 neurons in WT mice, but not in *Fmr1* KO mice. A previous *in vivo* imaging study found that a period of EE for 2 days in 1 month old WT mice led to a near doubling of spine formation (Yang et al., 2009), which is in line with our findings. Our study is the first, however, to demonstrate that this effect of EE is already apparent during the

critical period of L2/3 in barrel cortex development (P14) and requires only 8-10 h of novel experience. A 6% increase in spine density may seem rather modest at first glance, but consider the impact of similar daily increases over a 1 week or 2-week period. The Yang et. al (2009) study showed that experience-induced spines persisted longer than spines formed during SE, indicating that they were permanently incorporated into the circuit. Similarly, I found that spine density significantly increased, albeit modestly after EE, suggesting that newly added spines are retained. The fact that spines are added in response to new sensory inputs in early postnatal development is a critical step in circuit wiring in the cortex. Indeed, the fact the inability of spines in *Fmr1* KO mice to respond to novel sensory experiences may be a fundamental mechanism for circuit dysfunction in FXS.

Our finding that spines in 2 week-old *Fmr1* KO mice are insensitive to novel sensory experience is reminiscent of results in motor cortex of adult *Fmr1* KO mice, where spines do not respond to motor learning (Padmashri et al., 2013). This fits our theory that a central defect of dendritic spines in FXS is their lack of plasticity (He & Portera-Cailliau, 2013). I do not rule out the possibility that the defect is simply a delay in their responsivity to EE, and that if I had extended the period of EE, *Fmr1* KO mice would have shown an increase in spine density. There is evidence that the increased abundance of immature spines in L2/3 neurons is rescued when *Fmr1* KO mice reared in EE (Restivo 2005, Nagaoka 2016). However, in that fixed tissue study, the authors did not appreciate changes in spine density as a result of EE, and they were not able to assess spine dynamics.

In the future, it will be important to determine the functional impact of spine gains due to sensory experience. For example, using *in vivo* two-photon calcium imaging in single spines, one could test whether newly added spines in barrel cortex also have larger whisker-evoked signals in WT mice. Thus, the protocol I developed for rAAV-dependent expression of the indicator GCaMP6s in neonatal brain will be a significant resource for those experiments (see below). It is also fair to assume that our EE paradigm would yield similar synaptic gains in other brain regions, including visual or auditory cortex, as well as motor cortex, but that *Fmr1* KO mice would not show those changes. Because EE-induced improvements in synaptic and behavioral abnormalities have been shown in other models of autism (Lonetti 2010, Yamaguchi 2017), I believe our results have broad implications regarding the effects of EE in autism.

Our protocol detailing a method for imaging activity in early post-natal mice is ideally suited to implement for follow-up experiments to the L 2/3 spine data presented in **Chapter 2**. Given that spines are insensitive to environmental enrichment in FXS mice at P14, I would expect to see a functional correlate of spine insensitivity to whisker stimulus. Pairing whisker stimulation with L2/3 GCaMP6s imaging of spines in the barrel cortex will be an important set of experiments to link structural dynamics to functional responsivity. I would hypothesize that similar to the maladaptive responses in shown in L2/3 somata (He et al., 2017), calcium transients in spines might also show lack of adaptation following repeated stimuli trains. But how spine individual spine structures might change in response to repeated stimuli may be more nuanced given their dynamic nature.

Caveats for calcium imaging of spines

In the spirit of full disclosure, I would like to end by highlighting some specific challenges of GCaMP6s spine imaging in early post-natal mice and offer and tips to mitigate the effect of these obstacles:

- The first challenge is that introduction of an additional fluorescent marker is crucial for finding the same dendrites for longitudinal studies, otherwise locating the same dendrite relies on activity and is akin to finding a needle in a field of haystacks. A suitable fluorescent marker for structural imaging that is spectrally distinct from GCaMP6s is tdTomato. A couple advantages of tdTomato are its brightness and resistance to photobleaching. However, because tdTomato emitted fluorescence is so bright, it can cause 'bleed-though' in the green channel, especially since in practice, GCaMP6s requires higher laser power. Therefore, I would recommend obtaining high quality filters to minimize this effect. An alternate approach would be to use a red-shifted calcium indicator such as jR-GECO and a green fluorescent protein to label dendritic structures.

- Another, perhaps more significant challenge, is that imaging activity is done so on a single plane of focus and finding a dendrite completely parallel to the imaging plane can be difficult, especially for longitudinal studies. When imaging cell bodies, the focal plane has a minimal effect given that their diameter is ~25 μm. Dendritic spines, however, range in length from about 0.5 μm to 4 μm, so finding the same imaging plane is essential for longitudinal studies. Because the brain undergoes rapid enlargement during the first few post-natal weeks, this can hinder the chances of locating the same dendritic segment over

repeated imaging sessions. For chronic imaging over a single session, I recommend keeping the animal on the imaging rig for the duration of the imaging protocol, as long as the imaging period does not exceed more than 3 h. Removal from the rig will likely lead to small, but significant variations of the imaging focal plane.

- At P14, the skull is still slightly soft, so securing the head completely is not feasible. Unfortunately, small movements elicited by arousal or gasping can affect the imaging plane. I recommend using low levels of isoflurane (~0.5%) in conjunction with chlorprothixene (see **Chapter 3 METHODS**) to help reduce motion of the animal without affecting the excitability of neurons (which occurs with higher levels of isoflurane, unpublished observations). Importantly, dams become anxious when 1.) mouse pups have been removed from the home cage for extended periods of time (especially pups that have been operated on) and 2.) when pups aren't fully alert, so full recovery from chlorprothixene is critical to minimize cannibalism. Recovery generally takes a minimum of several hours.

Future directions

One of the challenges of early post-natal studies is the lack of behavioral paradigms. Learning and memory tasks can take days to weeks in adult mice, which is not an option for mice at younger ages. As discussed in the *Introduction*, our lab recently demonstrated differences in tactile defensiveness in early postnatal *Fmr1* KO mice. *Fmr1* KO mice appear to actively avoid whisker stimuli by turning away more so than WT mice. To address whether or not spine dynamic

dysregulation contributes to sensory overreactivity one could perform structural imaging of spines of L2/3 neurons before and after short-term EE and measure tactile defensive behavior in the same mice. If errors in spine dynamics modulation underpin sensory over-reactivity, I would expect to see a positive relationship between spine insensitivity to EE and aversive behavior. Furthermore, if GCaMP6s imaging of cell bodies was also performed in the same mice, links between spine dynamics, cell activity of microcircuits and behavior could be revealed, which is the next step in parsing apart how sensory information processing deficits impact sensory hypersensitivity. Similar sophisticated experiments illustrate the potential power of future studies but require initial phenotypic discovery in young post-natal mice for initial experimental design. The work presented in this thesis along with other studies from our lab are the first to use chronic two-photon microscopy to elucidate possible sensory-related cortical disruptions in early post-natal *Fmr1* KO mice.

References

Abekhoukh S, Bardoni B (2014) CYFIP family proteins between autism and intellectual disability: links with Fragile X syndrome. Front Cell Neurosci 8:81 Available at: http://www.pubmedcentral.nih.gov/articlerender.fcgi?artid=3973919&tool=pmcentrez&rendertype=abstract [Accessed May 30, 2014].

Adusei DC, Pacey LKK, Chen D, Hampson DR (2010) Early developmental alterations in GABAergic protein expression in fragile X knockout mice. Neuropharmacology 59:167–171 Available at: https://www.sciencedirect.com/science/article/pii/S002839081000119X?via%3Dihub [Accessed May 18, 2018].

Akins MR, Berk-Rauch HE, Fallon JR (2009) Presynaptic translation: stepping out of the postsynaptic shadow. Front Neural Circuits 3:17 Available at: http://www.pubmedcentral.nih.gov/articlerender.fcgi?artid=2776480&tool=pmcentrez&rendertype=abstract [Accessed November 16, 2014].

Arakawa H, Erzurumlu RS (2015) Role of whiskers in sensorimotor development of C57BL/6 mice. Behav Brain Res 287:146–155 Available at: http://www.ncbi.nlm.nih.gov/pubmed/25823761 [Accessed April 18, 2018].

Arnett MT, Herman DH, McGee AW (2014) Deficits in tactile learning in a mouse model of fragile x syndrome. PLoS One 9.

Bailey DB, Berry-Kravis E, Wheeler A, Raspa M, Merrien F, Ricart J, Koumaras B, Rosenkranz G, Tomlinson M, von Raison F, Apostol G, Apostol G (2016) Mavoglurant in adolescents with fragile X syndrome: analysis of Clinical Global Impression-Improvement source data from a double-blind therapeutic study followed by an open-label, long-term extension study. J Neurodev Disord 8:1 Available at: http://www.ncbi.nlm.nih.gov/pubmed/26855682 [Accessed May 18, 2018].

Bailey DB, Raspa M, Olmsted M, Holiday DB (2008) Co-occurring conditions associated with *FMR1* gene variations: Findings from a national parent survey. Am J Med Genet Part A 146A:2060–2069 Available at: http://www.ncbi.nlm.nih.gov/pubmed/18570292 [Accessed

May 9, 2018].

Baranek GT, Roberts JE, David FJ, Sideris J, Mirrett PL, Hatton DD, Bailey DB (2008) Developmental trajectories and correlates of sensory processing in young boys with fragile X syndrome. Phys Occup Ther Pediatr 28:79–98 Available at: http://www.ncbi.nlm.nih.gov/pubmed/18399048 [Accessed May 9, 2018].

Bassell GJ, Warren ST (2008) Fragile X syndrome: loss of local mRNA regulation alters synaptic development and function. Neuron 60:201–214 Available at: http://www.ncbi.nlm.nih.gov/entrez/query.fcgi?cmd=Retrieve&db=PubMed&dopt=Citation&list_uids=18957214.

Bear MF, Huber KM, Warren ST (2004) The mGluR theory of fragile X mental retardation. Trends Neurosci 27:370–377 Available at: http://www.ncbi.nlm.nih.gov/entrez/query.fcgi?cmd=Retrieve&db=PubMed&dopt=Citation&list_uids=15219735.

Begum MR, Sng JCG (2017) Molecular mechanisms of experience-dependent maturation in cortical GABAergic inhibition. J Neurochem 142:649–661 Available at: http://www.ncbi.nlm.nih.gov/pubmed/28628196 [Accessed May 17, 2018].

Belmonte MK, Bourgeron T (2006) Fragile X syndrome and autism at the intersection of genetic and neural networks. Nat Neurosci 9:1221–1225 Available at: http://www.nature.com/articles/nn1765 [Accessed May 18, 2018].

Belmonte MK, Cook Jr. EH, Anderson GM, Rubenstein JL, Greenough WT, Beckel-Mitchener A, Courchesne E, Boulanger LM, Powell SB, Levitt PR, Perry EK, Jiang YH, DeLorey TM, Tierney E (2004) Autism as a disorder of neural information processing: directions for research and targets for therapy. Mol Psychiatry 9:646–663 Available at: http://www.ncbi.nlm.nih.gov/pubmed/15037868.

Ben-Ari Y, Gaiarsa J-L, Tyzio R, Khazipov R (2007) GABA: A Pioneer Transmitter That Excites Immature Neurons and Generates Primitive Oscillations. Physiol Rev 87:1215–1284 Available at: http://www.ncbi.nlm.nih.gov/pubmed/17928584 [Accessed May 8,

2018].

Ben-Sasson A, Hen L, Fluss R, Cermak SA, Engel-Yeger B, Gal E (2009) A Meta-Analysis of Sensory Modulation Symptoms in Individuals with Autism Spectrum Disorders. J Autism Dev Disord 39:1–11 Available at: http://link.springer.com/10.1007/s10803-008-0593-3 [Accessed May 18, 2018].

Berry-Kravis EM, Hessl D, Rathmell B, Zarevics P, Cherubini M, Walton-Bowen K, Mu Y, Nguyen D V, Gonzalez-Heydrich J, Wang PP, Carpenter RL, Bear MF, Hagerman RJ (2012) Effects of STX209 (arbaclofen) on neurobehavioral function in children and adults with fragile X syndrome: a randomized, controlled, phase 2 trial. Sci Transl Med 4:152ra127 Available at: http://www.ncbi.nlm.nih.gov/pubmed/22993294.

Bobrov E, Wolfe J, Rao RP, Brecht M (2014) The Representation of Social Facial Touch in Rat Barrel Cortex. Curr Biol 24:109–115 Available at: https://www.sciencedirect.com/science/article/pii/S0960982213015042?via%3Dihub [Accessed May 11, 2018].

Bystron I, Blakemore C, Rakic P (2008) Development of the human cerebral cortex: Boulder Committee revisited. Nat Rev Neurosci 9:110–122 Available at: http://www.nature.com/articles/nrn2252 [Accessed May 17, 2018].

Cariaga-Martínez A, Gutiérrez K, Alelú-Paz R (2018) The Vast Complexity of the Epigenetic Landscape during Neurodevelopment: An Open Frame to Understanding Brain Function. Int J Mol Sci 19:1333 Available at: http://www.mdpi.com/1422-0067/19/5/1333 [Accessed May 12, 2018].

Cascio CJ (2010) Somatosensory processing in neurodevelopmental disorders. J Neurodev Disord 2:62–69 Available at: http://www.ncbi.nlm.nih.gov/pubmed/22127855 [Accessed May 2, 2018].

Chancey JH, Adlaf EW, Sapp MC, Pugh PC, Wadiche JI, Overstreet-Wadiche LS (2013) GABA Depolarization Is Required for Experience-Dependent Synapse Unsilencing in Adult-Born Neurons. J Neurosci 33:6614–6622 Available at:

http://www.ncbi.nlm.nih.gov/pubmed/23575858 [Accessed May 8, 2018].

Chang KT, Ro H, Wang W, Min K-T (2013) Meeting at the crossroads: common mechanisms in Fragile X and Down syndrome. Trends Neurosci 36:685–694 Available at: http://www.ncbi.nlm.nih.gov/pubmed/24075449 [Accessed July 3, 2014].

Chen Q, Cichon J, Wang W, Qiu L, Lee SJ, Campbell NR, Destefino N, Goard MJ, Fu Z, Yasuda R, Looger LL, Arenkiel BR, Gan WB, Feng G (2012) Imaging neural activity using Thy1-GCaMP transgenic mice. Neuron 76:297–308 Available at: http://www.ncbi.nlm.nih.gov/pubmed/23083733.

Chen TW, Wardill TJ, Sun Y, Pulver SR, Renninger SL, Baohan A, Schreiter ER, Kerr RA, Orger MB, Jayaraman V, Looger LL, Svoboda K, Kim DS (2013) Ultrasensitive fluorescent proteins for imaging neuronal activity. Nature 499:295–300 Available at: http://www.ncbi.nlm.nih.gov/pubmed/23868258.

Comery TA, Harris JB, Willems PJ, Oostra BA, Irwin SA, Weiler IJ, Greenough WT (1997) Abnormal dendritic spines in fragile X knockout mice: maturation and pruning deficits. Proc Natl Acad Sci U S A 94:5401–5404 Available at: http://www.ncbi.nlm.nih.gov/entrez/query.fcgi?cmd=Retrieve&db=PubMed&dopt=Citation&list_uids=9144249.

Cruz-Martin A, Crespo M, Portera-Cailliau C, Cruz-Martín A, Crespo M, Portera-Cailliau C (2012) Glutamate induces the elongation of early dendritic protrusions via mGluRs in wild type mice, but not in fragile X mice. PLoS One 7:e32446 Available at: http://www.pubmedcentral.nih.gov/articlerender.fcgi?artid=3288094&tool=pmcentrez&rendertype=abstract [Accessed July 3, 2014].

Cruz-Martín A, Crespo M, Portera-Cailliau C, Cruz-Martin A, Crespo M, Portera-Cailliau C (2010) Delayed stabilization of dendritic spines in fragile X mice. J Neurosci 30:7793–7803 Available at: http://www.pubmedcentral.nih.gov/articlerender.fcgi?artid=2903441&tool=pmcentrez&rendertype=abstract [Accessed January 26, 2014].

Curia G, Papouin T, Seguela P, Avoli M (2009) Downregulation of tonic GABAergic inhibition in a mouse model of fragile X syndrome. Cereb Cortex 19:1515–1520 Available at: http://www.ncbi.nlm.nih.gov/entrez/query.fcgi?cmd=Retrieve&db=PubMed&dopt=Citation&list_uids=18787232.

D'Hulst C, De Geest N, Reeve SP, Van Dam D, De Deyn PP, Hassan BA, Kooy RF (2006) Decreased expression of the GABAA receptor in fragile X syndrome. Brain Res 1121:238–245 Available at: http://www.ncbi.nlm.nih.gov/entrez/query.fcgi?cmd=Retrieve&db=PubMed&dopt=Citation&list_uids=17046729.

Dana H, Chen T-W, Hu A, Shields BC, Guo C, Looger LL, Kim DS, Svoboda K (2014) Thy1-GCaMP6 Transgenic Mice for Neuronal Population Imaging In Vivo. PLoS One 9:e108697.

Dansie LE, Phommahaxay K, Okusanya AG, Uwadia J, Huang M, Rotschafer SE, Razak KA, Ethell DW, Ethell IM (2013) Long-lasting effects of minocycline on behavior in young but not adult Fragile X mice. Neuroscience Available at: http://www.ncbi.nlm.nih.gov/pubmed/23660195.

Darnell JC, Klann E (2013) The translation of translational control by FMRP: therapeutic targets for FXS. Nat Neurosci 16:1530–1536 Available at: http://dx.doi.org/10.1038/nn.3379 [Accessed October 7, 2014].

Darnell JC, Van Driesche SJ, Zhang C, Hung KY, Mele A, Fraser CE, Stone EF, Chen C, Fak JJ, Chi SW, Licatalosi DD, Richter JD, Darnell RB (2011) FMRP stalls ribosomal translocation on mRNAs linked to synaptic function and autism. Cell 146:247–261 Available at: http://www.ncbi.nlm.nih.gov/entrez/query.fcgi?cmd=Retrieve&db=PubMed&dopt=Citation&list_uids=21784246.

Deng P-YY, Rotman Z, Blundon JAA, Cho Y, Cui J, Cavalli V, Zakharenko SSS, Klyachko VAA (2013) FMRP regulates neurotransmitter release and synaptic information

transmission by modulating action potential duration via BK channels. Neuron 77:696–711 Available at: https://www.sciencedirect.com/science/article/pii/S0896627312011567?via%3Dihub [Accessed April 29, 2018].

Dutch-Belgian Fragile X Consortium (1994) Fmr1 knockout mice: a model to study fragile X mental retardation. Cell 78:23–33 Available at: http://www.ncbi.nlm.nih.gov/entrez/query.fcgi?cmd=Retrieve&db=PubMed&dopt=Citation&list_uids=8033209.

Erickson CA, Davenport MH, Schaefer TL, Wink LK, Pedapati E V., Sweeney JA, Fitzpatrick SE, Brown WT, Budimirovic D, Hagerman RJ, Hessl D, Kaufmann WE, Berry-Kravis E (2017) Fragile X targeted pharmacotherapy: lessons learned and future directions. J Neurodev Disord 9:7 Available at: http://jneurodevdisorders.biomedcentral.com/articles/10.1186/s11689-017-9186-9 [Accessed May 18, 2018].

Erzurumlu RS, Gaspar P (2012) Development and critical period plasticity of the barrel cortex. Eur J Neurosci 35:1540–1553 Available at: http://www.ncbi.nlm.nih.gov/pubmed/22607000 [Accessed May 11, 2018].

Fagiolini M, Leblanc JJ (2011) Autism: A critical period disorder? Neural Plast 2011:921680 Available at: http://www.ncbi.nlm.nih.gov/pubmed/21826280 [Accessed May 17, 2018].

Ferron L, Nieto-Rostro M, Cassidy JS, Dolphin AC (2014) Fragile X mental retardation protein controls synaptic vesicle exocytosis by modulating N-type calcium channel density. Nat Commun 5:3628 Available at: http://www.pubmedcentral.nih.gov/articlerender.fcgi?artid=3982139&tool=pmcentrez&rendertype=abstract [Accessed May 30, 2014].

Fiala JC, Feinberg M, Popov V, Harris KM, Warren S, Hersch S (1998) Synaptogenesis via dendritic filopodia in developing hippocampal area CA1. J Neurosci 18:8900–8911 Available at:

http://www.ncbi.nlm.nih.gov/entrez/query.fcgi?cmd=Retrieve&db=PubMed&dopt=Citation&list_uids=9786995 [Accessed April 29, 2018].

Filipek PA, Accardo PJ, Baranek GT, Cook EH, Dawson G, Gordon B, Gravel JS, Johnson CP, Kallen RJ, Levy SE, Minshew NJ, Prizant BM, Rapin I, Rogers SJ, Stone WL, Teplin S, Tuchman RF, Volkmar FR (1999) The Screening and Diagnosis of Autistic Spectrum Disorders. J Autism Dev Disord 29 Available at: https://link.springer.com/content/pdf/10.1023%2FA%3A1021943802493.pdf [Accessed May 17, 2018].

Frye CG, MacLean JN (2016) Spontaneous activations follow a common developmental course across primary sensory areas in mouse neocortex. J Neurophysiol 116:431–437 Available at: http://www.physiology.org/doi/10.1152/jn.00172.2016 [Accessed May 10, 2018].

Fu Y-H, Kuhl DPA, Pizzuti A, Pieretti M, Sutcliffe JS, Richards S, Verkert AJMH, Holden JJA, Fenwick RG, Warren ST, Oostra BA, Nelson DL, Caskey CT (1991) Variation of the CGG repeat at the fragile X site results in genetic instability: Resolution of the Sherman paradox. Cell 67:1047–1058 Available at: https://www.sciencedirect.com/science/article/pii/0092867491902835?via%3Dihub [Accessed May 11, 2018].

Gabis L V., Baruch YK, Jokel A, Raz R (2011) Psychiatric and autistic comorbidity in fragile X syndrome across ages. J Child Neurol 26:940–948 Available at: http://journals.sagepub.com/doi/10.1177/0883073810395937 [Accessed July 5, 2014].

Gantois I, Vandesompele J, Speleman F, Reyniers E, D'Hooge R, Severijnen L-A, Willemsen R, Tassone F, Kooy RF (2006) Expression profiling suggests underexpression of the GABAA receptor subunit δ in the fragile X knockout mouse model. Neurobiol Dis 21:346–357 Available at: https://www.sciencedirect.com/science/article/pii/S0969996105002135?via%3Dihub [Accessed May 18, 2018].

Garaschuk O, Linn J, Eilers J, Konnerth A (2000) Large-scale oscillatory calcium waves in the

immature cortex. Nat Neurosci 3:452–459 Available at: http://www.ncbi.nlm.nih.gov/entrez/query.fcgi?cmd=Retrieve&db=PubMed&dopt=Citation&list_uids=10769384.

Ghashghaei HT, Lai C, Anton ES (2007) Neuronal migration in the adult brain: are we there yet? Nat Rev Neurosci 8:141–151 Available at: http://www.nature.com/articles/nrn2074 [Accessed May 17, 2018].

Gliga T, Jones EJH, Bedford R, Charman T, Johnson MH (2014) From early markers to neuro-developmental mechanisms of autism. Dev Rev 34:189–207 Available at: http://www.ncbi.nlm.nih.gov/pubmed/25187673 [Accessed May 18, 2018].

Goel A, Buonomano D V. (2016) Temporal Interval Learning in Cortical Cultures Is Encoded in Intrinsic Network Dynamics. Neuron 91:320–327.

Golshani P, Goncalves JT, Khoshkhoo S, Mostany R, Smirnakis S, Portera-Cailliau C (2009) Internally mediated developmental desynchronization of neocortical network activity. J Neurosci 29:10890–10899 Available at: http://www.ncbi.nlm.nih.gov/entrez/query.fcgi?cmd=Retrieve&db=PubMed&dopt=Citation&list_uids=19726647.

Goncalves JT, Anstey JE, Golshani P, Portera-Cailliau C (2013) Circuit level defects in the developing neocortex of Fragile X mice. Nat Neurosci 16:903–909 Available at: http://www.ncbi.nlm.nih.gov/pubmed/23727819.

Grewe BF, Helmchen F (2009) Optical probing of neuronal ensemble activity. Curr Opin Neurobiol Available at: http://www.ncbi.nlm.nih.gov/entrez/query.fcgi?cmd=Retrieve&db=PubMed&dopt=Citation&list_uids=19854041.

Grillo FW, Song S, Teles-Grilo Ruivo LM, Huang L, Gao G, Knott GW, Maco B, Ferretti V, Thompson D, Little GE, De Paola V (2013) Increased axonal bouton dynamics in the aging mouse cortex. Proc Natl Acad Sci U S A 110:E1514-23 Available at: http://www.pubmedcentral.nih.gov/articlerender.fcgi?artid=3631669&tool=pmcentrez&ren

dertype=abstract [Accessed November 11, 2014].

Hadjikhani N, Åsberg Johnels J, Lassalle A, Zürcher NR, Hippolyte L, Gillberg C, Lemonnier E, Ben-Ari Y (2018) Bumetanide for autism: more eye contact, less amygdala activation. Sci Rep 8:3602 Available at: http://www.nature.com/articles/s41598-018-21958-x [Accessed May 17, 2018].

Hanson JE, Madison D V (2007) Presynaptic FMR1 genotype influences the degree of synaptic connectivity in a mosaic mouse model of fragile X syndrome. J Neurosci 27:4014–4018 Available at: http://www.ncbi.nlm.nih.gov/entrez/query.fcgi?cmd=Retrieve&db=PubMed&dopt=Citation&list_uids=17428978.

Harlow EG, Till SM, Russell TA, Wijetunge LS, Kind P, Contractor A (2010) Critical period plasticity is disrupted in the barrel cortex of FMR1 knockout mice. Neuron 65:385–398 Available at: http://www.ncbi.nlm.nih.gov/entrez/query.fcgi?cmd=Retrieve&db=PubMed&dopt=Citation&list_uids=20159451 [Accessed May 27, 2014].

He CX, Cantu DA, Mantri SS, Zeiger WA, Goel A, Portera-Cailliau C (2017) Tactile Defensiveness and Impaired Adaptation of Neuronal Activity in the *Fmr1* Knock-Out Mouse Model of Autism. J Neurosci 37:6475–6487.

He Q, Arroyo ED, Smukowski SN, Xu J, Piochon C, Savas JN, Portera-Cailliau C, Contractor A (2018) Critical period inhibition of NKCC1 rectifies synapse plasticity in the somatosensory cortex and restores adult tactile response maps in fragile X mice. Mol Psychiatry:1 Available at: http://www.nature.com/articles/s41380-018-0048-y [Accessed April 29, 2018].

He Q, Nomura T, Xu J, Contractor A (2014) The developmental switch in GABA polarity is delayed in fragile X mice. J Neurosci 34:446–450 Available at: http://www.ncbi.nlm.nih.gov/pubmed/24403144 [Accessed October 30, 2014].

Hensch TK (2005) Critical period plasticity in local cortical circuits. Nat Rev Neurosci 6:877–

888 Available at: http://www.ncbi.nlm.nih.gov/entrez/query.fcgi?cmd=Retrieve&db=PubMed&dopt=Citation&list_uids=16261181.

Hernandez RN, Feinberg RL, Vaurio R, Passanante NM, Thompson RE, Kaufmann WE (2009) Autism spectrum disorder in fragile X syndrome: A longitudinal evaluation. Am J Med Genet Part A 149A:1125–1137 Available at: http://doi.wiley.com/10.1002/ajmg.a.32848 [Accessed May 9, 2018].

Hinton VJ, Brown WT, Wisniewski K, Rudelli RD (1991) Analysis of neocortex in three males with the fragile X syndrome. Am J Med Genet 41:289–294 Available at: http://www.ncbi.nlm.nih.gov/entrez/query.fcgi?cmd=Retrieve&db=PubMed&dopt=Citation&list_uids=1724112.

Hofer SB, Mrsic-Flogel TD, Bonhoeffer T, Hubener M (2009) Experience leaves a lasting structural trace in cortical circuits. Nature 457:313–317 Available at: http://www.ncbi.nlm.nih.gov/entrez/query.fcgi?cmd=Retrieve&db=PubMed&dopt=Citation&list_uids=19005470.

Holderith N, Lorincz A, Katona G, Rózsa B, Kulik A, Watanabe M, Nusser Z (2012) Release probability of hippocampal glutamatergic terminals scales with the size of the active zone. Nat Neurosci 15:988–997 Available at: http://dx.doi.org/10.1038/nn.3137 [Accessed May 25, 2014].

Holtmaat A, Bonhoeffer T, Chow DK, Chuckowree J, De Paola V, Hofer SB, Hubener M, Keck T, Knott G, Lee WC, Mostany R, Mrsic-Flogel TD, Nedivi E, Portera-Cailliau C, Svoboda K, Trachtenberg JT, Wilbrecht L (2009) Long-term, high-resolution imaging in the mouse neocortex through a chronic cranial window. Nat Protoc 4:1128–1144 Available at: http://www.ncbi.nlm.nih.gov/entrez/query.fcgi?cmd=Retrieve&db=PubMed&dopt=Citation&list_uids=19617885.

Holtmaat A, de Paola V, Wilbrecht L, Trachtenberg JT, Svoboda K, Portera-Cailliau C (2012) Imaging neocortical neurons through a chronic cranial window. Cold Spring Harb Protoc

6:694–701.

Holtmaat A, Svoboda K (2009) Experience-dependent structural synaptic plasticity in the mammalian brain. Nat Rev Neurosci 10:647–658 Available at: http://www.ncbi.nlm.nih.gov/entrez/query.fcgi?cmd=Retrieve&db=PubMed&dopt=Citation&list_uids=19693029.

Holtmaat A, Wilbrecht L, Knott GW, Welker E, Svoboda K (2006) Experience-dependent and cell-type-specific spine growth in the neocortex. Nature 441:979–983 Available at: http://www.ncbi.nlm.nih.gov/entrez/query.fcgi?cmd=Retrieve&db=PubMed&dopt=Citation&list_uids=16791195.

Hubel DH, Wiesel TN (1970) The period of susceptibility to the physiological effects of unilateral eye closure in kittens. J Physiol 206:419–436 Available at: http://www.ncbi.nlm.nih.gov/entrez/query.fcgi?cmd=Retrieve&db=PubMed&dopt=Citation&list_uids=5498493.

Irwin SA, Galvez R, Greenough WT (2000) Dendritic spine structural anomalies in fragile-X mental retardation syndrome. Cereb Cortex 10:1038–1044 Available at: http://www.ncbi.nlm.nih.gov/pubmed/11007554 [Accessed July 3, 2014].

Irwin SA, Idupulapati M, Gilbert ME, Harris JB, Chakravarti AB, Rogers EJ, Crisostomo RA, Larsen BP, Mehta A, Alcantara CJ, Patel B, Swain RA, Weiler IJ, Oostra BA, Greenough WT (2002) Dendritic spine and dendritic field characteristics of layer V pyramidal neurons in the visual cortex of fragile-X knockout mice. Am J Med Genet 111:140–146 Available at: http://www.ncbi.nlm.nih.gov/pubmed/12210340 [Accessed July 3, 2014].

Isshiki M, Tanaka S, Kuriu T, Tabuchi K, Takumi T, Okabe S (2014) Enhanced synapse remodelling as a common phenotype in mouse models of autism. Nat Commun 5:4742 Available at: http://www.nature.com/doifinder/10.1038/ncomms5742 [Accessed May 17, 2018].

Itami C, Kimura F (2012) Developmental switch in spike timing-dependent plasticity at layers 4-2/3 in the rodent barrel cortex. J Neurosci 32:15000–15011 Available at:

http://www.ncbi.nlm.nih.gov/pubmed/23100422 [Accessed November 11, 2014].

Jacquemont S et al. (2011) Epigenetic modification of the FMR1 gene in fragile X syndrome is associated with differential response to the mGluR5 antagonist AFQ056. Sci Transl Med 3:64ra1 Available at: http://www.ncbi.nlm.nih.gov/pubmed/21209411.

Jessell TM, Sanes JR (2000) Development: The decade of the developing brain. Curr Opin Neurobiol 10:599–611 Available at: https://www.sciencedirect.com/science/article/pii/S0959438800001367?via%3Dihub [Accessed May 17, 2018].

Jiang Y et al. (2013) Detection of clinically relevant genetic variants in autism spectrum disorder by whole-genome sequencing. Am J Hum Genet 93:249–263 Available at: http://www.pubmedcentral.nih.gov/articlerender.fcgi?artid=3738824&tool=pmcentrez&rendertype=abstract [Accessed July 14, 2014].

Johnston DG, Denizet M, Mostany R, Portera-Cailliau C (2012) Chronic In Vivo Imaging Shows No Evidence of Dendritic Plasticity or Functional Remapping in the Contralesional Cortex after Stroke. Cereb cortex Available at: http://www.ncbi.nlm.nih.gov/pubmed/22499800.

Jung CKEE, Herms J (2014) Structural Dynamics of Dendritic Spines are Influenced by an Environmental Enrichment: An In Vivo Imaging Study. Cereb Cortex 24:377–384 Available at: http://www.ncbi.nlm.nih.gov/pubmed/23081882 [Accessed January 22, 2014].

Kaila K, Price TJ, Payne JA, Puskarjov M, Voipio J (2014) Cation-chloride cotransporters in neuronal development, plasticity and disease. Nat Rev Neurosci 15:637–654 Available at: http://www.ncbi.nlm.nih.gov/pubmed/25234263 [Accessed May 8, 2018].

Knoth IS, Vannasing P, Major P, Michaud JL, Lippé S (2014) Alterations of visual and auditory evoked potentials in fragile X syndrome. Int J Dev Neurosci Available at: http://www.sciencedirect.com/science/article/pii/S0736574814000732 [Accessed June 2, 2014].

Knott G, Holtmaat A (2008) Dendritic spine plasticity--current understanding from in vivo

studies. Brain Res Rev 58:282–289 Available at: http://www.ncbi.nlm.nih.gov/entrez/query.fcgi?cmd=Retrieve&db=PubMed&dopt=Citation&list_uids=18353441.

Knudsen EI (2004) Sensitive Periods in the Development of the Brain and Behavior. J Cogn Neurosci 16:1412–1425 Available at: http://www.mitpressjournals.org/doi/10.1162/0898929042304796 [Accessed May 17, 2018].

Lambroso PJ, Rubenstein JL (1998) Development of the Cerebral Cortex: V. Transcription Factors and Brain Development. J Am Acad Child Adolesc Psychiatry 37:561–562 Available at: https://ac.els-cdn.com/S0890856709629579/1-s2.0-S0890856709629579-main.pdf?_tid=8a474582-6223-4e40-9c03-8e94effa330b&acdnat=1526604714_e95519ec5289b5edfb3810f5989376c3 [Accessed May 17, 2018].

Landers MS, Sullivan RM (1999) Vibrissae-evoked behavior and conditioning before functional ontogeny of the somatosensory vibrissae cortex. J Neurosci 19:5131–5137 Available at: http://www.ncbi.nlm.nih.gov/pubmed/10366646 [Accessed May 11, 2018].

LeBlanc JJ, Fagiolini M (2011) Autism: a “critical period” disorder? Neural Plast 2011:921680 Available at: http://www.ncbi.nlm.nih.gov/pubmed/21826280.

Leekam SR, Nieto C, Libby SJ, Wing L, Gould J (2007) Describing the Sensory Abnormalities of Children and Adults with Autism. J Autism Dev Disord 37:894–910 Available at: http://link.springer.com/10.1007/s10803-006-0218-7 [Accessed May 17, 2018].

Leitner Y (2014) The Co-Occurrence of Autism and Attention Deficit Hyperactivity Disorder in Children â€“ What Do We Know? Front Hum Neurosci 8:268 Available at: http://journal.frontiersin.org/article/10.3389/fnhum.2014.00268/abstract [Accessed May 17, 2018].

Ligsay A, Van Dijck A, Nguyen D V., Lozano R, Chen Y, Bickel ES, Hessl D, Schneider A, Angkustsiri K, Tassone F, Ceulemans B, Kooy RF, Hagerman RJ (2017) A randomized

double-blind, placebo-controlled trial of ganaxolone in children and adolescents with fragile X syndrome. J Neurodev Disord 9:26 Available at: http://jneurodevdisorders.biomedcentral.com/articles/10.1186/s11689-017-9207-8 [Accessed May 18, 2018].

Lozano R, Hare EB, Hagerman RJ (2014) Modulation of the GABAergic pathway for the treatment of fragile X syndrome. Neuropsychiatr Dis Treat 10:1769–1779 Available at: http://www.ncbi.nlm.nih.gov/pubmed/25258535 [Accessed May 18, 2018].

Lu R, Wang H, Liang Z, Ku L, O'donnell WT, Li W, Warren ST, Feng Y (2004) The fragile X protein controls microtubule-associated protein 1B translation and microtubule stability in brain neuron development. Proc Natl Acad Sci U S A 101:15201–15206 Available at: http://www.pubmedcentral.nih.gov/articlerender.fcgi?artid=524058&tool=pmcentrez&rendertype=abstract [Accessed July 3, 2014].

Malter HE, Iber JC, Willemsen R, Graaff E de, Tarleton JC, Leisti J, Warren ST, Oostra BA (1997) Characterization of the full fragile X syndrome mutation in fetal gametes. Nat Genet 15:165–169 Available at: http://www.ncbi.nlm.nih.gov/pubmed/9020841 [Accessed May 11, 2018].

Maravall M, Mainen ZF, Sabatini BL, Svoboda K (2000) Estimating intracellular calcium concentrations and buffering without wavelength ratioing. Biophys J 78:2655–2667 Available at: http://www.ncbi.nlm.nih.gov/entrez/query.fcgi?cmd=Retrieve&db=PubMed&dopt=Citation&list_uids=10777761.

Matta JA, Ashby MC, Sanz-Clemente A, Roche KW, Isaac JT (2011) mGluR5 and NMDA receptors drive the experience- and activity-dependent NMDA receptor NR2B to NR2A subunit switch. Neuron 70:339–351 Available at: http://www.ncbi.nlm.nih.gov/pubmed/21521618.

Meredith RM (2015) Sensitive and critical periods during neurotypical and aberrant neurodevelopment: A framework for neurodevelopmental disorders. Neurosci Biobehav

Rev 50:180–188 Available at: http://www.ncbi.nlm.nih.gov/pubmed/25496903 [Accessed May 9, 2018].

Meredith RM, Dawitz J, Kramvis I (2012) Sensitive time-windows for susceptibility in neurodevelopmental disorders. Trends Neurosci Available at: http://www.ncbi.nlm.nih.gov/pubmed/22542246.

Metcalfe JS, Chang T-Y, Chen L-C, McDowell K, Jeka JJ, Clark JE (2005) Development of somatosensory-motor integration: An event-related analysis of infant posture in the first year of independent walking. Dev Psychobiol 46:19–35 Available at: http://doi.wiley.com/10.1002/dev.20037 [Accessed May 10, 2018].

Micheva KD, Beaulieu C (1996) Quantitative aspects of synaptogenesis in the rat barrel field cortex with special reference to GABA circuitry. J Comp Neurol 373:340–354 Available at: http://www.ncbi.nlm.nih.gov/entrez/query.fcgi?cmd=Retrieve&db=PubMed&dopt=Citation&list_uids=8889932.

Miller LJ, McIntosh DN, McGrath J, Shyu V, Lampe M, Taylor AK, Tassone F, Neitzel K, Stackhouse T, Hagerman RJ (1999) Electrodermal responses to sensory stimuli in individuals with fragile X syndrome: a preliminary report. Am J Med Genet 83:268–279 Available at: http://www.ncbi.nlm.nih.gov/pubmed/10208160 [Accessed July 5, 2014].

Miquelajauregui A, Kribakaran S, Mostany R, Badaloni A, Consalez GG, Portera-Cailliau C (2015) Layer 4 Pyramidal Neurons Exhibit Robust Dendritic Spine Plasticity In Vivo after Input Deprivation. J Neurosci 35 Available at: http://www.jneurosci.org/content/35/18/7287.long [Accessed April 17, 2017].

Miyazaki M, Phd M, Fujii E, Saijo T, Mori K, Hashimoto T, Kagami S, Kuroda Y (n.d.) Short-latency somatosensory evoked potentials in infantile autism: evidence of hyperactivity in the right primary somatosensory area. Available at: https://onlinelibrary.wiley.com/doi/pdf/10.1017/S0012162207000059.x [Accessed May 17, 2018].

Molliver ME, Kostovic´ I, Van Der Loos H (1973) The development of synapses in cerebral

cortex of the human fetus. Brain Res 50:403–407 Available at: https://www.sciencedirect.com/science/article/pii/0006899373907415?via%3Dihub [Accessed May 17, 2018].

Moy SS, Nadler JJ (2008) Advances in behavioral genetics: mouse models of autism. Mol Psychiatry 13:4–26 Available at: http://www.nature.com/articles/4002082 [Accessed May 18, 2018].

Muddashetty RS, Kelic S, Gross C, Xu M, Bassell GJ (2007) Dysregulated metabotropic glutamate receptor-dependent translation of AMPA receptor and postsynaptic density-95 mRNAs at synapses in a mouse model of fragile X syndrome. J Neurosci 27:5338–5348 Available at: http://www.ncbi.nlm.nih.gov/entrez/query.fcgi?cmd=Retrieve&db=PubMed&dopt=Citation&list_uids=17507556.

Nakamoto M, Nalavadi V, Epstein MP, Narayanan U, Bassell GJ, Warren ST (2007) Fragile X mental retardation protein deficiency leads to excessive mGluR5-dependent internalization of AMPA receptors. Proc Natl Acad Sci U S A 104:15537–15542 Available at: http://www.ncbi.nlm.nih.gov/entrez/query.fcgi?cmd=Retrieve&db=PubMed&dopt=Citation&list_uids=17881561.

Nimchinsky EA, Oberlander AM, Svoboda K (2001) Abnormal development of dendritic spines in FMR1 knock-out mice. J Neurosci 21:5139–5146 Available at: http://www.ncbi.nlm.nih.gov/pubmed/11438589 [Accessed July 3, 2014].

Nomura T, Kimura M, Horii T, Morita S, Soejima H, Kudo S, Hatada I (2008) MeCP2-dependent repression of an imprinted miR-184 released by depolarization. Hum Mol Genet 17:1192–1199 Available at: http://www.ncbi.nlm.nih.gov/pubmed/18203756 [Accessed October 29, 2014].

Oh WC, Lutzu S, Castillo PE, Kwon H-B (2016) De novo synaptogenesis induced by GABA in the developing mouse cortex. Science 353:1037–1040 Available at: http://www.ncbi.nlm.nih.gov/pubmed/27516412 [Accessed May 8, 2018].

Olmos-Serrano JL, Paluszkiewicz SM, Martin BS, Kaufmann WE, Corbin JG, Huntsman MM (2010) Defective GABAergic neurotransmission and pharmacological rescue of neuronal hyperexcitability in the amygdala in a mouse model of fragile X syndrome. J Neurosci 30:9929–9938 Available at: http://www.ncbi.nlm.nih.gov/pubmed/20660275.

Padmashri R, Reiner BC, Suresh A, Spartz E, Dunaevsky A (2013) Altered structural and functional synaptic plasticity with motor skill learning in a mouse model of fragile x syndrome. J Neurosci 33:19715–19723 Available at: http://www.pubmedcentral.nih.gov/articlerender.fcgi?artid=3858638&tool=pmcentrez&rendertype=abstract [Accessed January 21, 2014].

Pan F, Aldridge GM, Greenough WT, Gan W-BB (2010) Dendritic spine instability and insensitivity to modulation by sensory experience in a mouse model of fragile X syndrome. Proc Natl Acad Sci U S A 107:17768–17773 Available at: http://www.pubmedcentral.nih.gov/articlerender.fcgi?artid=2955121&tool=pmcentrez&rendertype=abstract [Accessed January 26, 2014].

Patel AB, Hays SA, Bureau I, Huber KM, Gibson JR (2013) A target cell-specific role for presynaptic Fmr1 in regulating glutamate release onto neocortical fast-spiking inhibitory neurons. J Neurosci 33:2593–2604 Available at: http://www.pubmedcentral.nih.gov/articlerender.fcgi?artid=3711607&tool=pmcentrez&rendertype=abstract [Accessed November 3, 2014].

Peñagarikano O, Mulle JG, Warren ST (2007) The pathophysiology of fragile x syndrome. Annu Rev Genomics Hum Genet 8:109–129 Available at: http://www.ncbi.nlm.nih.gov/entrez/query.fcgi?cmd=Retrieve&db=PubMed&dopt=Citation&list_uids=17477822.

Pencea V, Bingaman KD, Freedman LJ, Luskin MB (2001) Neurogenesis in the Subventricular Zone and Rostral Migratory Stream of the Neonatal and Adult Primate Forebrain. Exp Neurol 172:1–16 Available at: https://www.sciencedirect.com/science/article/pii/S0014488601977684?via%3Dihub [Accessed May 17, 2018].

Pihko E, Lauronen L (2004) Somatosensory processing in healthy newborns. Exp Neurol 190:2–7 Available at: https://www.sciencedirect.com/science/article/pii/S0014488604000494?via%3Dihub [Accessed May 9, 2018].

Pologruto TA, Sabatini BL, Svoboda K (2003) ScanImage : Flexible software for operating laser scanning microscopes. Biomed Eng Online 2:1–9.

Portera-Cailliau C, Weimer RM, De Paola V, Caroni P, Svoboda K (2005) Diverse modes of axon elaboration in the developing neocortex. PLoS Biol 3:e272 Available at: http://www.ncbi.nlm.nih.gov/entrez/query.fcgi?cmd=Retrieve&db=PubMed&dopt=Citation&list_uids=16026180.

Quiroz JA, Tamburri P, Deptula D, Banken L, Beyer U, Rabbia M, Parkar N, Fontoura P, Santarelli L (2016) Efficacy and Safety of Basimglurant as Adjunctive Therapy for Major Depression. JAMA Psychiatry 73:675 Available at: http://archpsyc.jamanetwork.com/article.aspx?doi=10.1001/jamapsychiatry.2016.0838 [Accessed May 18, 2018].

Rash BG, Grove EA (2006) Area and layer patterning in the developing cerebral cortex. Curr Opin Neurobiol 16:25–34 Available at: https://www.sciencedirect.com/science/article/pii/S0959438806000055?via%3Dihub [Accessed May 17, 2018].

Rochefort NL, Garaschuk O, Milos RI, Narushima M, Marandi N, Pichler B, Kovalchuk Y, Konnerth A (2009) Sparsification of neuronal activity in the visual cortex at eye-opening. Proc Natl Acad Sci U S A 106:15049–15054 Available at: http://www.ncbi.nlm.nih.gov/entrez/query.fcgi?cmd=Retrieve&db=PubMed&dopt=Citation&list_uids=19706480.

Rogers SJ, Hepburn S, Wehner E (2003) Parent reports of sensory symptoms in toddlers with autism and those with other developmental disorders. J Autism Dev Disord 33:631–642 Available at: http://www.ncbi.nlm.nih.gov/pubmed/14714932 [Accessed May 9, 2018].

Ronconi L, Molteni M, Casartelli L (2016) Building Blocks of Others' Understanding: A Perspective Shift in Investigating Social-Communicative Deficit in Autism. Front Hum Neurosci 10:144 Available at: http://journal.frontiersin.org/Article/10.3389/fnhum.2016.00144/abstract [Accessed May 18, 2018].

Rubenstein JLR, Merzenich MM (2003) Model of autism: increased ratio of excitation/inhibition in key neural systems. Genes, Brain Behav 2:255–267 Available at: http://doi.wiley.com/10.1034/j.1601-183X.2003.00037.x [Accessed May 18, 2018].

Rudelli RD, Brown WT, Wisniewski K, Jenkins EC, Laure-Kamionowska M, Connell F, Wisniewski HM (1985) Adult fragile X syndrome. Clinico-neuropathologic findings. Acta Neuropathol 67:289–295 Available at: http://www.ncbi.nlm.nih.gov/entrez/query.fcgi?cmd=Retrieve&db=PubMed&dopt=Citation&list_uids=4050344.

Ruthazer ES, Stryker MP (1996) The role of activity in the development of long-range horizontal connections in area 17 of the ferret. J Neurosci 16:7253–7269 Available at: http://www.ncbi.nlm.nih.gov/entrez/query.fcgi?cmd=Retrieve&db=PubMed&dopt=Citation&list_uids=8929433.

Siegel F, Heimel JA, Peters J, Lohmann C (2012) Peripheral and central inputs shape network dynamics in the developing visual cortex in vivo. Curr Biol 22:253–258.

Smith LE, Barker ET, Seltzer MM, Abbeduto L, Greenberg JS (2012) Behavioral phenotype of fragile X syndrome in adolescence and adulthood. Am J Intellect Dev Disabil 117:1–17 Available at: http://www.ncbi.nlm.nih.gov/pubmed/22264109 [Accessed May 2, 2018].

Soechting JF, Flanders M (2008) Sensorimotor control of contact force. Curr Opin Neurobiol 18:565–572 Available at: https://www.sciencedirect.com/science/article/pii/S095943880800158X?via%3Dihub [Accessed May 9, 2018].

Suvrathan A, Hoeffer CA, Wong H, Klann E, Chattarji S (2010) Characterization and reversal of

synaptic defects in the amygdala in a mouse model of fragile X syndrome. Proc Natl Acad Sci U S A 107:11591–11596 Available at: http://www.pubmedcentral.nih.gov/articlerender.fcgi?artid=2895119&tool=pmcentrez&rendertype=abstract [Accessed November 16, 2014].

Tam PPL, Fossat N, Wilkie E, Loebel DAF, Ip CK, Ramialison M (2016) Formation of the Embryonic Head in the Mouse: Attributes of a Gene Regulatory Network. Curr Top Dev Biol 117:497–521 Available at: https://www.sciencedirect.com/science/article/pii/S0070215315001854?via%3Dihub [Accessed May 17, 2018].

Tashiro A, Dunaevsky A, Blazeski R, Mason CA, Yuste R (2003) Bidirectional regulation of hippocampal mossy fiber filopodial motility by kainate receptors: a two-step model of synaptogenesis. Neuron 38:773–784 Available at: http://www.ncbi.nlm.nih.gov/entrez/query.fcgi?cmd=Retrieve&db=PubMed&dopt=Citation&list_uids=12797961.

Tau GZ, Peterson BS (2010) Normal Development of Brain Circuits. Neuropsychopharmacology 35:147–168 Available at: http://www.nature.com/articles/npp2009115 [Accessed May 17, 2018].

Thye MD, Bednarz HM, Herringshaw AJ, Sartin EB, Kana RK (2018) The impact of atypical sensory processing on social impairments in autism spectrum disorder. Dev Cogn Neurosci 29:151–167 Available at: https://www.sciencedirect.com/science/article/pii/S1878929316301736?via%3Dihub [Accessed May 17, 2018].

Tian L, Hires SA, Mao T, Huber D, Chiappe ME, Chalasani SH, Petreanu L, Akerboom J, McKinney SA, Schreiter ER, Bargmann CI, Jayaraman V, Svoboda K, Looger LL (2009) Imaging neural activity in worms, flies and mice with improved GCaMP calcium indicators. Nat Methods 6:875–881 Available at: http://www.ncbi.nlm.nih.gov/entrez/query.fcgi?cmd=Retrieve&db=PubMed&dopt=Citation&list_uids=19898485.

Till SM, Wijetunge LS, Seidel VG, Harlow E, Wright AK, Bagni C, Contractor A, Gillingwater TH, Kind PC (2012) Altered maturation of the primary somatosensory cortex in a mouse model of fragile X syndrome. Hum Mol Genet 21:2143–2156 Available at: http://www.ncbi.nlm.nih.gov/pubmed/22328088.

Tomchek SD, Dunn W (2007) Sensory processing in children with and without autism: a comparative study using the short sensory profile. Am J Occup Ther 61:190–200 Available at: http://www.ncbi.nlm.nih.gov/pubmed/17436841 [Accessed May 9, 2018].

Trachtenberg JT, Chen BE, Knott GW, Feng G, Sanes JR, Welker E, Svoboda K (2002) Long-term in vivo imaging of experience-dependent synaptic plasticity in adult cortex. Nature 420:788–794 Available at: http://www.ncbi.nlm.nih.gov/entrez/query.fcgi?cmd=Retrieve&db=PubMed&dopt=Citation&list_uids=12490942.

van der Bourg A, Yang J-W, Reyes-Puerta V, Laurenczy B, Wieckhorst M, Stüttgen MC, Luhmann HJ, Helmchen F (2016) Layer-Specific Refinement of Sensory Coding in Developing Mouse Barrel Cortex. Cereb Cortex:1–16.

Verkerk AJMH et al. (1991) Identification of a gene (FMR-1) containing a CGG repeat coincident with a breakpoint cluster region exhibiting length variation in fragile X syndrome. Cell 65:905–914 Available at: https://www.sciencedirect.com/science/article/pii/009286749190397H?via%3Dihub [Accessed May 11, 2018].

Wang DD, Kriegstein AR (2009) Defining the role of GABA in cortical development. J Physiol 587:1873–1879 Available at: http://www.ncbi.nlm.nih.gov/pubmed/19153158 [Accessed May 8, 2018].

Wang X-S, Peng C-Z, Cai W-J, Xia J, Jin D, Dai Y, Luo X-G, Klyachko VA, Deng P-Y (2014) Activity-dependent regulation of release probability at excitatory hippocampal synapses: a crucial role of fragile X mental retardation protein in neurotransmission. Eur J Neurosci 39:1602–1612 Available at: http://www.ncbi.nlm.nih.gov/pubmed/24646437 [Accessed

November 16, 2014].

Willemsen R, Kooy RF (2017) Fragile X syndrome from genetics to targeted treatment. Academic Press.

Wilt BA, Burns LD, Wei Ho ET, Ghosh KK, Mukamel EA, Schnitzer MJ (2009) Advances in light microscopy for neuroscience. Annu Rev Neurosci 32:435–506 Available at: http://www.ncbi.nlm.nih.gov/entrez/query.fcgi?cmd=Retrieve&db=PubMed&dopt=Citation&list_uids=19555292.

Winarni TI, Schneider A, Borodyanskara M, Hagerman RJ (2012) Early intervention combined with targeted treatment promotes cognitive and behavioral improvements in young children with fragile x syndrome. Case Rep Genet 2012:280813 Available at: http://www.pubmedcentral.nih.gov/articlerender.fcgi?artid=3447258&tool=pmcentrez&rendertype=abstract [Accessed June 2, 2014].

Wolfe J, Mende C, Brecht M (2011) Social facial touch in rats. Behav Neurosci 125:900–910 Available at: http://doi.apa.org/getdoi.cfm?doi=10.1037/a0026165 [Accessed May 11, 2018].

Won H, Mah W, Kim E (2013) Autism spectrum disorder causes, mechanisms, and treatments: focus on neuronal synapses. Front Mol Neurosci 6:19 Available at: http://www.pubmedcentral.nih.gov/articlerender.fcgi?artid=3733014&tool=pmcentrez&rendertype=abstract [Accessed November 10, 2014].

Yang G, Pan F, Gan W-B (2009) Stably maintained dendritic spines are associated with lifelong memories. Nature 462:920–924 Available at: http://www.ncbi.nlm.nih.gov/pubmed/19946265 [Accessed January 23, 2014].

Youssef EA, Berry-Kravis E, Czech C, Hagerman RJ, Hessl D, Wong CY, Rabbia M, Deptula D, John A, Kinch R, Drewitt P, Lindemann L, Marcinowski M, Langland R, Horn C, Fontoura P, Santarelli L, Quiroz JA, Group FS (2018) Effect of the mGluR5-NAM Basimglurant on Behavior in Adolescents and Adults with Fragile X Syndrome in a Randomized, Double-Blind, Placebo-Controlled Trial: FragXis Phase 2 Results.

Neuropsychopharmacology 43:503–512 Available at: http://www.nature.com/doifinder/10.1038/npp.2017.177 [Accessed May 18, 2018].

Yu X, Zuo Y (2011) Spine plasticity in the motor cortex. Curr Opin Neurobiol 21:169–174 Available at: http://www.ncbi.nlm.nih.gov/pubmed/20728341.

Yuste R, Bonhoeffer T (2001) Morphological changes in dendritic spines associated with long-term synaptic plasticity. Annu Rev Neurosci 24:1071–1089 Available at: http://www.ncbi.nlm.nih.gov/entrez/query.fcgi?cmd=Retrieve&db=PubMed&dopt=Citation&list_uids=11520928.

Zariwala HA, Borghuis BG, Hoogland TM, Madisen L, Tian L, De Zeeuw CI, Zeng H, Looger LL, Svoboda K, Chen TW (2012) A Cre-dependent GCaMP3 reporter mouse for neuronal imaging in vivo. J Neurosci 32:3131–3141 Available at: http://www.ncbi.nlm.nih.gov/pubmed/22378886.

Zhang Y, Bonnan A, Bony G, Ferezou I, Pietropaolo S, Ginger M, Sans N, Rossier J, Oostra B, LeMasson G, Frick A (2014) Dendritic channelopathies contribute to neocortical and sensory hyperexcitability in Fmr1−/y mice. Nat Neurosci 17:1701–1709 Available at: http://www.nature.com/doifinder/10.1038/nn.3864%5Cnhttp://dx.doi.org/10.1038/nn.3864.

Zucker E, Welker WI (1969) Coding of somatic sensory input by vibrissae neurons in the rat's trigeminal ganglion. Brain Res 12:138–156 Available at: https://www.sciencedirect.com/science/article/pii/0006899369900614?via%3Dihub [Accessed April 18, 2018].

Zukin RS, Richter JD, Bagni C (2009) Signals, synapses, and synthesis: how new proteins control plasticity. Front Neural Circuits 3:14 Available at: http://www.ncbi.nlm.nih.gov/entrez/query.fcgi?cmd=Retrieve&db=PubMed&dopt=Citation&list_uids=19838324.